CRANFIELD UNIVERSITY

ANNA MACLENNAN HULME

SCHOOL OF WATER, ENERGY AND ENVIRONMENT
Cranfield Water Science Institute

PhD
Academic Year: 2017 - 2020

Supervisor: Prof. Ewan McAdam
Associate Supervisor: Dr Marc Pidou

CRANFIELD UNIVERSITY

SCHOOL OF WATER, ENERGY AND ENVIRONMENT
Cranfield Water Science Institute

PhD

Academic Year 2017 - 2020

ANNA MACLENNAN HULME

Operation and configuration of reverse electrodialysis for thermal to electric conversion applications

Supervisor: Prof. Ewan McAdam
Associate Supervisor: Dr Marc Pidou
December 2020

Abstract

Reverse electrodialysis (RED) is a membrane-based technology which enables the sustainable production of electricity through harnessing the Gibbs free energy of mixing solutions with a salinity gradient. Whilst RED research has largely focussed on power production from sea water and river water, efforts to decarbonise the energy sector have led to interest in 'closed-loop' RED, which utilises synthetic saline solutions for applications in energy storage and thermal to electric conversion. To realise the potential of RED for these applications, research is required to determine the operating conditions and configurations which enable high power output and energy efficiency and reduce the levelised cost of electricity. In this work, the use of sodium chloride solutions with an increased concentration gradient in a recycle configuration is demonstrated to maximise the work produced from a fixed volume when current density is optimised, minimising the unitary cost of electricity produced by RED. However, these conditions exacerbate phenomena such as osmosis, ionic transport, and concentration polarisation, introducing complex temporal effects which must be managed. Features of electrodialysis modules such as an increased intermembrane distance and the low water permeability of membranes have been demonstrated to improve energy efficiency obtained using these feeds at low current densities, however, compromises power density at higher current densities. Membranes with low water permeability and low resistance are required to maximise power and energy efficiency using these feeds. Whilst the use of larger stack size has been shown to be associated with greater exergy losses due to water transport, increasing the cell pair number has been identified as an effective strategy to increase the process scale, enabling improvements to both power and efficiency.

Keywords: Closed-loop, reverse electrodialysis heat engine, salinity gradient energy, brine, blue energy, low-grade heat

Acknowledgements

I would like to extend my thanks to my supervisor Professor Ewan McAdam for providing so much invaluable time, guidance and feedback throughout the project - thank you for always pushing me to do my best and taking my 'attention to detail' to the next level! I would also like to thank Dr Marc Pidou for his input into the project. I am very grateful to Dr Chris Davey for all his advice, support and assistance, particularly in the lab, and for always making time to help me troubleshoot! I would also like to thank the Bill & Melinda Gates Foundation for funding this research (grant number OPP1149204). Finally, I would like to thank all those who made Cranfield Water Science Institute such an enriching environment.

Table of Contents

List of Figures

List of Tables

Nomenclature

Roman symbols

A	Active membrane area	m^2
C	Counter-ion concentration	mol
CAF	Capital amortization factor	-
F	Faraday constant	$C\ mol^{-1}$
h	Intermembrane thickness	m
I	Current	A
K_{mem}	Membrane cost	$\$\ m^{-2}$
K_{PT}	Pre-treatment cost	€ $m^{-3}\ day^{-1}$
l	Channel length	m
N	Number of moles	mol
n	Number of cell pairs	-
NPV	Net present value	$
OCV	Open circuit voltage	V
P	Power	W
P_d	Gross power density	$W\ m^{-2}$
$P_{d,PT}$	Pre-treatment power density	$W\ m^{-2}$
$P_{d,pump}$	Pumping power density	$W\ m^{-2}$
P_{net}	Net power	W
P_p	Pumping power	W
P_{RED}	Gross power produced by RED	W
Q	Volumetric flow rate	$m^3\ s^{-1}$
R	Universal gas constant	$J\ mol^{-1}\ K^{-1}$
r	Annualised cost of capital	%
T	Temperature	K
t	Time	s
U	Voltage	V
v	Velocity	$m\ s^{-1}$
w	Stack width	m
W	Work	J
x_i	Mole fraction of species i	-
z	Valency of ion	-

Greek symbols

ΔG	Gibbs free energy	J
Δp	Pressure drop	Pa
ΔS	Molar entropy	J mol $^{-1}$ K^{-1}
μ	Viscosity	Pa s
γ	Activity coefficient	-
Γ	Years of operation	years
η	Energy efficiency	%
τ	Residence time	s

Subscripts

c	Concentrated
d	Dilute
m	Mixed outlet

Abbreviations

AD	Adsorption desalination
CAF	Capital amortisation factor
ED	Electrodialysis
EU	European Union
GOR	Gain output ratio
IEM	Ion exchange membrane
MD	Membrane distillation
MED	Multi-effect distillation
MSRED	Multi-stage reverse electrodialysis
NPV	Net present value
OCV	Open circuit voltage
ORC	Organic rankine cycle
PRO	Pressure retarded osmosis
RED	Reverse electrodialysis
RED-HE	Reverse electrodialysis heat engine
SGE	Salinity gradient energy
TEG	Thermoelectric generator
UK	United Kingdom

1. Introduction

1.1 Drivers for thermal to electric conversion of low-grade heat

Decarbonisation of energy is urgently required to mitigate global warming [1]. Innovative energy solutions are required to achieve this, whilst simultaneously meeting increasing demand for electricity [2]. Legislative drivers for alternative low emission energy sources include the European Union (EU) Emissions Trading Scheme, which applies to all power stations and industrial plants producing emissions including methane, carbon dioxide, nitrous oxide, or perfluorocarbons. The 'cap and trade' system places an upper limit on the emissions which can be produced by each plant and requires permits for emissions exceeding this limit to be purchased, thus incentivising innovations which foster reductions in emissions [3]. In the United Kingdom (UK), the Climate Change Levy serves as a further driver for alternative technologies for sustainable power production by taxing energy from coal, gas, and solid fuels used by businesses [4]. The EU Renewable Energy Directive aims to decarbonise the energy sector by 2050, with a target of achieving 32 % of energy from renewable sources by 2030 [5]. This directive has been implemented in the UK through the Renewable Heat Incentive which provides financial incentives for renewable heat technologies such as biomass boilers, heat pumps and combined heat and power in homes, businesses, the public sector and non-profit organisations [6]. Whilst such regulations do not currently cover thermal to electric conversion, heat from renewable sources could provide future opportunities for power production.

Waste heat represents a large and underutilised source of energy, with 246 PJ estimated to be available globally [7] from sources including industry, power generation, transportation, commercial services, and residential buildings [7,8]. The thermal to electric conversion of this energy could provide low-carbon power. In the EU, industrial heat alone is estimated to be equivalent to 300 TWh per year [9]. However, a third of this heat has a temperature below 200 °C [9], with up to 63 % of the global waste heat potential similarly classified as low-grade waste heat with a temperature <100 °C [7]. At present, low efficiency and high cost are barriers preventing thermal to electric conversion of low-grade waste heat.

1.2 Thermal to electric technologies

Current technologies for the conversion of waste heat to electricity include the Organic Rankine Cycle (ORC) and thermoelectric generators (TEG) [10]. In the ORC, a working fluid is pressurised and evaporated before being expanded in a turbine to produce electricity. The ORC is currently the most used thermodynamic cycle for thermal to electric applications of low-medium grade heat (80 °C–350 °C) [11]. However, Carnot efficiency is limited to 5 % to 10 % when using low-grade waste heat [12]. Whilst suitable for large-scale applications (MW), the unit cost of electricity is also too high to be commercially viable for applications in the range of 1 kW to 100 kW [13]. Thermoelectric generators produce electricity using the Seebeck effect, where a difference in temperatures between the two surfaces generate electricity. TEGs are suitable for both small-scale applications and large-scale applications producing >100 kW [14] and have been demonstrated in industrial, domestic and transportation applications [14–16]. TEGs have the advantages of no moving parts and minimal maintenance requirements however, TEGS require a large temperature difference and the high cost of materials and low efficiencies obtained have thus far prohibited their widespread use [16].

1.3 Salinity gradient systems as a next generation thermal to electric technology

Salinity gradient heat engines have been demonstrated to theoretically enable high exergy efficiency utilising low-grade (<100 °C) waste heat for thermal to electric conversion [10]. The salinity gradient heat engine comprises two stages: (i) a power production stage which harvests the energy available from the mixing of two solutions of differing salinities; and (ii) a thermal separation stage which utilises available heat to 'unmix' the solutions and regenerate the concentration gradient [17] (Figure 1.1).

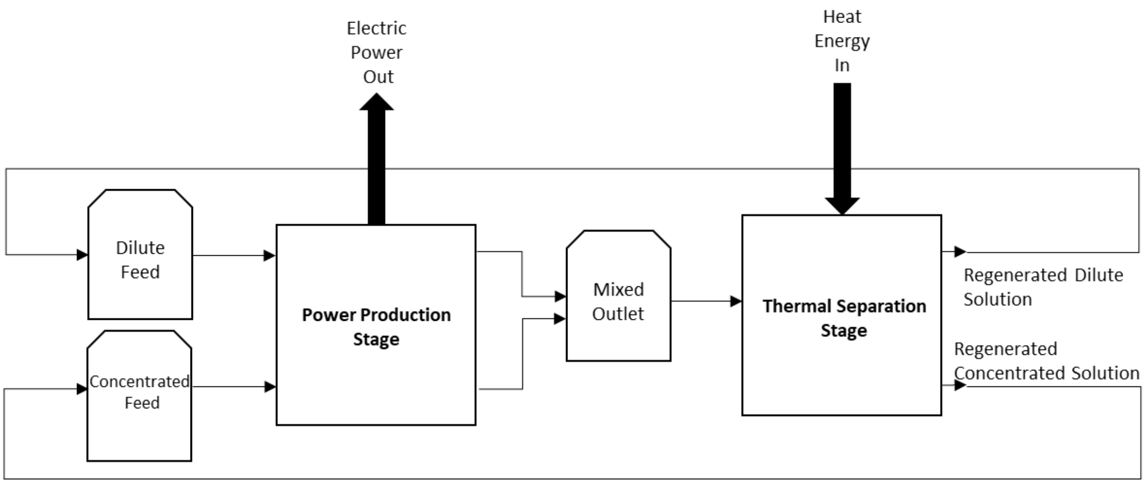

Figure 1.1. *Schematic illustrating the working principles of a salinity gradient heat engine.*

Technologies which exploit salinity gradient energy (SGE) or 'blue energy' for power production include pressure retarded osmosis (PRO), reverse electrodialysis (RED), capacitive-mixing, reverse vapour compression and hydrogels [18]. Of these, the membrane-based PRO and RED are considered the most commercially viable [19] and have been investigated for heat engine applications [10,20]. In PRO, a membrane separating a dilute feed and concentrated draw solution is permeable to water and rejects ions. The draw solution is pressurised and subsequently used to generate electricity using a turbine [21]. The increase in osmotic pressure facilitated by large concentration gradients theoretically enables power densities up to 38 W m^{-2} and energy efficiency up to 56 % to be achieved by PRO [4]. Whilst modelling demonstrates that the cost of electricity produced by a small-scale PRO heat engine (<2.5 MW) is infeasibly high (> \$0.85 kWh^{-1}) in comparison to alternative thermal to electric and power generation technologies, a reduction in the cost of electricity as system size was increased indicates that larger systems could be a competitive technology in future, following improvements to PRO membranes [23]. However, due to the requirement for turbines and pressure exchangers, a large area of land is required for PRO in comparison to conventional thermal to electric technologies such as ORCs [23,24]. Reverse electrodialysis uses alternately arranged anion and cation exchange membranes to create high concentration and low concentration compartments, facilitating the controlled movement of ions across the membranes driven by the concentration gradient. A redox couple circulating the stack converts the movement of ions to an electrical current [25]. Power densities up to 6.7 W m^{-2} have been achieved using aqueous sodium chloride (NaCl) feeds at increased concentration gradients at elevated temperatures [26], with improved power densities of 8 W m^{-2} obtained using mixtures of salts such as lithium chloride (LiCl) with NaCl at room temperature [27]. RED has been demonstrated on the pilot-scale using a range of feed waters [28] and has also been employed in the first working osmotic heat engine [29]. In contrast to PRO, RED has been demonstrated for nano-scale applications [30], indicating the potential of RED to be utilised for a wide range of applications from small-scale to industrial applications [31]. Additionally, the ability to stack RED membrane modules minimises land requirements for RED applications [32].

Thermal separation techniques can be divided into: (i) salt extraction; and (ii) solvent extraction processes [10]. Salt extraction processes utilise thermolytic salts such as ammonium bicarbonate, which degrades to gaseous ammonia and carbon dioxide at low temperature. This enables removal from the dilute effluent using a vapour stripping column, for example, and subsequent reabsorption by the concentrated stream to regenerate the salinity gradient [29]. However, this process is only applicable to thermolytic salts which produce limited power densities, with a maximum power density of 1.21 W m^{-2} achieved by RED using ammonium bicarbonate following investigation into the effect of process conditions [33]. Solvent extraction processes which may be used for SGE heat engine applications using a more diverse range of feeds include multi-effect distillation (MED) [34,35], membrane distillation (MD) [36,37], and adsorption desalination (AD) [38]. MED is a multi-stage process, in which a portion of water from the feed is evaporated in each stage, concentrating the feed [35]. The concentrated brine effluent and the condensation of vapour produces two solutions with a salinity gradient which can be utilised for power production. Steam is required to heat the first stage, however the use of the vapour produced as a heat source in subsequent stages minimises energy requirements, producing a high gain output ratio (GOR). Modelling by Tamburini et al. [10] demonstrated the potential for high exergy efficiency to be obtained by an RED-MED heat engine, with exergy efficiency up to 28 % theoretically achievable using existing state-of-the-art RED and MED modules, increasing to a maximum of 85 % assuming significant improvements in the efficiency of future ion exchange membranes. A subsequent study estimated exergy efficiency in the range of 7 – 31 % could theoretically be expected from an RED-MED heat engine [35]. As efficiency increases with stage number, MED is well-suited to large-scale applications, however is less appropriate for smaller-scale systems [38]. Membrane distillation uses a vapour-permeable membrane which rejects ions, producing pure water and concentrated brine. MD has a high GOR and can be used across process scales [39]. Whereas MED offers improved energetic performance over MD at large-scale, MD is preferable for use at smaller scales (<1000 m^3) [39]. Adsorption desalination has also been investigated due to its potential to utilise heat with a temperature as low as 40 °C [38]. In AD, water vapour is adsorbed onto an unsaturated adsorption material, with low-grade waste heat subsequently used to desorb the vapour [38,40]. The thermal separation stage selected for heat engine applications depends on the available heat source and scale of application. RED is currently the most promising salinity gradient technology for heat engine applications. In comparison to PRO, RED offers simplicity due to its direct conversion of salinity gradient energy in a single unit [18], in addition to flexibility to be used across process scale from nano-scale to industrial applications [41]. However, the configuration and operation of RED for integration with a thermal separation stage for closed-loop applications has not been well investigated.

1.4 Fundamentals of Reverse Electrodialysis

A reverse electrodialysis stack consists of repeating cell pairs of alternately arranged anion and cation exchange membranes. The membranes are separated by gaskets and woven spacers, which determine the intermembrane distance. The stack is bookended by endplates into which mesh electrodes are fixed (Figure 1.2).

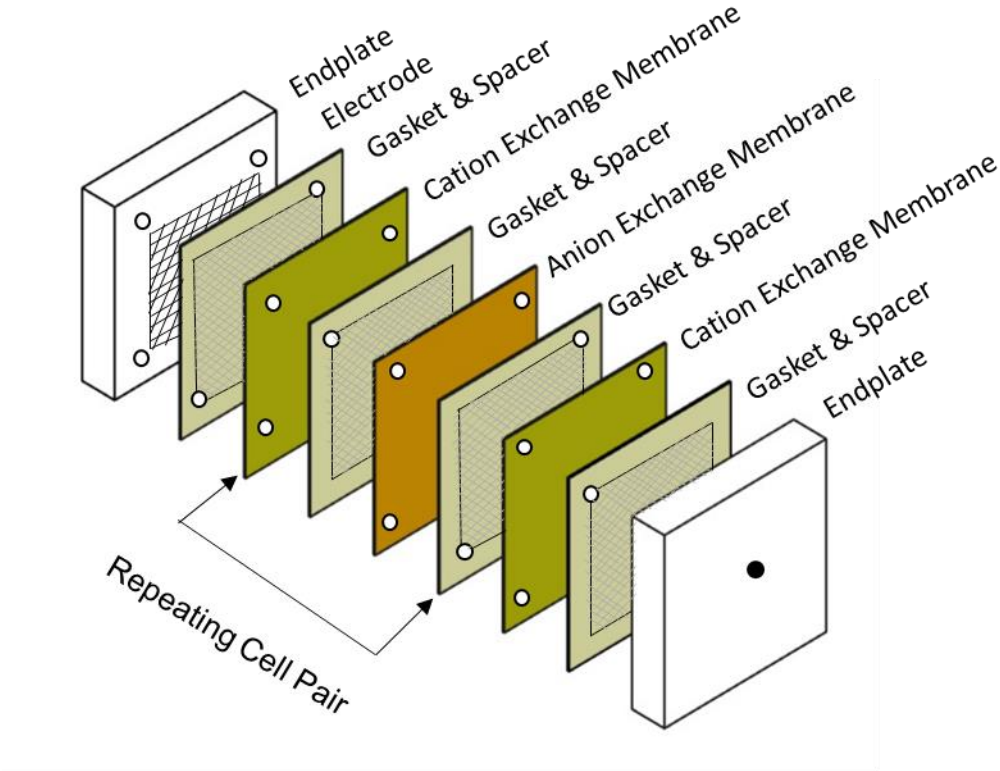

Figure 1.2. *Schematic figure of a reverse electrodialysis stack. Alternately arranged anion and cation exchange membranes are separated by gaskets and woven spacers. At each end of the stack is an endplate containing an electrode.*

Electricity is produced through the controlled mixing of two solutions with a salinity gradient through ion exchange membranes in an RED stack (Figure 1.3). A dilute saline solution and a concentrated saline solution are pumped to the stack, creating a concentration difference across each membrane. By alternately arranging anion exchange membranes, which allow only cations to pass, and cation exchange membranes, which allow only anions to pass, the movements of cations and anions in opposite directions is facilitated, creating a voltage across the stack. A reversible redox couple circulates the electrodes and converts the flow of ions to an electrical current [25]. This is the opposite process to electrodialysis, in which an electrical current is applied to move ions against the concentration gradient, removing salt to produce desalinated water [25].

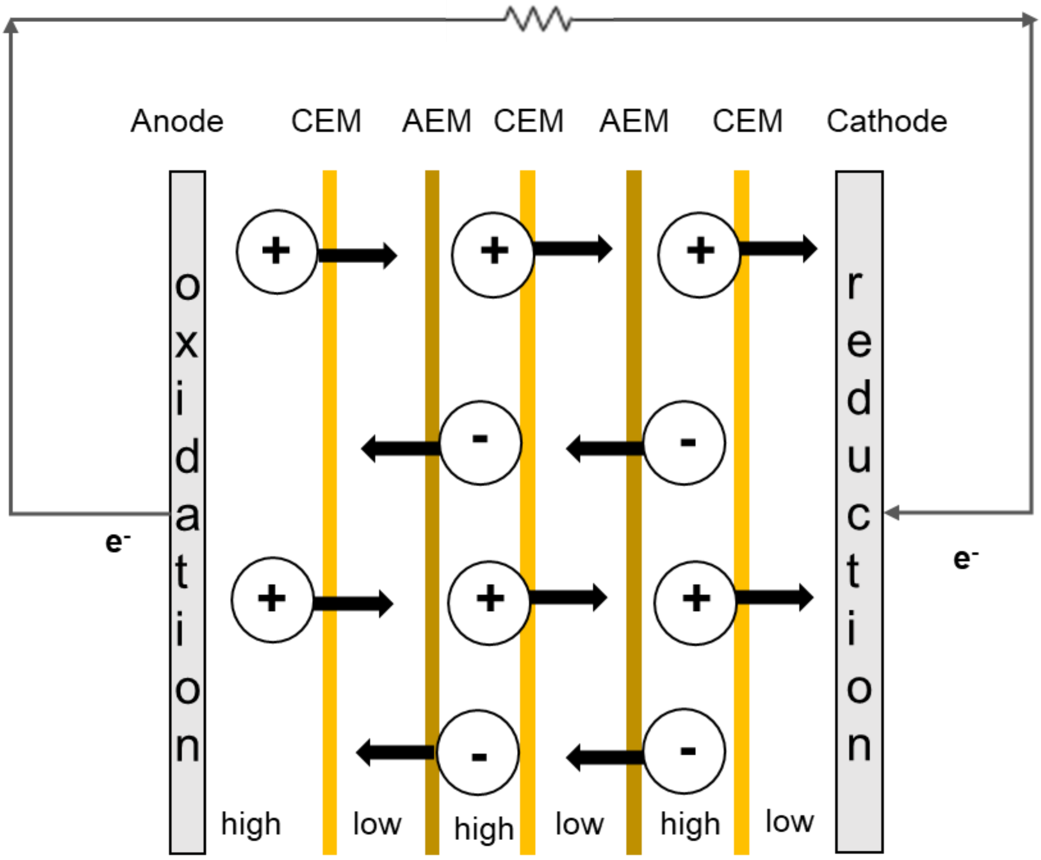

Figure 1.3. *Schematic figure of working principles of reverse electrodialysis. The high concentration and low concentration compartments create a concentration difference across each ion exchange membrane. The anion exchange membranes (AEM) allow only cations to be transported across the membranes and cation exchange membranes (CEM) allow only anions to cross the membrane, causing positive and negative ions to move in opposite directions. A reversible redox couple circulating the electrodes converts the ionic flow to an electrical current.*

A typical experimental RED set-up consists of an RED stack connected to a potentiostat, with saline solutions with a concentration gradient pumped to the stack from a dilute feed reservoir and a concentrated feed reservoir, and a reversible redox couple circulating the electrode from the electrode rinse reservoir (Figure 1.4). Placing the reservoirs on balances and measuring the inlet and outlet conductivity of feeds enables mass balances to be carried out and the temporal decline in concentration gradient to be monitored.

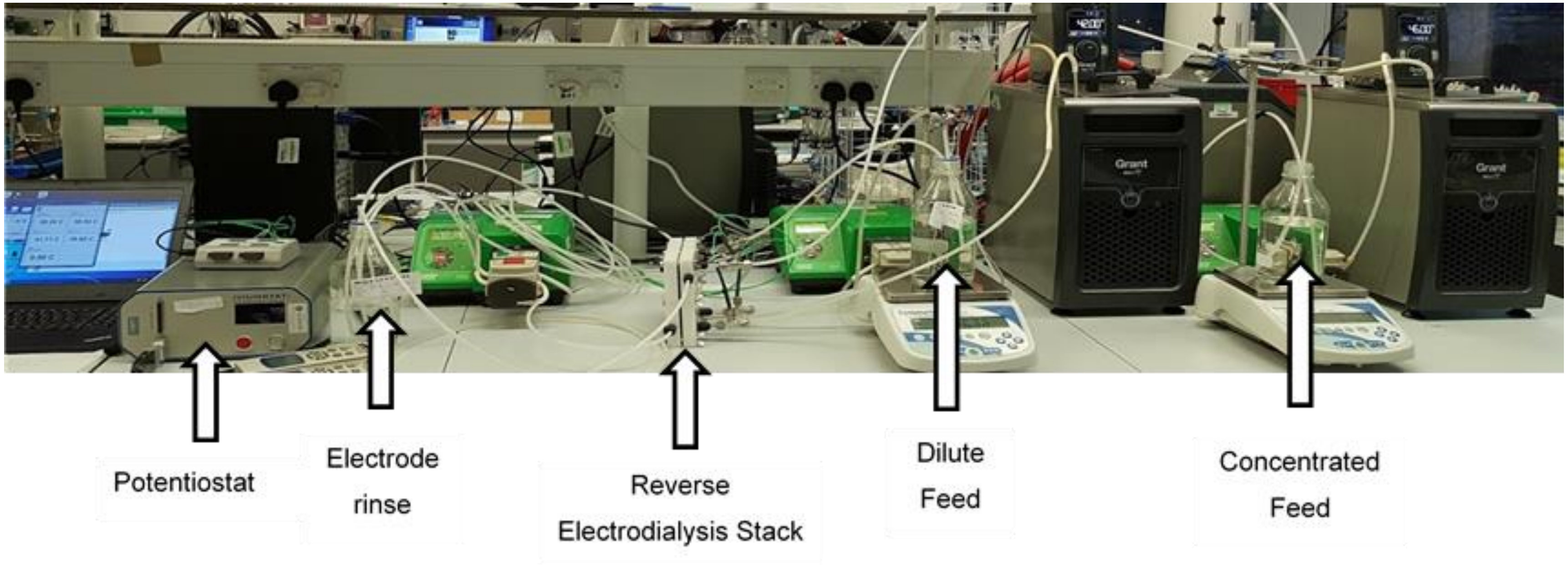

Figure 1.4. *Example of reverse electrodialysis experimental set-up. A reverse electrodialysis stack is connected to a potentiostat, with dilute and concentrated sodium chloride solutions pumped to the stack from a reservoir. An electrode rinse circulates the electrodes. Reservoirs were placed on balances and conductivity meters were fitted inline to enable mass balances to be carried out.*

Key performance parameters in reverse electrodialysis include power density and energy efficiency [22]. The maximum gross power density of an RED stack can be determined experiementally. A current-voltage curve is generated by varying the current during single pass operation and recording the cell potential. A parabolic power density curve can then be produced:

$$P_d = \frac{UI}{A} \tag{1-1}$$

where P_d is the power density (W m^{-2}), I is the current (A), U is the voltage (V) and A is the total active membrane area of the RED stack (m^2). The maximum power density is subsequently determined from the power-density curve and varies depending on process conditions including salinity gradient, flow rate and temperature, and stack features including ion exchange membranes, intermembrane distance and stack hydrodynamics [25]. Increasing the power density is critical to reduce the membrane area required for high power, and hence the unitary cost of electricity [26].

Energy efficiency is defined as the proportion of available Gibbs free energy which is converted to electricity by RED:

$$\eta_{RED} = \frac{W_{RED}}{\Delta G_{mix}} \times 100\ \% \tag{1-2}$$

where, $\eta_{RED,}$ is energy efficiency (%), W_{RED} is the work produced by RED (J) and $\triangle G_{mix}$ is the total Gibbs free energy of mixing available upon mixing two solutions with a salinity gradient (J).

These performance parameters must be maximised for RED to be viable for closed-loop applications.

1.5 Development of Reverse Electrodialysis to-date

Reverse electrodialysis was first demonstrated as a means of producing electricity from the mixing of two solutions with a salinity gradient by Pattle in 1954, achieving a maximum power density of 15 mW m^{-2} at a temperature of 39 °C [42]. In 1976, Weinstein and Leitz [43] expanded on this work, producing an experimentally validated model of RED predicting that power density up to 1.7 W m^{-2} could theoretically be achieved utilising pure NaCl solutions with an equivalent concentration to sea water and river water following development of thinner membranes and the use of thinner compartment channels. Loeb (1979) subsequently patented the reverse electrodialysis heat engine (RED-HE), proposing the integration of reverse electrodialysis with a regeneration stage such as distillation for the thermal 'unmixing' of solutions [17]. However, the low power densities achieved of up to 0.24 W m^{-2}, and the high cost of ion exchange membranes (IEMs) prevented the practical realisation of the RED-HE at this time.

Driven by the need for alternative energy sources, RED has seen a resurgence in interest over the last two decades [41]. With up to 980 GW estimated to be available from the mixing of sea and river water, RED activities were initially largely focussed on exploiting this energy source [44]. Developments in membranes and stack design have produced rapid improvements in power densities obtained using artificial NaCl feeds with an equivalent concentration to sea and river water (approximately 30 g L^{-1} and 1 g L^{-1}, respectively) [25]. In 2009, an evaluation of commercially available ion exchange membranes for RED by Veerman et al. [45], experimentally demonstrated that power density up to 1.18 W m^{-2} could be achieved using membranes with low resistance and high permselectivity. The use of thinner spacers to reduce the intermembrane distance from 0.5 mm to 0.2 mm further increased power densities using these feeds to 2.2 W m^{-2} [46]. Selection of process conditions such as flow rates and temperatures also impact on the performance of RED and have been investigated for the sea and river water matrix. Zhu et al. [47], experimentally demonstrated that net power density and energy efficiency was highest at flow rates of 20 ml min^{-1} to 50 ml min^{-1}, and modelling showed that increasing feed temperature from room temperature to 40 °C could theoretically improve power densities up to 2.75 W m^{-2} [48].

Whilst the power output using artificial sea and river water feeds has improved significantly following modifications to RED stacks and operating conditions, increased Gibbs free energy is available from mixing solutions with a larger concentration gradient, which therefore have the potential to produce even greater power densities [26]. Alternative sources of salinity including wastewater and concentrated brines have been investigated for power production by RED, however, challenges in the realisation of power production from these feed waters include the availability of freshwater and extensive pre-treatment requirements [49]. Closed-loop RED applications for energy storage and thermal to electric conversion utilise artificial saline solutions and thus enable opportunities for greater power output without these limitations. The highest power density achieved experimentally using aqueous NaCl solutions of 6.7 W m^{-2} used a 5M concentrated feed and a 0.01M dilute feed at a temperature of 40 °C [26]. However, the use of increased concentration gradients has been shown to decrease energy efficiency as the increased osmotic gradient exacerbates water transport and hence concentration polarisation [50]. Alternative aqueous salt solutions have also been investigated for RED and could theoretically produce higher power densities due to the increased Gibbs free energy which they provide [10,51]. Increased power densities of up to 8 W m^{-2} have been experimentally obtained using binary mixtures of NaCl and salts such as LiCl at room temperature [27]. However, the same challenges of increased exergy losses and decreased energy efficiency will apply when utilising these feeds for RED. For thermal to electric applications, the work produced per volume of feed is critical during RED for integration with a distillation thermal separation process [52], as the volume of water which must be evaporated determines the requirement of heat energy and hence overall system efficiency. For sea and river water feeds, recirculating or recycling feeds has been demonstrated to improve efficiency [53], however the effect of recycling feeds with a larger concentration gradient on water flux and power production over time has not previously been examined. Modifications to operating conditions such as current density and fluid flow rates could improve power density due to their dominant role in governing resistance to ionic transport. To illustrate, of the few studies that have investigated concentrated brines, the RED stacks used have been optimised for a sea/river water matrix, thus improved power densities and energy efficiencies could be obtained by modifying RED stacks for use with larger concentration gradients. Features of electrodialysis modules such as increased intermembrane distance and membrane properties such as low water permeability could be preferable over conventional RED design for these feeds.

For closed-loop RED to be practically realised, the process scale must be increased from the lab-scale [54] and an understanding of how current and voltage scale when utilising high concentration gradients is required. Vermaas et al. [55], reported that power density increased approximately linearly as cell pair number was increased for sea and river water, however it is unclear whether this relationship will hold for larger concentration gradients which exhibit increased water transport [50] and hence increased concentration polarisation, phenomena which can be hypothesised to be exacerbated by an increase in process scale. Several studies have demonstrated that the performance of RED stacks of varying dimensions can be estimated using residence time when sea/river water feeds are utilised [54,56]. Whilst RED has been demonstrated at the pilot-scale RED using a diverse range of feed waters with a salinity gradient, including sea water and river water at Afsluitdijk, the Netherlands [57]; brackish water and brines from saltworks at Trapani, Italy; and municipal wastewater and seawater at Jeju Island, Korea [58]; there have been no studies to determine how best to manage exergy losses and maximise power production when scaling-up using increased concentration gradients.

1.6 Aims and Objectives

The aim of this thesis is to experimentally demonstrate the potential of reverse electrodialysis for closed-loop applications such as the thermal to electric conversion of low-grade waste heat, by determining the preferred operating conditions and configuration for this application.

Specific objectives to meet this aim are to:

1. Determine whether feed properties, configuration and operating conditions which differ from conventional sea/river RED can increase work produced by RED from a fixed volume of solutions.
2. Identify whether RED from large concentration gradients in recycle can benefit from closer alignment to ED stack design principles by evaluating the performance of commercially available ED and RED modules, and the effect of membranes and intermembrane distance on power density and energy efficiency using these feeds.
3. Establish the scalability of RED using larger concentration gradients in recycle by determining the effect of increasing path length and cell pair number on power output and energy efficiency.

1.7 Thesis structure

The thesis objectives are addressed in three technical chapters, Chapters 2 to 4 (Figure 1.5), which have been formatted as journal articles. Chapter 2, "*Managing power dissipation in closed-loop reverse electrodialysis to maximise energy recovery during thermal to electric conversion*" determines how RED performance can be improved through selection of feed properties and operating conditions. This chapter has been published [59]. Chapter 3, "*Transitioning from electrodialysis (ED) to reverse electrodialysis (RED) stack design for energy generation from high salinity gradients in recycle*" investigates how features of ED module design such as membrane properties and intermembrane distances can be utilised in RED to minimise exergy losses and improve power production from large concentration gradients in recycle. Chapter 4 *'Scale-up of reverse electrodialysis for energy generation from high concentration salinity gradients'* establishes how to scale-up RED using concentrated brines in recycle. Chapters 3 and 4 are being submitted for publication. An overall discussion of the thesis is presented in Chapter 5. This is followed by conclusions and recommendations for further work in Chapter 6. Anna Hulme was lead author of all chapters and led experimental work. Technical chapters were edited by Professor Ewan McAdam, Dr Marc Pidou and Dr Chris Davey.

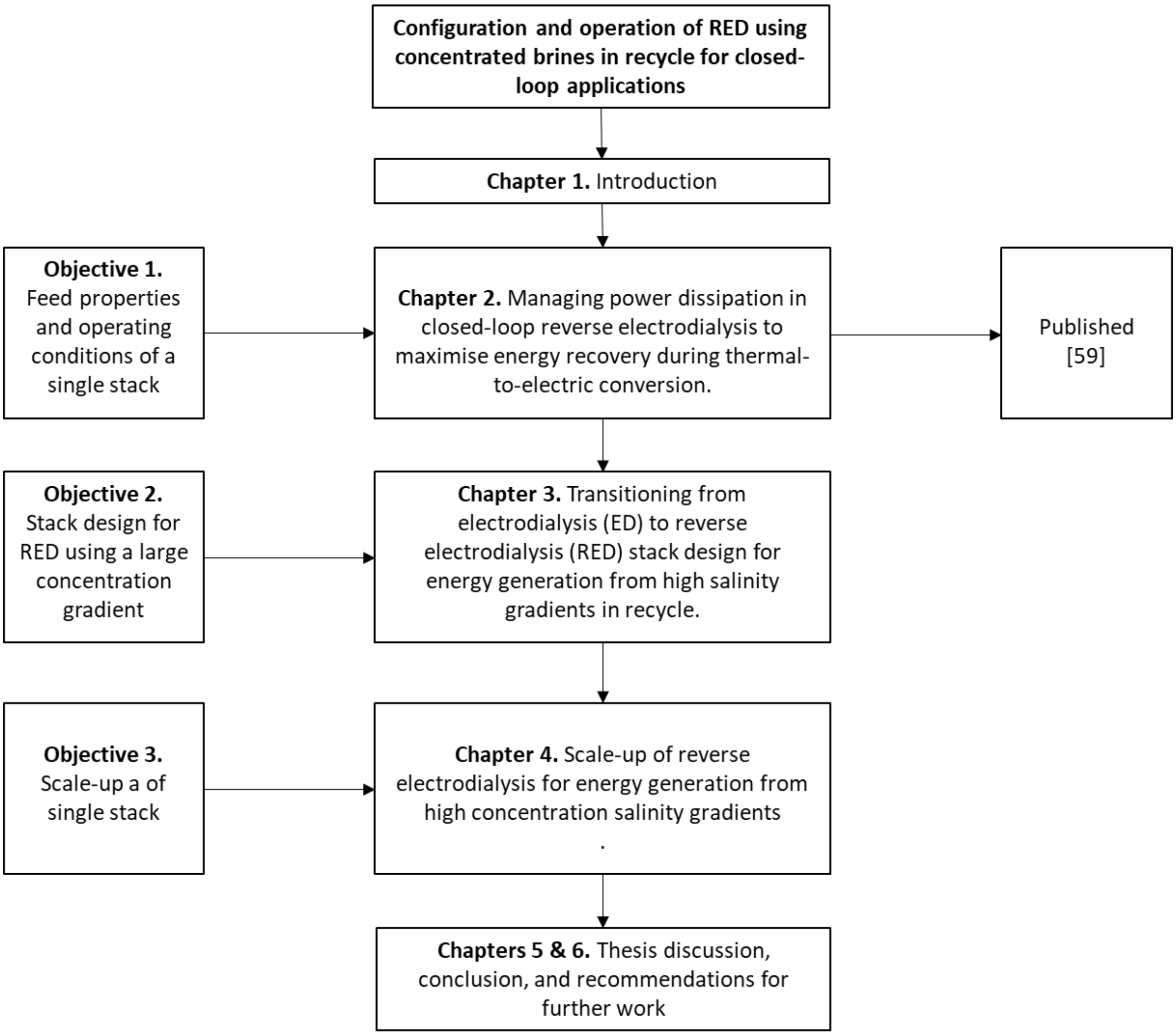

Figure 1.5. *Schematic detailing the structure of the thesis to meet the objectives.*

References

[1] J. Rogelj, D. Shindell, K. Jiang, S. Fifita, Mitigation Pathways Compatible with 1.5°C in the Context of Sustainable Development, in: Glob. Warm. 1.5°C. An IPCC Spec. Rep. Impacts Glob. Warm. 1.5°C above Pre-Industrial Levels Relat. Glob. Greenh. Gas Emiss. Pathways, Context Strength. Glob. Response to Threat Clim. Chang., IPCC, Geneva, Switzerland, 2018: pp. 93–174.

[2] International Energy Agency, World Energy Outlook 2019: Executive Summary. https://www.iea.org/reports/world-energy-outlook-2019, 2019 (accessed 7 October 2020).

[3] European Parliament, Directive 2003/87/EC of the European Parliament and of the Council of 13 October 2003 establishing a scheme for greenhouse gas emission allowance trading within the Community and amending Council Directive, 96/61/EC. Off. J. Eur. Union. 275 (2003) 33-46.

[4] National Audit Office, The Climate Change Levy and Climate Change Agreements. https://www.nao.org.uk/wp-content/uploads/2012/11/climate_change_review.pdf, 2017 (accessed 7 September 2020).

[5] European Parliament, Council of the European Union, Directive (EU) 2018/2001 of 11 December 2018 on the promotion of the use of energy from renewable sources. Off. J. Eur. Union. 328 (2018) 82-209.

[6] Department of Energy and Climate Change. Renewable Heat Incentive (RHI). https://assets.publishing.service.gov.uk/government/uploads/system/uploads/attachment_data/file/48041/1387-renewable-heat-incentive.pdf, 2011 (accessed 15 September 2020).

[7] C. Forman, I.K. Muritala, R. Pardemann, B. Meyer, Estimating the global waste heat potential, Renew. Sustain. Energy Rev. 57 (2016) 1568–1579.

[8] A. Firth, B. Zhang, A. Yang, Quantification of global waste heat and its environmental effects, Appl. Energy. 235 (2019) 1314–1334.

[9] M. Papapetrou, G. Kosmadakis, A. Cipollina, U. La Commare, G. Micale, Industrial waste heat: Estimation of the technically available resource in the EU per industrial sector, temperature level and country, Appl. Therm. Eng. 138 (2018) 207–216.

[10] A. Tamburini, M. Tedesco, A. Cipollina, G. Micale, M. Ciofalo, M. Papapetrou, W. Van Baak, A. Piacentino, Reverse electrodialysis heat engine for sustainable power production, Appl. Energy. 206 (2017) 1334–1353.

[11] H. Zhai, Q. An, L. Shi, V. Lemort, S. Quoilin, Categorization and analysis of heat sources for organic Rankine cycle systems, Renew. Sustain. Energy Rev. 64 (2016) 790–805.

[12] S. Iglesias Garcia, R. Ferreiro Garcia, J. Carbia Carril, D. Iglesias Garcia, A review of thermodynamic cycles used in low temperature recovery systems over the last two years, Renew. Sustain. Energy Rev. 81 (2018) 760–767.

[13] L. Tocci, T. Pal, I. Pesmazoglou, B. Franchetti, Small scale Organic Rankine Cycle (ORC): A techno-economic review, Energies. 10 (2017) 1–26.

[14] R. Freer, A. V. Powell, Realising the potential of thermoelectric technology: A Roadmap, J. Mater. Chem. C. 8 (2020) 441–463.

[15] M.A. Zoui, S. Bentouba, J.G. Stocholm, M. Bourouis, A review on thermoelectric generators: Progress and applications, Energies. 13 (2020) 3606.

[16] D. Champier, Thermoelectric generators: A review of applications, Energy Convers. Manag. 140 (2017) 167–181.

[17] S. Loeb, 4171409A, Method and Apparatus for Generating Power Utilizing Reverse Electrodialysis, United States Patent and Trademark Office, 1979. https://patents.google.com/patent/US4171409A/en (accessed 7 October 2020).

[18] G. Micale, A. Cipollina, A. Tamburini, Salinity gradient energy, in: A. Cipollina, G.M. Micale (Eds.), Sustain. Energy from Salin. Gradients, Woodhead Publishing, Cambridge, United Kingdom, 2016: pp. 1–17.

[19] N.Y. Yip, M. Elimelech, Comparison of energy efficiency and power density in pressure retarded osmosis and reverse electrodialysis, Environ. Sci. Technol. 48 (2014) 11002–11012.

[20] R.L. McGinnis, J.R. McCutcheon, M. Elimelech, A novel ammonia-carbon dioxide osmotic heat engine for power generation, J. Memb. Sci. 305 (2007) 13–19.

[21] A. Achilli, K.L. Hickenbottom, Pressure retarded osmosis, in: A. Cipollina, G.M. Micale (Eds.), Sustain. Energy from Salin. Gradients, Woodhead Publishing, Cambridge, United Kingdom, 2016: pp. 55–75.

[22] J.W. Post, J. Veerman, H.V.M. Hamelers, G.J.W. Euverink, S.J. Metz, K. Nymeijer, C.J.N. Buisman, Salinity-gradient power: Evaluation of pressure-retarded osmosis and reverse electrodialysis, J. Memb. Sci. 288 (2007) 218–230.

[23] K.L. Hickenbottom, J. Vanneste, L. Miller-Robbie, A. Deshmukh, M. Elimelech, M.B. Heeley, T.Y. Cath, Techno-economic assessment of a closed-loop osmotic heat engine, J. Memb. Sci. 535 (2017) 178–187.

[24] R. Kleiterp, The feasibility of a commercial osmotic power plant, MSc thesis, Delft University of Technology, 2012.

[25] J. Veerman, D.A. Vermaas, Reverse electrodialysis: Fundamentals, in: A. Cipollina, G.M. Micale (Eds.), Sustain. Energy from Salin. Gradients, Woodhead Publishing, Cambridge, United Kingdom, 2016: pp. 77–133.

[26] A. Daniilidis, D.A. Vermaas, R. Herber, K. Nijmeijer, Experimentally obtainable energy from mixing river water, seawater or brines with reverse electrodialysis, Renew. Energy. 64 (2014) 123–131.

[27] M. Micari, M. Bevacqua, A. Cipollina, A. Tamburini, W. Van Baak, T. Putts, G. Micale, Effect of different aqueous solutions of pure salts and salt mixtures in reverse electrodialysis systems for closed-loop applications, J. Memb. Sci. 551 (2018) 315–325.

[28] M. Tedesco, A. Cipollina, A. Tamburini, G. Micale, Towards 1 kW power production in a reverse electrodialysis pilot plant with saline waters and concentrated brines, J. Memb. Sci. 522 (2017) 226–236.

[29] F. Giacalone, F. Vassallo, F. Scargiali, A. Tamburini, A. Cipollina, G. Micale, The first operating thermolytic reverse electrodialysis heat engine, J. Memb. Sci. 595 (2019) 117522.

[30] D.K. Kim, C. Duan, Y.F. Chen, A. Majumdar, Power generation from concentration gradient by reverse electrodialysis in ion-selective nanochannels, Microfluid. Nanofluidics. 9 (2010) 1215–1224.

[31] K. Branker, M.J.M. Pathak, J.M. Pearce, A review of solar photovoltaic levelized cost of electricity, Renew. Sustain. Energy Rev. 15 (2011) 4470–4482.

[32] M. Papapetrou, K. Kumpavat, Environmental aspects and economics of salinity gradient power (SGP) processes, in: A. Cipollina, G.M. Micale (Eds.), Sustain. Energy from Salin. Gradients, Woodhead Publishing, Cambridge, United Kingdom, 2016: pp. 315–335.

[33] M. Bevacqua, A. Tamburini, M. Papapetrou, A. Cipollina, G. Micale, A. Piacentino, Reverse electrodialysis with NH_4CO_3-water systems for heat-to-power conversion, Energy. 137 (2017) 1293-1307.

[34] F. Giacalone, A. Tamburini, A. Cipollina, G. Micale, Reverse Electrodialysis-Multi Effect Distillation Heat Engine Fed by Lithium Chloride Solutions, Chem. Eng. Trans. 74 (2019) 787-792.

[35] P. Palenzuela, M. Micari, B. Ortega-Delgado, F. Giacalone, G. Zaragoza, D.-C.C. Alarcón-Padilla, A. Cipollina, A. Tamburini, G. Micale, Performance Analysis of a RED-MED Salinity Gradient Heat Engine, Energies. 11 (2018) 3385.

[36] R. Long, B. Li, Z. Liu, W. Liu, Hybrid membrane distillation-reverse electrodialysis electricity generation system to harvest low-grade thermal energy, J. Memb. Sci. 525 (2017) 107–115.

[37] M. Micari, A. Cipollina, F. Giacalone, G. Kosmadakis, M. Papapetrou, G. Zaragoza, G. Micale, A. Tamburini, Towards the first proof of the concept of a Reverse ElectroDialysis - Membrane Distillation Heat Engine, Desalination. 453 (2019) 77–88.

[38] C. Olkis, G. Santori, S. Brandani, An Adsorption Reverse Electrodialysis system for the generation of electricity from low-grade heat, Appl. Energy. 231 (2018) 222–234.

[39] A. Deshmukh, C. Boo, V. Karanikola, S. Lin, A.P. Straub, T. Tong, D.M. Warsinger, M. Elimelech, Membrane distillation at the water-energy nexus: Limits, opportunities, and challenges, Energy Environ. Sci. 11 (2018) 1177–1196.

[40] K.C. Ng, K. Thu, Y. Kim, A. Chakraborty, G. Amy, Adsorption desalination: An emerging low-cost thermal desalination method, Desalination. 308 (2013) 161–179.

[41] R.A. Tufa, S. Pawlowski, J. Veerman, K. Bouzek, E. Fontananova, S. Velizarov, J. Goulão, K. Nijmeijer, E. Curcio, Progress and prospects in reverse electrodialysis for salinity gradient energy conversion and storage, 225 (2018) 290–331.

[42] R. Pattle, Production of Electric Power by mixing Fresh and Salt Water in the Hydroelectric Pile, Nature. 174 (1954) 660.

[43] J. Weinstein, F. Leitz, Electric Power from Differences in Salinity: The Dialytic Battery, Science 191 (1976) 557–559.

[44] B.E. Logan, M. Elimelech, Membrane-based processes for sustainable power generation using water, Nature. 488 (2012) 313–319.

[45] J. Veerman, R.M. de Jong, M. Saakes, S.J. Metz, G.J. Harmsen, Reverse electrodialysis: Comparison of six commercial membrane pairs on the thermodynamic efficiency and power density, J. Memb. Sci. 343 (2009) 7–15.

[46] D.A. Vermaas, M. Saakes, K. Nijmeijer, Doubled power density from salinity gradients at reduced intermembrane distance, Environ. Sci. Technol. 45 (2011) 7089–7095.

[47] X. Zhu, W. He, B.E. Logan, Reducing pumping energy by using different flow rates of high and low concentration solutions in reverse electrodialysis cells, J. Memb. Sci. 486 (2015) 215–221.

[48] P. Długołęcki, A. Gambier, K. Nijmeijer, M. Wessling, Practical potential of reverse electrodialysis as process for sustainable energy generation, Environ. Sci. Technol. 43 (2009) 6888–6894.

[49] B.E. Logan, M. Elimelech, Membrane-based processes for sustainable power generation using water, Nature. 488 (2012) 313–319.

[50] F. Giacalone, P. Catrini, A. Tamburini, A. Cipollina, A. Piacentino, G. Micale, Exergy analysis of reverse electrodialysis, Energy Convers. Manag. 164 (2018) 588–602.

[51] F. Giacalone, C. Olkis, G. Santori, A. Cipollina, S. Brandani, G. Micale, Novel solutions for closed-loop reverse electrodialysis: Thermodynamic characterization and perspective analysis, Energy. 166 (2019) 674–689.

[52] J. Hu, X. Wu, Q. Leng, D. Jin, P. Wang, S. Xu, D. Wu, Multi-stage reverse electrodialysis: Strategies to harvest salinity gradient energy, Energy Convers. Manag. 183 (2019) 803–815.

[53] D.A. Vermaas, J. Veerman, N.Y. Yip, M. Elimelech, M. Saakes, K. Nijmeijer, High efficiency in energy generation from salinity gradients with reverse electrodialysis, ACS Sustain. Chem. Eng. 10 (2013) 1295–1302.

[54] J. Moreno, S. Grasman, R. Van Engelen, K. Nijmeijer, Upscaling Reverse Electrodialysis, Environ. Sci. Technol. 52 (2018) 10856–10863.

[55] J. Veerman, M. Saakes, S.J. Metz, G.J. Harmsen, Reverse electrodialysis: Performance of a stack with 50 cells on the mixing of sea and river water, J. Memb. Sci. 327 (2009) 136–144.

[56] J. Veerman, M. Saakes, S.J. Metz, G.J. Harmsen, Electrical power from sea and river water by reverse electrodialysis: A first step from the laboratory to a real power plant, Environ. Sci. Technol. 44 (2010) 9207–9212.

[57] A. Cipollina, G. Micale, A. Tamburini, M. Tedesco, L. Gurreri, J. Veerman, S. Grasman, Reverse electrodialysis: Applications, in: A. Cipollina, G.M. Micale (Eds.), Sustain. Energy from Salin. Gradients, Woodhead Publishing, Cambridge, United Kingdom, 2016: pp. 135–180.

[58] J.-Y. Nam, K.-S. Hwang, H.-C. Kim, H. Jeong, H. Kim, E. Jwa, S. Yang, J. Choi, C.-S. Kim, J.-H. Han, N. Jeong, Assessing the behavior of the feed-water constituents of a pilot-scale 1000-cell-pair reverse electrodialysis with seawater and municipal wastewater effluent, Water Res. 148 (2019) 261–271.

[59] A.M. Hulme, C.J. Davey, A. Parker, L. Williams, S. Tyrrel, Y. Jiang, M. Pidou, C. Water, B. Mk, Managing power dissipation in closed-loop reverse electrodialysis to maximise energy recovery during thermal to electric conversion, Desalination. 496 (2020) 114711.

2. Managing power dissipation in closed-loop reverse electrodialysis to maximise energy recovery during thermal to electric conversion

Managing power dissipation in closed-loop reverse electrodialysis to maximise energy recovery during thermal to electric conversion

A.M. Hulme[a], C.J. Davey[a], A. Parker[a], L. Williams[b], S. Tyrrel[a], Y. Jiang[c], M. Pidou[a], E.J. McAdam[a]*

[a]Cranfield Water Science Institute, Cranfield University, Bedfordshire, MK43 0AL, UK

[b]Centre for Creative and Competitive Design, Cranfield University, Bedfordshire, MK43 0AL, UK

[c]Centre for Thermal Energy Systems and Materials, Cranfield University, Bedfordshire, MK43 0AL, UK

*Corresponding author: e.mcadam@cranfield.ac.uk

Abstract

Whilst the efficiency of reverse electrodialysis (RED) for thermal to electrical conversion has been theoretically demonstrated for low-grade waste heat, the specific configuration and salinity required to manage power generation has been less well described. This study demonstrates that operating RED by recycling feed solutions provides the most suitable configuration for energy recovery from a fixed solution volume, providing a minimum unitary cost for energy production. For a fixed membrane area, recycling feeds achieves energy efficiency seven times higher than single pass (conventional operation), and with an improved power density. However, ionic transport, water flux and concentration polarisation introduce complex temporal effects when concentrated brines are recirculated, that are not ordinarily encountered in single pass systems. Regeneration of the concentration gradient at around 80 % energy dissipation was deemed most economically pragmatic, due to the increased resistance to mass transport beyond this threshold. However, this leads to significant exergy destruction that could be improved by interventions to better control ionic build up in the dilute feed. Further improvements to energy efficiency were fostered through optimising current density for each brine concentration independently. Whilst energy efficiency was greatest at lower brine concentrations, the work produced from a fixed volume of feed solution was greatest at higher saline concentrations. Since the thermal to electrical conversion proposed is governed by volumetric heat utilisation (distillation to reset the concentration gradient), higher brine concentrations are therefore recommended to improve total system efficiency. Importantly, this study provides new evidence for the configuration and boundary conditions required to realise RED as a practical solution for application to sources of low-grade waste heat.

Keywords: distillation, closed-loop, recycle, heat engine, salinity gradient energy, brine concentrate

2.1 Introduction

Approximately 20 % of the world's population are without power, due to the absence of networked electricity, and the fragility of existing power grids, resulting in frequent large-scale power outages, particularly in low-income countries [1–3]. Conversely, waste heat energy is abundant, estimated to be equivalent to 246 PJ globally [4]. Thermal to electric conversion of this waste heat could provide a reliable source of off-grid power for small-scale applications. However, 63 % of this energy source is classified as low-grade heat below 100 °C [4]. Conventional thermal to electric technologies, such as the Organic Rankine Cycle (ORC), are unsuitable for the conversion of low-grade heat as Carnot efficiency is directly proportional to the hot source temperature [5]. Furthermore, the specific cost per kW of small-scale ORCs in the range of 1 kW – 100 kW is prohibitively high [6]. Thermoelectric generators have recently been proposed for applications to transportation and manufacturing sectors, however widespread use is similarly hindered by high cost and low efficiency (<10 %) [7].

In a reverse electrodialysis – membrane distillation heat engine, waste heat is utilised for the thermal separation of salt and water to produce two feeds with differing salinities [8]. The Gibbs free energy released by mixing solutions with a concentration gradient is then harnessed by reverse electrodialysis (RED) to produce power (Figure 2.1).

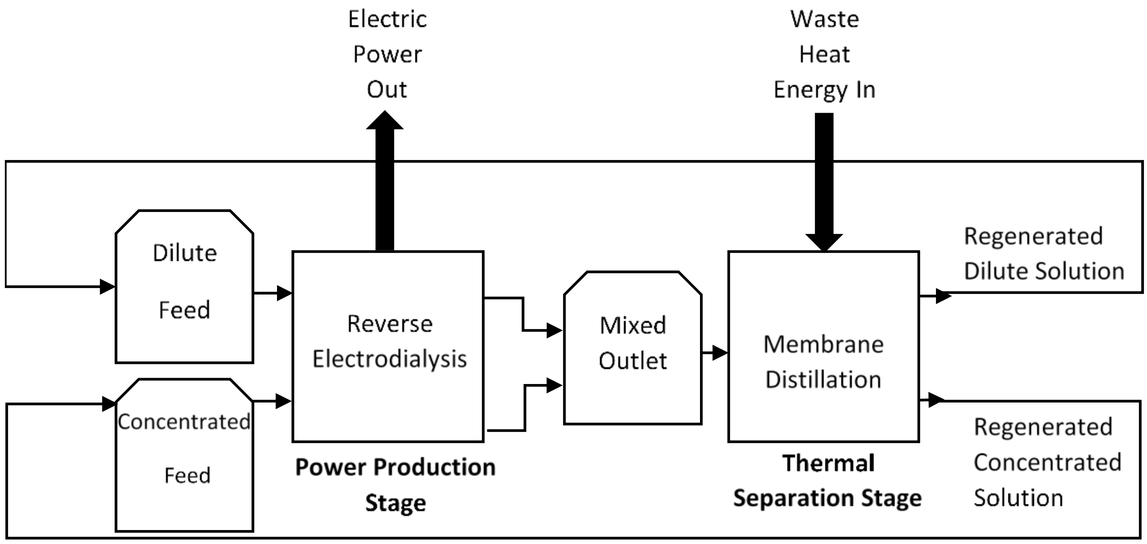

Figure 2.1. *Diagram illustrating the principles of a reverse electrodialysis heat engine. Waste heat is utilised in the thermal separation stage to regenerate two solutions with differing salinities. These solutions are subsequently used to produce power by reverse electrodialysis.*

The proposed heat engine can theoretically achieve high energy efficiency of up to 85 % [8]. Overall heat engine efficiency depends on both the thermal efficiency of solvent regeneration, and on maximising the Gibbs free energy which is recovered for power production. It has been theoretically demonstrated that membrane distillation (MD) can achieve exceptionally high 'gain output ratios', indicating substantial latent heat utilisation efficiency [9]. For small-scale applications of <1000 m^3 day^{-1}, MD outperforms alternative thermal separation stages such as multi-effect distillation in terms of energy consumption and gain output ratio [9]. Power production by RED has also been demonstrated to be scalable, from nano-scale and micro-fluidic applications [10] to large-scale (1 kW) pilot plants [11]. In an RED stack, anion and cation exchange membranes are alternately placed between two electrodes, creating concentrated and dilute compartments that initiate a concentration gradient driving ionic transport, where the separation of anions and cations is mediated by the membranes applied. An electrode rinse solution circulating at the electrode then converts ionic transport to an electric current [12]. Typically, RED applications have exploited naturally occurring feeds such as seawater and river water for power production, however, several critical differences must be considered when adapting RED for thermal to electric applications.

Initial RED research focussed on large-scale power production using seawater and river water. Following optimisation of stack design and operating conditions, power densities up to 2.2 W m^{-2} have been obtained using these feeds at ambient temperature [13]. The addition of a separation stage to restore the concentration gradient from the mixed RED effluent - enabling cyclic depletion and regeneration of the salinity gradient in a 'closed-loop' - has subsequently been investigated, with potential applications in energy storage and thermal to electric conversion. In the case of thermal to electric RED, the key distinction is that the working solution volume is fixed by the availability of heat energy to regenerate solution and restore the salinity gradient. The criticality is therefore to maximise the total power output from this fixed volume of solution prior to regeneration [14,15]. In contrast to conventional RED using naturally occurring saline feeds, the utilisation of pure artificial solutions in closed-loop RED minimises the likelihood of membrane fouling due to an absence of co-ions and impurities entering the system, in addition to enabling the selection of optimal fluid properties and operating conditions [8]. The available Gibbs free energy in a limited feed volume can therefore be increased by using a larger salinity gradient or alternative aqueous salt solutions. Consequently, a range of high solubility salts such as lithium bromide have been investigated for closed-loop RED and theoretically demonstrated to produce high overall system efficiency [8,15]. Regardless of the salt selected, power dissipation from a limited volume of working solution must be managed for closed-loop RED applications. In this work, sodium chloride is used as an example to determine how energy recovery from a fixed volume can be maximised. High power densities up to 6.7 W m^{-2} have been experimentally demonstrated using NaCl at high concentration and increased feed temperatures [17]. However, RED performance from a finite volume is a trade-off between power density and energy efficiency [18]. Energy efficiency is defined as the proportion of Gibbs free energy recovered for power production. Recycling feeds (i.e. reusing the feeds) increases the energy efficiency compared to typical single pass operation, without requiring a greater membrane area [14,17]. However, power densities decrease over time as exergy is lost from the system [14]. Management of exergy destruction is therefore paramount for overall system efficiency. Despite this, few studies have considered operating RED in recycle, or the effect of operating conditions and fluid properties on resulting exergy losses within the system.

Van Egmond et al. [14], investigated the effect of current density and temperature on the efficiency of an RED battery which is regenerated by electrodialysis. However, low efficiency in the electrodialysis charging stage (analogous to solution regeneration) limited the working domain to relatively low concentration gradients. In an RED heat engine, thermal separation by MD can be used to produce larger concentration gradients but it is unclear whether use of these feeds will benefit closed-loop performance. Daniilidis et al. [17], experimentally determined the energy efficiency and total work obtained by recirculating feeds across a range of concentrations but neglected to consider the impact of operating conditions such as flow rate and current density. Giacalone et al. [18] modelled sources of exergy loss in RED but did not examine the effect of feed temperature.

This work aims to determine how to manage discharge in closed-loop RED, by establishing boundary conditions which maximise the electrochemical potential harnessed for power production, whilst minimising exergy losses for high overall system efficiency in RED for thermal to electric applications. Specific objectives are to: (i) Benchmark the system in single pass, to characterise power density and open circuit voltage at maximum concentration gradient; (ii) Compare RED operation in single pass and recycle at different fluid velocities, to establish the trade-off between power density and energy efficiency, and identify for the first time the process conditions and preferred configuration to minimise exergy destruction and enable high energy efficiency; (iii) Examine power dissipation with a fixed volume in recycle, to identify the threshold for initiating thermal regeneration to maximise efficiency due to the limiting return on energy recovered; (iv) Determine the effect of sensible heat retention from thermal regeneration on the performance of RED in recycle.

2.2 Materials and Methods

2.2.1 Experimental setup for reverse electrodialysis stack

A custom-made 5 cell-pair reverse electrodialysis stack was used. Neosepta AMX and CMX (Eurodia Industrie SA, Pertuis, France) ion exchange membranes with an active area of 10 cm x 10 cm were alternately stacked. Nylon woven spacers (SEFAR, Heiden, Switzerland) and silicon gaskets (Silex Silicones Ltd, Hampshire, UK) with a thickness of 0.3 mm separated the membranes. An extra cation exchange membrane sealed the electrode rinse compartment. Titanium mesh electrodes coated with a Ru/Ir mixed metal oxide with dimensions of 10 cm x 10 cm (MAGNETO special anodes, Schiedam, The Netherlands) were fixed inside each custom-made acetal endplate (Model Products LT, Bedfordshire, UK). The cell was bolted closed through the endplates. Peristaltic pumps fed the feed and electrode rinse solutions to the stack (Watson Marlow, Cornwall, UK). Feed temperature was controlled using refrigerated heating circulating baths (Model LT ecocool 150, Grant Instruments Cambridge Ltd, Cambridgeshire, UK). All tubes were insulated using nitrile rubber pipe insulation (Thick Kaiflex ST Class O, Pipelagging, Manchester UK). Four conductivity meters (2 CDH-SD1, Omega Engineering Limited, Manchester, UK and 2 Mettler Toledo Seven2Go Pro S7, Wolf Laboratories, York, UK) were fitted inline on the stack inlets and outlets. The feed reservoirs were each placed on a precision top loading balance (Model 4202E PT, Cole-Parmer Instrument Company, London, UK). This enabled a mass balance to be carried out and water transport within the stack to be quantified. Initial experiments were carried out in single pass to determine optimal operating conditions. Feed flow rates were varied from 5 ml min^{-1} to 200 ml min^{-1} using peristaltic pumps (Watson Marlow, Cornwall, UK). Feed temperature was increased from 10 ^{o}C to 50 ^{o}C, to determine the effect on stack performance. To maximise energy efficiency, 250 g of each feed was continuously recycled through the stack.

2.2.2 Preparation of solutions

Aqueous sodium chloride solutions were prepared using 99 % NaCl (Alfa-Aesar, Lancashire, UK) and deionised water. Solutions of concentration 0M, 0.005M, 0.01M, 0.02M, 0.04M, 0.08M, and 0.16M were prepared for the dilute feed and 0.5M, 1M, 2M, 3M, 4M, 5M and a saturated solution prepared for the concentrated feed. A 1 litre volume of electrode rinse was circulated through the stack at 200 ml min^{-1}. The electrode rinse solution contained 0.1M $K_3Fe(CN)_6$, 0.1M $K_4Fe(CN)_6$ (Fisher Scientific, Leicestershire, UK) and NaCl (Alfa-Aesar, Lancashire, UK). A NaCl concentration halfway between the concentrated and dilute concentrations was used to minimise salt and water transport between the feeds and electrode rinse.

2.2.3 Electrochemical Measurements

Electrochemical measurements were made using a potentiostat (IviumStat.h, Alvatek, UK) and data was logged using IviumSoft (IviumStat.h, Alvatek, UK). Prior to running a test, feed solutions were pumped through the stack until a stable (< 0.01 V s^{-1}) open circuit voltage (OCV) was obtained, indicating steady-state. All experiments were carried out at least three times and reported as mean, with error bars indicating standard deviation. In the single pass experiments, linear sweeps were carried out in galvanostatic mode, with current increased in steps of 2×10^{-3} A s^{-1} to determine the cell potential, maximum current and maximum power density. The power density, P_d, (W m^{-2}) at time t is defined as the power produced per membrane area and can be calculated as follows:

$$P_d = \frac{UI}{A} \qquad \textbf{(2-1)}$$

where I is the current (A), U is the voltage (V) produced by the stack and A is the total active membrane area (m^2).

To determine energy efficiency, a constant current was drawn until no more work was produced at 0 V. The current was varied to determine its effect on energy efficiency at each salinity gradient. The total work which is produced by reverse electrodialysis can be determined:

$$W_{RED} = \sum_{t_o}^{t_{end}} UI \triangle t \qquad \textbf{(2-2)}$$

where $\triangle t$ is the time interval (s), t_o and t_{end} are the times at which work produced by RED started and ended, respectively [17].

The theoretical Gibbs free energy of mixing, $\triangle G_{mix}$, available if total mixing of the two solutions occurs is calculated using the Gibbs equation:

$$\Delta G_{mix} = \Delta G_m - (\Delta G_c + \Delta G_d) \qquad \textbf{(2-3)}$$

where $\triangle G$ is the Gibbs energy (J) with the subscripts m, c and d denoting the mixed outlet stream, the concentrated and dilute feeds, respectively. Assuming the solutions are ideal:

$$\Delta G_{mix} = -(N_c + N_d)T\Delta S_m - (-N_cT\Delta S_c - N_dT\Delta S_d) \qquad \textbf{(2-4)}$$

where N is the number of moles (mol), T is the temperature (K) and $\triangle S$ is the molar entropy (J K^{-1} mol^{-1}) which can be calculated from:

$$\Delta S = -R \sum_i x_i \ln x_i \quad \textbf{(2-5)}$$

where R is the universal gas constant (8.314 J mol^{-1} K^{-1}), x is the mole fraction of species i. The energy efficiency η_{RED}, (%) can then be determined as the ratio of the work produced, $W_{RED,}$ to the theoretical Gibbs energy, ΔG_{mix} [20]:

$$\eta_{RED} = \frac{W_{RED}}{\Delta G_{mix}} \times 100\,\% \quad \textbf{(2-6)}$$

2.3 Results and discussion

2.3.1 Large concentration gradients required for high power density in single pass

To evidence the maximum achievable power density for the RED stack which comprised a fixed membrane area, evaluation was conducted in single pass (i.e. no reuse of feed), as this excludes the cumulative exergetic loss imposed by recycling the feed. Standard salt solutions with NaCl concentrations equivalent to sea and river water, 0.51M and 0.02M, respectively, were initially used to benchmark with literature. Dilute and concentrated feeds were pumped to the cell at equal flow rates of 20 ml min^{-1}. Experiments were then repeated at 200 ml min^{-1} to ensure flow rate did not limit performance due to the development of concentration polarisation. Open circuit voltage (OCV) is the voltage produced by the system at 0 A and is a measure of the electrochemical potential difference across the RED stack. An OCV of 0.73 V to 0.75 V was obtained for sea/river water feeds (Figure 2.2A), which compares well to the theoretical OCV of 0.77 V. This demonstrates high membrane permselectivity of 94 % to 97 %, calculated from the ratio of the measured electrochemical potential to theoretical electrochemical potential [10]. Maximum power densities of 0.64 W m^{-2} at 20 ml min^{-1} and 0.67 W m^{-2} at 200 ml min^{-1} were obtained at the same conditions (Figure 2.2B), falling in the range of 0.59 W m^{-2} - 0.87 W m^{-2} expected from the literature for comparable systems using the same ion exchange membranes and electrodes at a range of compartment widths [13].

As the concentrated feed concentration was increased from 0.51M to saturation at a fixed 0.02M dilute feed, OCV increased up to 1.0 V at 20 ml min^{-1} and 1.2 V at 200 ml min^{-1} compared to a theoretical OCV of 1.4 V (Figure 2.2A). Power densities approximately tripled to 1.79 W m^{-2} at 4M (Figure 2.2B). Large concentration gradients expectedly lead to improved voltages and power densities, due to the corresponding increase in Gibbs free energy available [17,21]. However, power density decreased as the concentration approached saturation. Similarly, Zhu et al [21] established a peak in power density at 3.6M. Conversely, Daniilidis et al. [17] reported the highest power density in the literature using 5M and 0.01M feeds at high temperature. This difference can be attributed to membrane ion exchange capacity [21]. Increasing the flow rate to 200 ml min^{-1} increased power density by 23 % to 2.33 W m^{-2}, due to the reduction in concentration polarisation at high flow rates [22]. As the dilute feed concentration was increased from 0 M – 0.15M at a fixed 4M concentrated feed, OCV halved from 1.5 V to 0.65 V at 200 ml min^{-1} (Figure 2.2C). This dramatic reduction in OCV following a small change in concentration demonstrates the increased sensitivity of the OCV to the dilute feed concentration in comparison to the concentrated feed and highlights the importance of maintaining a low dilute feed concentration. Maximum power densities peaked at a dilute feed concentration of 0.02M and decreased with further increases to the dilute concentration. Membrane, solution, and spacer resistances dominate at lower dilute feed concentration; however, these resistances decrease as the concentration of salt and hence ion conductivity is increased [17,21]. Above an optimal concentration, the benefit of reduced resistances is outweighed by the reduction in salinity gradient which limits power density [21]. Previous studies have similarly identified an optimal concentration of 0.005 - 0.02M for the dilute feed [10]. The concentration gradient is the most significant factor governing achievable power density in single pass; increased power being achieved when complemented with an increased flow rate to reduce stack resistance and concentration polarisation effects.

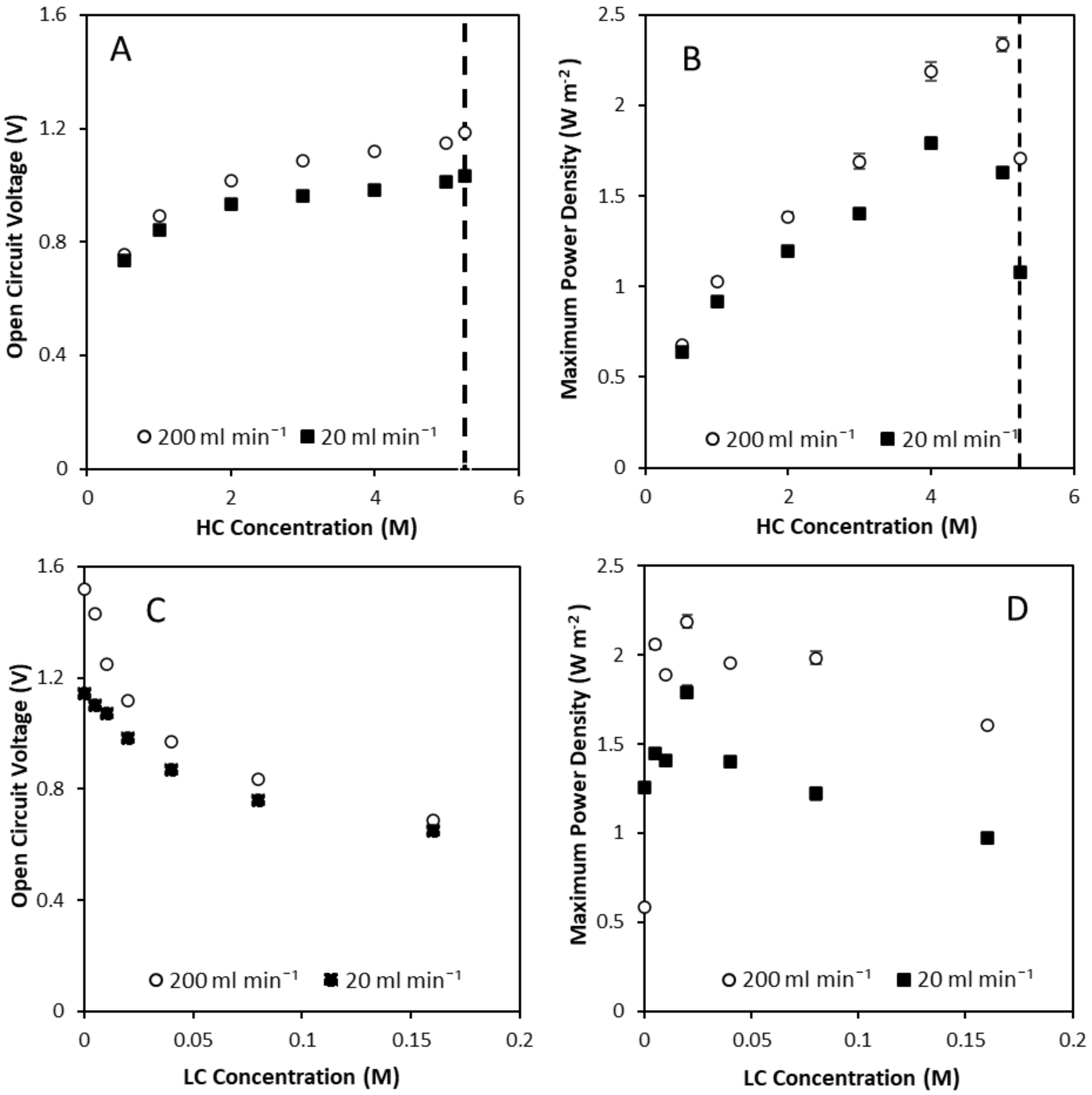

Figure 2.2. *Effect of varying concentrated feed concentration with the dilute concentration fixed at 0.02M on (A) open circuit voltage, and (B) maximum power density. Dilute feed concentration was then varied at a fixed 4M concentrated feed on (C) open circuit voltage and (D) maximum power density. Galvanostatic sweeps were carried out in single pass (25 °C; Q_d/Q_c = 1). Error bars represent the standard deviation of a triplicate. Dashed line in A and B shows the solubility limit of NaCl at the reference temperature.*

2.3.2 Recycling feeds maximises energy efficiency from a fixed volume

In single pass operation, increasing the flow rate of both feeds simultaneously from 0.06 cm s^{-1} to 0.55 cm s^{-1} caused OCV to increase from 0.8 V to 1.1 V, approaching the theoretical OCV of 1.3 V (Figure 2.3A). Power density also increased up to a maximum of 2.1 W m^{-2} at 0.55 cm s^{-1} due to reduced concentration polarisation at increased flow rates [23,24]. The reduction in residence time is also likely to reduce exergy loss due to water and salt flux, further improving power density. Further increases to fluid velocity above 0.55 cm s^{-1} provided no additional benefit to power density or OCV, as concentration polarisation is minimised. Similarly, Tedesco et al. [25] determined an optimal velocity of 1 cm s^{-1} for concentrated brines (5M and 0.5M), above which net power density reduces significantly.

Power density is initially constant in single pass when the feed volume is fixed and is subsequently followed by a dissipation in power output, corresponding to the exhaustion of the available feed. Therefore, increasing the residence time through a reduction in velocity increases the duration of constant power production, but at significantly reduced power densities (Figure 2.3B). For example, energy efficiency improved from 0.5 % to 3 % as fluid velocity was decreased from 2.2 cm s^{-1} to 0.06 cm s^{-1} (Figure 2.3D). However, a significant residual concentration gradient of 3M remained after a single pass (Figure 2.3C). RED heat engine efficiency is dependent on both the energy recovered for power production by RED, and the efficiency of thermal regeneration. A residual concentration gradient between the streams exiting the RED stack represents unused electrochemical potential. Therefore, remixing these solutions prior to thermal regeneration represents an exergetic destruction, and maximum utilisation of the concentration gradient prior to thermal regeneration is critical for overall system efficiency.

By recycling the feeds continuously, a similar maximum power density to single pass at an equivalent velocity was achieved (P_d, 0.8 W m^{-2}; 2.2 cm s^{-1}), and sustained for an order of magnitude longer, before a slow decline in power density is observed. This latter region enabled further energy recovery, but at a lower specific power output. The residual salinity gradient was reduced to less than 1M, enabling energy efficiency of 18 % to be obtained (Figure 2.3D). This demonstrates that for a stack of equivalent membrane surface area, exergy destruction is best managed under recycle. In single pass, maximum energy efficiency is obtained at the lowest flow rate, as this extends residence time, which improves the utilisation of the concentration gradient. However, this reduction in velocity increases concentration polarisation and lowers power density. To illustrate, a power density of 0.4 W m^{-2} was obtained at 0.06 cm s^{-1}, equating to 3 % efficiency but half the power density achieved at 2.2 cm s^{-1}. Whilst doubling the membrane area at 0.06 cm s^{-1} in single pass could deliver an equivalency in power output, this would increase the unitary energy cost (€ kWh^{-1}) due to the capital investment. Furthermore, increased concentration polarisation at reduced flow rates would inevitably prevent energy efficiency equivalent to recycle from being obtained. Alternatively, equivalent energy efficiency to recycle could be achieved in single pass at an equivalent velocity (Figure 2.3B, 2.2 cm s^{-1}) through multiple stacks in series. Whilst delivering a higher absolute power output, this would also increase the unitary cost for energy production. Therefore, when scaling up RED for thermal to electrical applications, recycling feeds provides the most capitally efficient option for power production, through better governance over energy dissipation.

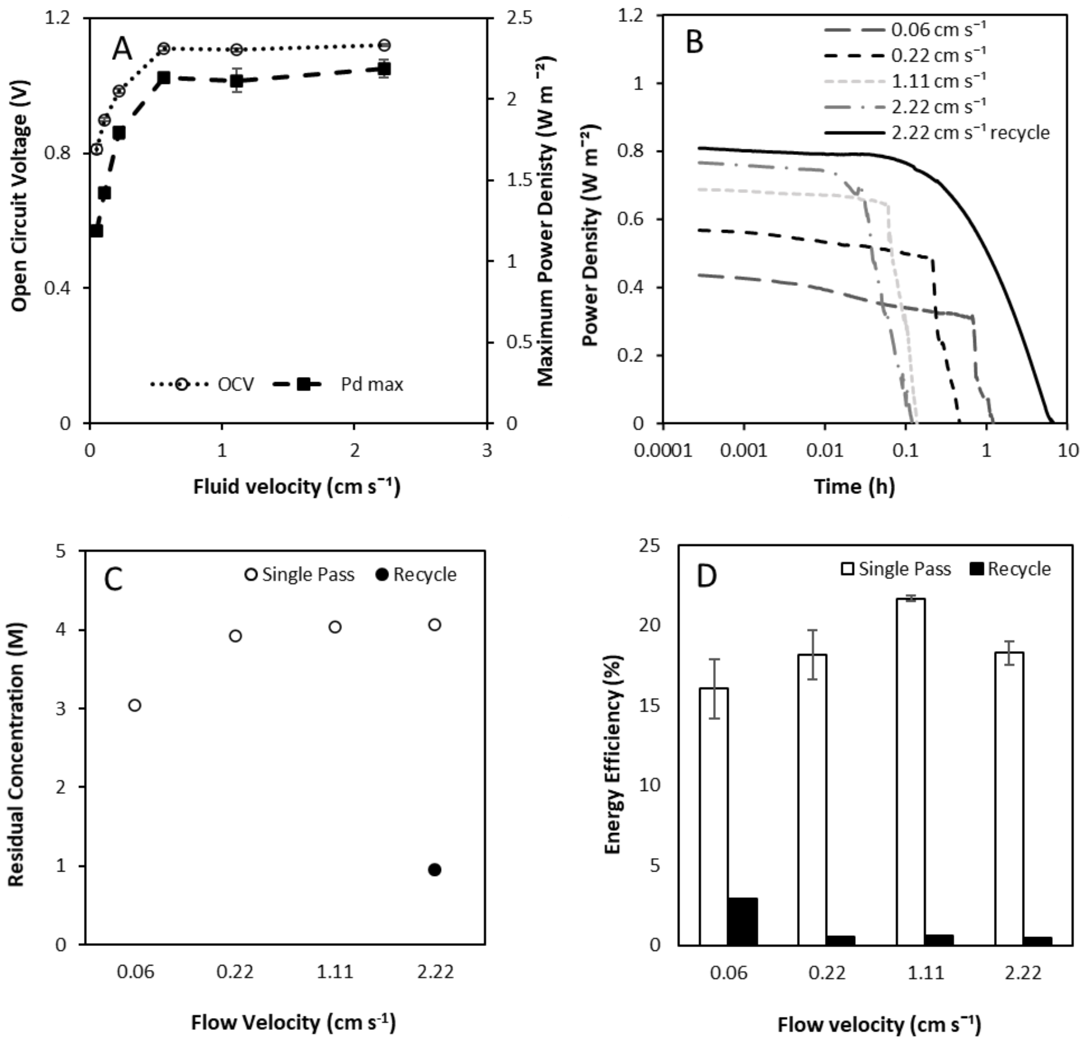

Figure 2.3. *(A) Effect of fluid velocity in single pass on open circuit voltage and maximum power density with an excess of 4M and 0.02M feeds in single pass at 25°C. (B) Power density over time from a fixed feed volume in single pass and recycle. (C) Residual outlet concentration gradient from a fixed feed volume in single pass and recycle. (D) Effect of fluid velocity on energy efficiency from 250 g of 4M and 0.02M at 25 °C in single pass and recycle.*

Varying the flow rate in recycle had little effect on performance; a plateau in maximum energy efficiency of 18 % to 21 % was obtained above a fluid velocity of 0.56 cm s^{-1} (Figure 2.3D). We propose the relative insensitivity to flow rate in recycle, when compared to single pass (Figure 2.2A) was due to increase ionic migration into the dilute feed which presents the primary resistance to power production. However, there is a temporal limit to be observed between sustaining power density above a set threshold, whilst seeking to minimise the unused electrochemical potential when operating in recycle (Figure 2.4). Specifically, as the number of retention times increases, energy efficiency in recycle can be described in two stages: (i) a proportonal increase in work (J kg^{-1}) with time whilst high power densities are sustained, followed by (ii) a subsequent rapid decline in work produced (Figure 2.4A). Power densities decrease over time as exergy losses due to resistance, water transport and co-ion transport contribute to a dynamic concentration gradient (Figure 2.4B) [14]. After approximately 4 hours, the cumulative energy efficiency was observed to plateau. To maximise the return on investment in heat engine applications, it is therefore prudent to regenerate solutions to re-establish the salinity gradient at the intersection of these two regions, equivalent to around 80 % of the maximum work available. However, the residual 2M concentration gradient at this threshold represents substantial electrochemical potential, which in single pass could deliver a power density exceeding 1 W m^{-2} at the same concentration gradient (Figure 2.2). This can be explained by the more complex boundary layer phenomenon which develops across channel length [24] over time in recycle. In contrast to single pass, where the dilute feed was fixed at 0.02M, in recycle the concentration of the dilute feed has progressively increased to 1M (Figure 2.4B). At this concentration, we can infer that concentration polarisation has developed on the dilute and concentrated feed sides due to simultaneous ionic transport and water flux, and the dynamic temporal shift in these phenomena, with the attributable resistance inhibiting power production. Therefore, management of the dilute concentration is critical for energy efficiency in RED for thermal to electric conversion.

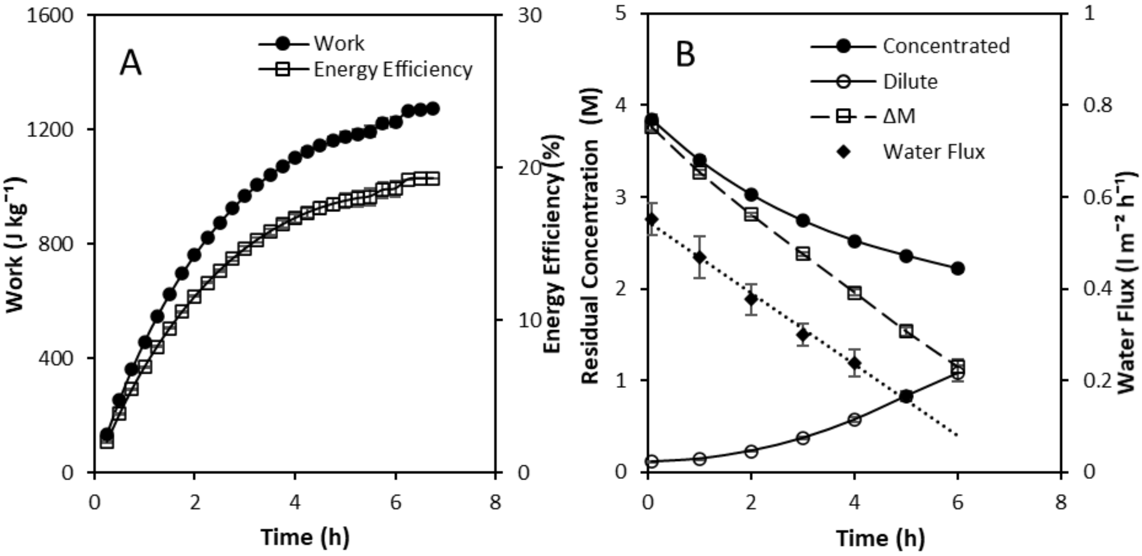

Figure 2.4. *(A) Energy efficiency and work recovered over time, and (B) water flux and feed concentration profile over time from 250 g of 4M and 250 g of 0.02M in recycle. Feed flow rate, 200 ml min^{-1}; feed temperature, 25 °C; current, 100 mA.*

2.3.3 Large salinity gradients improve total work produced from a fixed volume at optimised current density

For an RED-MD heat engine, the availability of waste heat determines the total feed volume which can be regenerated. Therefore, the work produced per volume of feed solution is an important performance parameter for closed-loop RED. The available Gibbs free energy in the fixed volume can be increased by using a larger salinity gradient. However, increasing the concentration gradient also increases the driving force for exergy losses from salt and water transport [19]. It must therefore be determined whether the increased potential energy established in the system using larger salinity gradients results in greater total work produced. At a 0.5M concentrated feed concentration, equivalent to seawater, an energy efficiency of 43 % was obtained at an optimised current density of 5 A m^{-2} (Figure 2.5). For comparison, at the equivalent current density (5 A m^{-2}), the energy efficiency at 2M concentrated feed concentration was 21 %. Daniilidis et al. [17] similarly determined that the highest energy efficiencies were obtained at low concentration gradients. The same author reported a maximum total recovered energy of approximately 300 J kg^{-1} of feed solution at 2.5M concentrated feed; recovered energy then decreased as the concentrated feed concentration was increased further. However this was carried out at a fixed current density, whereas, an enhancement in energy efficiency was observed in this study, through identification of optimal current density, which increased as the salinity gradient increased (Figure 2.5A), the final maximum energy efficiencies being equal to 31 % and 18% for 2M and 4M, respectively. Whilst maximum energy efficiencies were below those identified at 0.5M (work 456 J kg^{-1}), increasing the concentration gradient vastly increased the total work produced from a fixed volume, to 1086 J kg^{-1} and 1206 J kg^{-1} for 2M and 4M, respectively (Figure 2.5B) and facilitated higher power densities (Figure 2.6). However, above this optimum current density, the work produced per volume vastly reduces, which can be accounted for by the limited time available for power dissipation (Figure 2.6). As such, despite the lower overall efficiency, large concentration gradients at optimised current densities are preferable for high power applications, due to the increased work available from the fixed solution volume. The difference in work provided by an increase from 2 to 4M was not linear, which should be considered in the integrated RED-MD system, since the higher salinity gradient will reduce the vapour pressure, and therefore impact upon the thermal efficiency of MD, unless consideration has been given in the design.

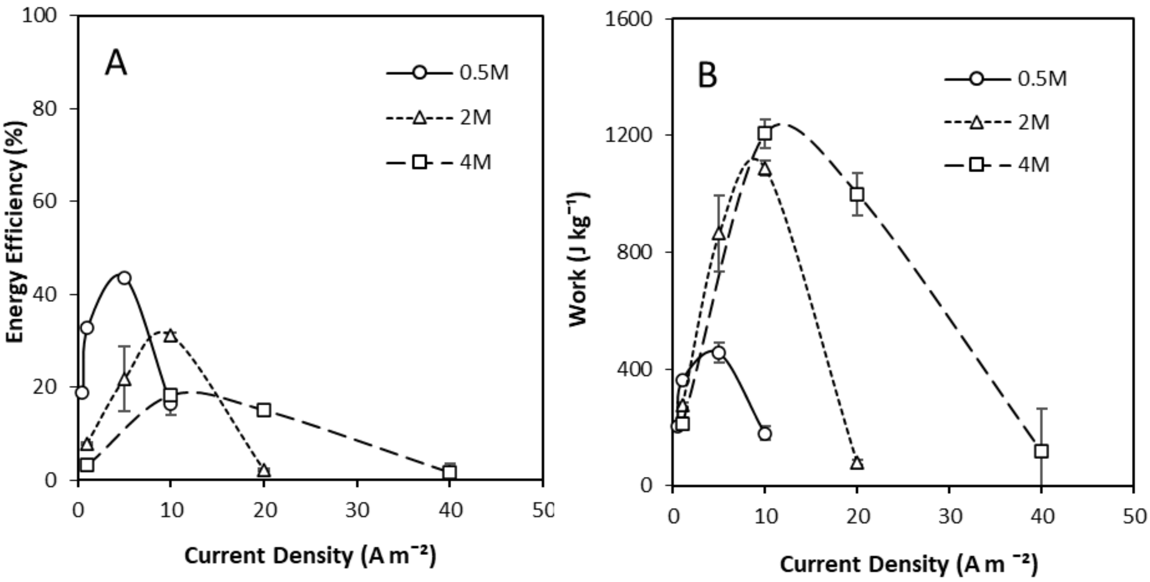

Figure 2.5. *Effect of feed concentration and current density on: (A) energy efficiency; and (B) total work obtained from dilute and concentrated feeds in recycle. Feed flow rate, 200 ml min^{-1}; feed temperature, 25 °C; solution mass, 250 g; dilute concentration, 0.02M.*

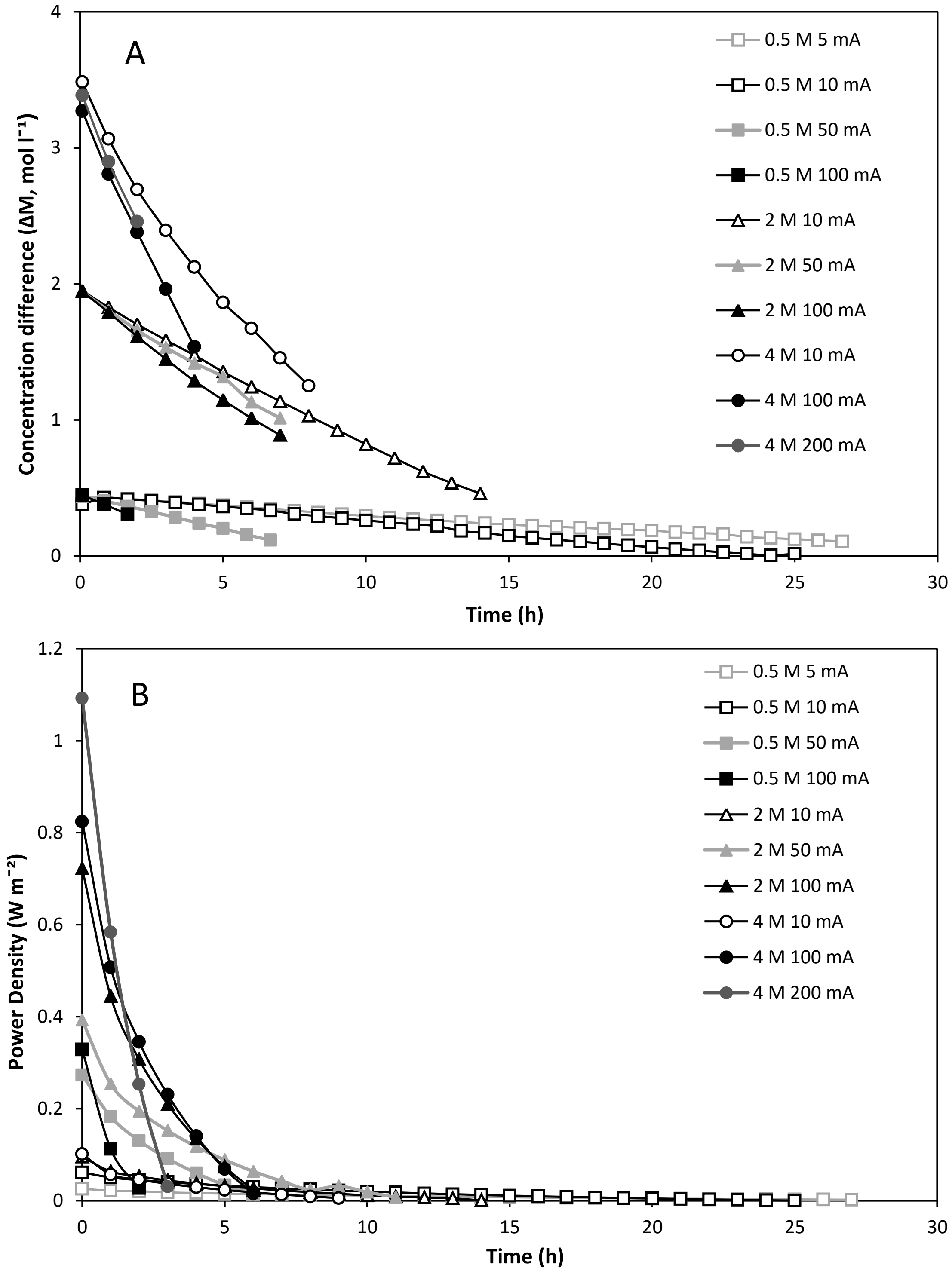

Figure 2.6. *Effect of feed concentration and current density on: (A) change in concentration gradient over time; and (B) power density over time in recycle. Feed flow rate, 200 ml min^{-1}; feed temperature, 25 °C; solution mass, 250 g; dilute concentration, 0.02M.*

2.3.4 Heating the feed doubles power density in single pass but reduces total work in recycle

The retention of sensible heat from thermal regeneration presents an opportunity to increase RED feed temperatures at no additional cost, enabling increased power densities at a reduced membrane area and hence reduced capital investment. The impact of feed temperature from 10 °C to 60 °C was first tested in single pass, where a modest increase in OCV was observed from 1.1 V to 1.2 V, whilst power density almost doubled from 1.6 W m^{-2} to 3.0 W m^{-2} (Figure 2.7). This is because membrane and solution resistances and permselectivity are reduced at increased temperatures [27]. A near linear increase in power density with temperature has previously been reported at high concentrations [17] and sea/river water concentrations [26]. Retention of sensible heat from thermal regeneration in RED could therefore represent a cost-effective method of producing higher power densities in thermal to electric applications; the sensible heat applied being potentially recoverable in spent solution to support the subsequent regeneration cycle. However, increasing feed temperature has the disadvantages of decreasing membrane permselectivity, and increasing ionic shortcuts, the spacer shadow effect and concentration polarisation [17,21]. Therefore, despite the positive effect on power density in single pass, the cumulative effect of these phenomena in recycle may adversely affect power dissipation in recycle. This was evidenced by the decrease in time for power production as the temperature was increased (Figure 2.8A). Energy efficiency decreased from 18 % to 13 % as the feed temperature was increased from 25 °C to 60 °C (Figure 2.8B). This is because of the increase in water flux which causes the concentration gradient to decrease more rapidly at higher temperatures. At 40 °C, the concentration gradient was reduced to 1.5M after 5 hours (Figure 2.8C). At 60 °C, the depletion in concentration gradient was significantly faster due to the increased water flux, which reached a concentration gradient of 1.3M after only 3 hours (Figure 2.8D). As heating the feeds had a detrimental impact on RED performance, it is therefore proposed that heat recovery should be fully managed within the thermal separation stage, independent of RED. By utilising all available heat energy in the regeneration stage, instead of diverting heat to increase feed temperature in the power production stage, the total volume recovered by thermal regeneration could be improved. The improvement in efficiency of RED, coupled with the increased working volume is expected to improve the overall energy efficiency of the heat engine.

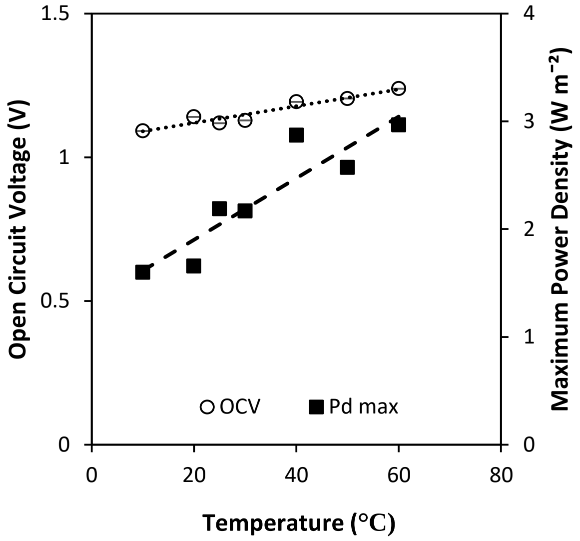

Figure 2.7. *Effect of feed temperature on open circuit voltage and maximum power density in single pass. Concentrate and feed solution concentrations, 4M and 0.02M, respectively; temperature, 25 °C; flow rate, 200 ml min^{-1}.*

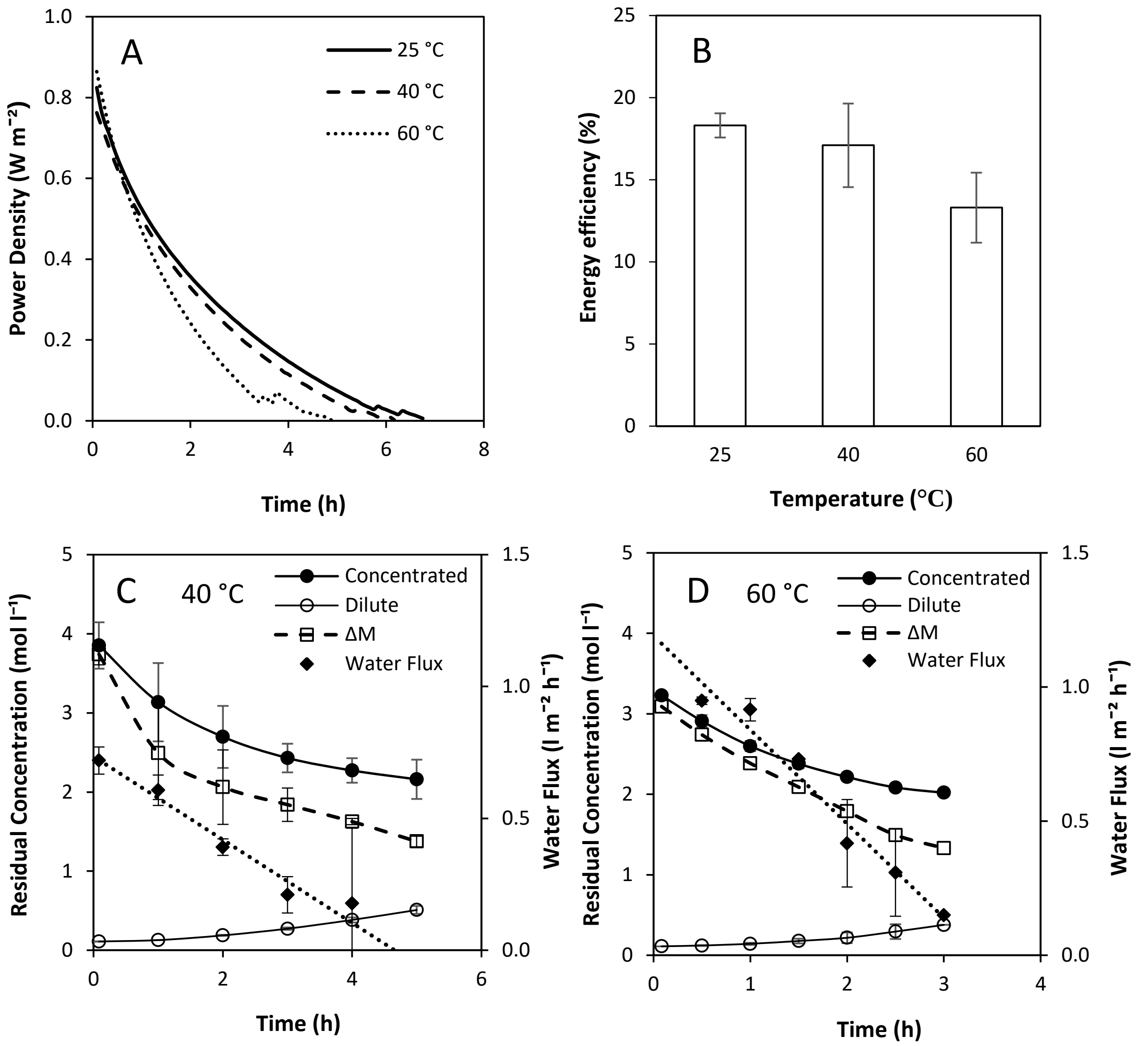

Figure 2.8. *Effect of temperature on: (A) power density over time; and (B) energy efficiency obtained in recycle. Concentrate and feed solution concentrations, 4M and 0.02M, respectively; solution mass, 250 g; flow rate, 200 ml min* $^{-1}$*. Concentration profile and water flux at feed temperature of: (C) 40 °C; and (D) 60 °C.*

2.4 Conclusions

In this study, recirculating RED feeds in a recycle mode has been demonstrated to provide the most suitable configuration for energy recovery from a fixed solution volume, providing a minimum unitary cost for energy production. This is significant as both unit cost and energy efficiency are acknowledged barriers to the viability of thermal to electric conversion for low-grade waste heat. Whilst application of RED to a sea water/ river water matrix has been widely reported, high concentration gradients and operation in recycle present different challenges to optimisation. In single pass, power densities up to 3 W m^{-2} can be achieved through high concentration gradients and elevated temperatures (60°C). However, when feeds are recycled, comparable conditions can promote water transport and concentration polarisation phenomena, which exert an exergy destruction that must be managed. Evaluation of power dissipation evidenced a two-phase transition, in which 80 % of the work was recoverable over half of the discharge cycle, which appears the most economically pragmatic operating point to initiate regeneration. However, this results in a significant exergetic loss due to the high residual concentration gradient. The dilute feed has been identified as the critical limitation to energy recovery within discharge, due to polarisation and water flux effects. To reduce the exergetic loss from the fixed solution before regeneration, a staged configuration could therefore be considered through application of the residual concentrated feed to a second RED cell with a separate dilute feed, or inclusion of a new dilute feed to the existing cell. Optimum current density is specific to concentrated feed concentration, and whilst improved efficiencies are exhibited for lower concentrations, the recovered work from an equivalent working volume is far more significant at higher concentrations, although this is not proportional to feed concentration. When evaluated as an integrated system, an intermediate concentrated feed concentration may therefore present an optimum between work produced from a fixed solution volume, and the energy required for volumetric regeneration due to the raised vapour pressure gradient. Optimising RED stack configuration and process conditions can improve energy efficiency further, however, the present work evidences RED in recycle as a viable strategy for power generation from concentrated brines, improving the potential for delivering cost effective thermal to electrical conversion for application to small-scale, low-grade waste heat solutions.

2.5 Appendices

The use of differing flow rates for the concentrated and dilute feeds has been proposed as a strategy to minimise pumping energy whilst maintaining performance. For sea/river RED, Zhu et al. [27] demonstrated that a higher flow rate is required for the dilute feed in comparison to the concentrated feed, due to the increased solution resistance. For larger salinity gradients, a higher flow rate may be required for the concentrated feed to overcome increased concentration polarisation. To examine this, the flow rate of the dilute was varied at a fixed concentrate flow rate in single pass, to produce ratios defined as Q_D/Q_C. At 25 °C and 200 ml min^{-1} similar power densities of approximately 1.5 W m^{-2} were obtained at all ratios (Figure 2.9). This is because the rapid diffusion of ions from the concentrated to the dilute feed, which is increased at higher concentration gradients, reduces the solution resistance of the dilute feed and so dilute flow rate no longer limits RED performance. However, increasing the concentrated feed flow rate from 20 ml min^{-1} to 200 ml min^{-1} significantly improved both OCV and power density at all ratios. This is because concentration polarisation on the concentrated feed was limiting power production. Increasing the temperature to 40 °C further improved OCV and maximum power density at all flow ratios with a maximum power density of 2.87 W m^{-2} obtained at equal feed flow rates.

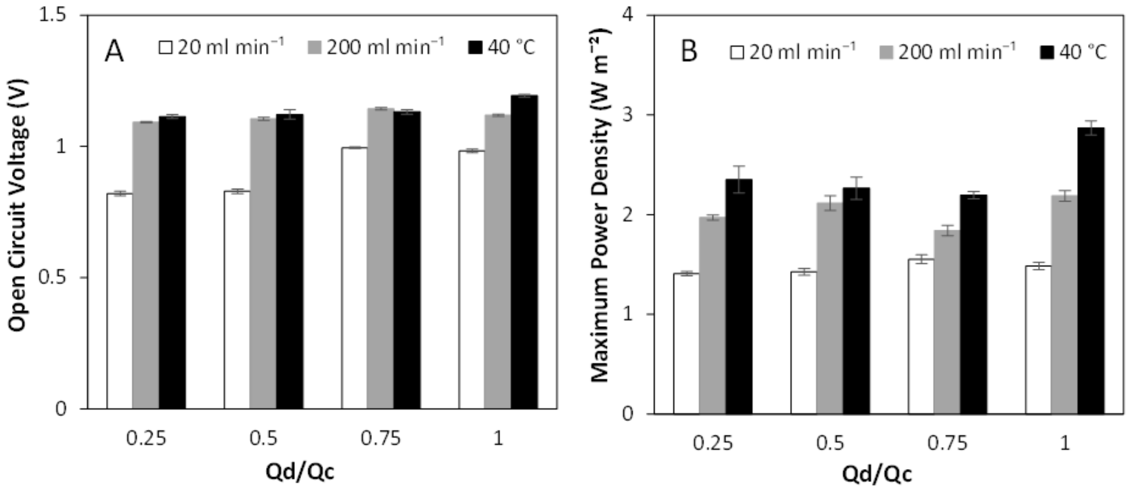

Figure 2.9. *Effect of differing feed flow rates on: (A) open circuit voltage; and (B) maximum power density in single pass. Concentrate and feed solution concentrations, 4M and 0.02M, respectively; concentrate flow rate was initially fixed at 20 ml min $^{-1}$ and the dilute flow rate varied to produce flow ratios Q_d/Q_c at 25 °C. Experiments repeated at a concentrate flow rate of 200 ml min^{-1} at 25 °C and 40 °C.*

Acknowledgements

This publication is based on research funded by the Bill & Melinda Gates Foundation (grant number OPP1149204). The findings and conclusions contained within are those of the authors and do not necessarily reflect positions or policies of the funders. Data underlying this paper can be accessed at: 10.17862/cranfield.rd.12645842.

References

[1] 2018 World Energy Outlook: Executive Summary. https://doi.org/10.1787/weo-2018-en, 2018 (accessed March 3, 2020).

[2] E. Panos, M. Densing, K. Volkart, Access to electricity in the World Energy Council's global energy scenarios: An outlook for developing regions until 2030, Energy Strateg. Rev. 9 (2016) 28–49.

[3] Z. Bo, O. Shaojie, Z. Jianhua, S. Hui, W. Geng, Z. Ming, An analysis of previous blackouts in the world: Lessons for China's power industry, Renew. Sustain. Energy Rev. 42 (2015) 1151–1163.

[4] C. Forman, I.K. Muritala, R. Pardemann, B. Meyer, Estimating the global waste heat potential, Renew. Sustain. Energy Rev. 57 (2016) 1568–1579.

[5] S. Iglesias Garcia, R. Ferreiro Garcia, J. Carbia Carril, D. Iglesias Garcia, A review of thermodynamic cycles used in low temperature recovery systems over the last two years, Renew. Sustain. Energy Rev. 81 (2018) 760–767.

[6] L. Tocci, T. Pal, I. Pesmazoglou, B. Franchetti, Small scale Organic Rankine Cycle (ORC): A techno-economic review, Energies. 10 (2017) 1–26.

[7] D. Champier, Thermoelectric generators: A review of applications, Energy Convers. Manag. 140 (2017) 167–181.

[8] A. Tamburini, M. Tedesco, A. Cipollina, G. Micale, M. Ciofalo, M. Papapetrou, W. Van Baak, A. Piacentino, Reverse electrodialysis heat engine for sustainable power production, Appl. Energy. 206 (2017) 1334–1353.

[9] A. Deshmukh, C. Boo, V. Karanikola, S. Lin, A.P. Straub, T. Tong, D.M. Warsinger, M. Elimelech, Membrane distillation at the water-energy nexus: Limits, opportunities, and challenges, Energy Environ. Sci. 11 (2018) 1177–1196.

[10] Y. Mei, C.Y. Tang, Recent developments and future perspectives of reverse electrodialysis technology: A review, Desalination. 425 (2018) 156–174.

[11] M. Tedesco, A. Cipollina, A. Tamburini, G. Micale, Towards 1 kW power production in a reverse electrodialysis pilot plant with saline waters and concentrated brines, J. Memb. Sci. 522 (2017) 226–236.

[12] J. Veerman, D.A. Vermaas, Reverse electrodialysis: Fundamentals, in: A. Cipollina, G.M. Micale (Eds.), Sustain. Energy from Salin. Gradients, Woodhead Publishing, Cambridge, United Kingdom, 2016: pp. 77–133.

[13] R.A. Tufa, S. Pawlowski, J. Veerman, K. Bouzek, E. Fontananova, S. Velizarov, J. Goulão, K. Nijmeijer, E. Curcio, Progress and prospects in reverse electrodialysis for salinity gradient energy conversion and storage, 225 (2018) 290–331.

[14] W.J. van Egmond, U.K. Starke, M. Saakes, C.J.N. Buisman, H.V.M. Hamelers, Energy efficiency of a concentration gradient flow battery at elevated temperatures, J. Power Sources. 340 (2017) 71–79.

[15] M. Micari, A. Cipollina, F. Giacalone, G. Kosmadakis, M. Papapetrou, G. Zaragoza, G. Micale, A. Tamburini, Towards the first proof of the concept of a Reverse ElectroDialysis - Membrane Distillation Heat Engine, Desalination. 453 (2019) 77–88.

[16] F. Giacalone, C. Olkis, G. Santori, A. Cipollina, S. Brandani, G. Micale, Novel solutions for closed-loop reverse electrodialysis: Thermodynamic characterization and perspective analysis, Energy. 166 (2019) 674–689.

[17] A. Daniilidis, D.A. Vermaas, R. Herber, K. Nijmeijer, Experimentally obtainable energy from mixing river water, seawater or brines with reverse electrodialysis, Renew. Energy. 64 (2014) 123–131.

[18] N.Y. Yip, D.A. Vermaas, K. Nijmeijer, M. Elimelech, Thermodynamic, energy efficiency, and power density analysis of reverse electrodialysis power generation with natural salinity gradients, Environ. Sci. Technol. 48 (2014) 4925–4936.

[19] F. Giacalone, P. Catrini, A. Tamburini, A. Cipollina, A. Piacentino, G. Micale, Exergy analysis of reverse electrodialysis, Energy Convers. Manag. 164 (2018) 588–602.

[20] W.J. Van Egmond, M. Saakes, S. Porada, T. Meuwissen, C.J.N. Buisman, H.V.M. Hamelers, The concentration gradient flow battery as electricity storage system: Technology potential and energy dissipation, J. Power Sources. 325 (2016) 129–139.

[21] X. Zhu, W. He, B.E. Logan, Influence of solution concentration and salt types on the performance of reverse electrodialysis cells, J. Memb. Sci. 494 (2015) 154–160.

[22] P. Długołecki, P. Ogonowski, S.J. Metz, M. Saakes, K. Nijmeijer, M. Wessling, On the resistances of membrane, diffusion boundary layer and double layer in ion exchange membrane transport, J. Memb. Sci. 349 (2010) 369–379.

[23] P. Długołecki, B. Anet, S.J. Metz, K. Nijmeijer, M. Wessling, Transport limitations in ion exchange membranes at low salt concentrations, J. Memb. Sci. 346 (2010) 163–171.

[24] S. Pawlowski, P. Sistat, J.G. Crespo, S. Velizarov, Mass transfer in reverse electrodialysis: Flow entrance effects and diffusion boundary layer thickness, J. Memb. Sci. 471 (2014) 72–83.

[25] M. Tedesco, E. Brauns, A. Cipollina, G. Micale, P. Modica, G. Russo, J. Helsen, Reverse electrodialysis with saline waters and concentrated brines: A laboratory investigation towards technology scale-up, J. Memb. Sci. 492 (2015) 9–20.

[26] P. Długołęcki, A. Gambier, K. Nijmeijer, M. Wessling, Practical potential of reverse electrodialysis as process for sustainable energy generation, Environ. Sci. Technol. 43 (2009) 6888–6894.

[27] X. Zhu, W. He, B.E. Logan, Reducing pumping energy by using different flow rates of high and low concentration solutions in reverse electrodialysis cells, J. Memb. Sci. 486 (2015) 215–221.

3. Transitioning from electrodialysis (ED) to reverse electrodialysis (RED) stack design for energy generation from high salinity gradients in recycle

Transitioning from electrodialysis (ED) to reverse electrodialysis (RED) stack design for energy generation from high salinity gradients in recycle

A.M. Hulme[a], C.J. Davey[a], M. Pidou[a], E.J. McAdam[a]*

[a]Cranfield Water Science Institute, Cranfield University, Bedfordshire, MK43 0AL, UK

*Corresponding author: e.mcadam@cranfield.ac.uk

Abstract

In this study, stack design for high concentration gradient reverse electrodialysis (RED) operating in recycle is addressed. High concentration gradients introduce complex transport phenomena, which are exacerbated when recycling feeds; a strategy employed to improve system level energy efficiency. This challenge indicates that membrane properties and spacer thickness requirements may differ considerably from single pass RED for lower concentration gradients (e.g. seawater/river water), drawing closer parallels to electrodialysis (ED) stack design. Consequently, commercially available ED and RED stack designs were first compared for power generation from high concentration gradients. Higher gross power densities were identified for the RED stack in single pass, due to the use of thinner membranes characterised by reduced resistance, which improved current. However, energy efficiency of the ED stack was twice that recorded for the RED stack at low current densities with solution recycling, which was attributed to: (i) an increased residence time provided by the larger intermembrane distance, and (ii) reduced exergy losses of the ED membranes, which provided comparatively lower water permeance. Further in-depth investigation into membrane properties and intermembrane distance identified that membranes characterised by low water permeability and ohmic resistance provided the highest power density and energy efficiency (Neosepta ACS/CMS), whilst wider intermembrane distances up to 0.3 mm improved net power density. This study identifies that RED stacks for high concentration gradients in recycle therefore do demand design more comparable to ED stacks to drive energy efficiency, but membrane selection must also consider water permeability to ensure economic viability.

Keywords: intermembrane distance, spacer thickness; closed-loop; desalination; blue energy; membrane thickness; brine

3.1 Introduction

Electrodialysis (ED) is a commercially mature technology, with applications in multiple industries ranging from food manufacturing to wastewater treatment [1]. Through revisiting stack design, ED has now been demonstrated to be economically and energetically competitive to reverse osmosis for the desalination of brackish waters [2,3]. In an ED stack, anion and cation ion exchange membranes are alternately arranged between two electrodes to form concentrated and dilute compartments. The controlled movement of ions across the ion exchange membranes (IEMs) is driven by an applied electrical current to produce desalinated water [2,4]. Spacers and gaskets separating the membranes determine the intermembrane distance. An intermembrane distance of 0.3 mm to 2 mm is typically used in ED units [1]. Larger intermembrane distances are preferable as the increased volume of salt enables a higher potential to be applied [5]. Water transport across the membranes from the dilute to concentrated stream hinders separation [6] and occurs by: (i) osmosis, facilitated by the concentration difference across the membrane; and, (ii) electro-osmosis, in which ionic transport across the membrane facilitates the co-transport of associated water molecules [1,6]. Therefore, membranes with low water permeability are required to decrease water transport and reduce energy consumption [5]. Industrial ED modules can contain over 500 cell pairs, with the active area of each membrane pair up to 1 m^2, however, multi-stage or feed recycling configurations are generally proposed to deliver high quality desalinated water [1,7].

In reverse electrodialysis (RED), the opposite process to ED is employed, where ionic transport across alternately stacked IEMs is driven by the concentration gradient, to liberate the Gibbs free energy of mixing between solutions of different salinities. A redox couple circulating across the electrodes converts the ionic flow to an electric current [8]. Whilst sharing mechanistically comparable separation principles, coupled with their application to equivalent saline concentration gradients, the modules used for desalination by ED and those used for power production by RED exhibit several key differences. In contrast to ED, compartment widths in the region of 0.1 mm to 0.3 mm have typically been adopted for RED stacks [9]. This is because the smaller intermembrane distance benefits power output by RED due to a reduction in resistance, although this is negated by the increased pressure drop at distances < 0.1 mm [10]. Whilst low water permeability membranes are critical to minimise water transport in ED, low resistance membranes with high permselectivity are prioritised for RED applications using artificial sea and river water [11–13]. In RED, electro-osmosis occurs in the opposite direction to osmosis and thus acts to reduce net water transport [13,14]. Despite this, water transport is detrimental to power output and energy efficiency in RED applications [13,15]. Whilst these effects are less evident when seawater/river water is used in RED, such phenomena can conceivably pose a significant resistance to ionic transport when higher salinity gradients, or solution recycling are employed as strategies to improve power output and energy efficiency [15]. The principles of RED stack design in these scenarios may therefore require much closer alignment to those of ED for desalination applications.

Research on RED has largely centred around the exploitation of seawater/river water to develop the concentration gradient driving force, with power densities up to 0.93 W m^{-2} obtained [16]. However, higher salinity differences found in concentrated brines associated with natural and engineered systems (e.g. desalination reject brine) [17], or artificial concentrates that can be exploited for energy storage or thermal to electrical opportunities, increase the system electrochemical potential (Nernst potential) such that power densities up to 6.7 W m^{-2} have been reported at elevated temperatures [18]. For energy storage and thermal to electric conversion systems, closed-loop RED is proposed, where mixed solutions exiting the RED stack subsequently pass through a separation stage which restores the concentration gradient [19]. Artificial saline solutions enable opportunities to improve electrochemical potential through increasing concentration gradient, temperature, or valence of the salt [20,21]. However, higher salinity gradients increase the driving force for water transport as well as ionic transport across the membrane resulting in increased exergy losses [6,22,23]. Consequently, RED stack design has migrated away from conventional ED stack design for feed waters of equivalent salinity by introducing membranes which promote higher permselectivity and reduced resistance at the cost of water transport to improve power density [8]. It is postulated that the critical membrane characteristics, channel dimensions and hydrodynamics required to overcome the more complex transport behaviour imposed in RED by higher concentration gradients in recycle may be more comparable to ED stack design. Further exergetic advantage can be achieved in closed-loop RED systems by feedwater recycling which has been demonstrated to increase net energy recovery [18,24], and is analogous to ED where feed recirculation is used to improve final product quality in desalination [1]. However, feed recirculation introduces complex temporal phenomena due to the cumulative effect of water transport on the concentration gradient, which is exacerbated by the elevated concentration gradient [25]. The aim of this paper is therefore to determine how to transition from ED stack design towards the practical implementation of an RED stack design suitable for high concentration gradients when operated in recycle, for applications such as thermal to electrical conversion and energy storage. To facilitate engineering rationalisation, commercially available stack designs for ED and RED of equivalent stack dimensions and surface area are initially compared and are benchmarked on concentrated brines in single pass before evaluation in recycle. Subsequent investigation as to: the contribution of membrane properties and intermembrane distance on power density and energy efficiency is undertaken during concentrated brine recirculation, in order to better characterise the trade-off between membrane permselectivity and water permeability and to limit exergy losses.

3.2 Materials and methods

3.2.1 Experimental setup for reverse electrodialysis stacks

A FumaTech RED-800-2-25 module (FumaTech, Bietigheim-Bissingen, Germany) and MemBrain EDR-Y module (MemBrain, Czech Republic) were tested to determine the performance of commercially available modules using high concentration gradients. Both stacks had dimensions of 10 cm x 40 cm and were equipped with 25 pairs, giving a total active membrane area of 2 m^2 (Table 3.1). A custom-made 10cm x 10cm stack was used to identify the contribution of individual stack components on RED performance. Titanium electrodes with Ru/Ir mixed metal oxide coating were fitted into custom-made endplates (Model Products, Bedfordshire, UK). 5 pairs of ion exchange membranes were stacked alternately in the module, separated by nylon woven spacers (SEFAR, Heiden, Switzerland) and silicon gaskets (Silex Silicones Ltd, Hampshire, UK). Membrane type, intermembrane distance and electrode material were individually varied to determine the effect of energy efficiency and work produced from a fixed volume. The membranes tested were Neosepta AMX and CMX; Neosepta ACS and CMS (Eurodia Industrie SA, Pertuis, France); Selemion ASA and CSO (AGC Engineering, Japan); Ralex AMH-PES and CMH-PES (MemBrain, Czech Republic); and Fumasep FAS-50 and FKS-50 (FumaTech, Bietigheim-Bissingen, Germany). Intermembrane distance was varied by using spacers and gaskets with thicknesses of 0.1 mm, 0.155 mm, 0.2 mm, 0.3 mm and 0.5 mm. Peristaltic pumps recirculated the electrode rinse, dilute and concentrated feeds to the modules (Watson Marlow, Cornwall, UK). Conductivity meters were fitted inline to enable feed concentration to be monitored throughout the experiment (2 CDH-SD1, Omega Engineering Limited, Manchester, UK and 2 Mettler Toledo Seven2Go Pro S7, Wolf Laboratories, York, UK). Feed reservoirs were placed on balances to quantify water flux and enable a full mass balance to be carried out (Kern SFB 20K2HIP, Scales and Balances, Thetford, UK).

3.2.2 Preparation of solutions

Sodium chloride solutions were prepared for the concentrated and dilute feeds using 99 % NaCl (Alfa-Aesar, Lancashire, UK) and deionised water. For the concentrated feed, solutions of 0.5M, typically used to represent sea water in the literature, and 4M were prepared. For the dilute feed, a 0.02M solution was prepared. The electrode rinse consisted of 0.1M $K_3Fe(CN)_6$, 0.1M $K_4Fe(CN)_6$ (Fisher Scientific, Leicestershire, UK) and 2M NaCl (Alfa-Aesar, Lancashire, UK) and was continuously recirculated to the stacks. For experiments using the large commercially available stacks, a feed reservoir containing 5 L of electrode rinse solution was prepared and 1 L for the 10 cm x 10 cm stack and wrapped in tin foil to avoid contact with light.

3.2.3 Electrochemical measurements

A potentiostat (IviumStat.h, Alvatek, UK) was used to make electrochemical measurements, with the data logged using IviumSoft (IviumStat.h, Alvatek, UK). A consistent open circuit voltage <0.01 V s^{-1} was obtained before electrochemical measurements were made to ensure steady-state. All measurements were carried out at least three times, with the mean reported and error bars used to represent the standard deviation of the triplicate. In single pass, chronopotentiometry was carried out at a range of current densities until a stable voltage was achieved. Power density, Pd (W m^{-2}) was calculated:

$$P_d = \frac{UI}{A} \tag{3-1}$$

where I is the current (A), U is the voltage (V) produced by the stack and A is the total active membrane area (m^2). To determine energy efficiency, feeds were recirculated with the potentiostat set at a constant current, enabling total work produced, W_{RED}, to be calculated:

$$W_{RED} = \sum_{t_o}^{t_{end}} UI \triangle t \tag{3-2}$$

Where t_o and t_{end} is the time at which work was produced by RED started and ended, respectively, where U is the voltage produced (V) and I is the current, (A) [18]. The Gibbs free energy in the system, ΔG_{mix}, is the theoretical maximum energy which can be recovered, assuming total mixing and no exergy losses:

$$\Delta G_{mix} = \Delta G_m - (\Delta G_c + \Delta G_d) \tag{3-3}$$

where ΔG_{mix} is the Gibbs energy (J) and the subscripts m, c and d represent the mixed outlet stream, concentrated and dilute feeds, respectively. For ideal solutions:

$$\Delta G_{mix} = -(N_c + N_d)T\Delta S_m - (-N_cT\Delta S_c - N_dT\Delta S_d) \tag{3-4}$$

where N is the number of moles (mol), T is the temperature (K) and ΔS is the molar entropy (J mol^{-} K^{-1}). The molar entropy is determined by:

$$\Delta S = -R \sum_i x_i \ln x_i \tag{3-5}$$

where R is the universal gas constant (8.315 J mol^{-1} K^{-1}) and x is the mole fraction of species i. [6]. The energy efficiency, $\eta_{RED,}$ is defined as the work produced from the total available Gibbs free energy:

$$\eta_{RED} = \frac{W_{RED}}{\Delta G_{mix}} \times 100 \tag{3-6}$$

3.3 Results and Discussion

3.3.1 Improved performance of RED stack compared to ED stack using a large concentration gradient

Measurements were initially carried out in single pass to evidence the maximum power density that can be achieved using the two commercially available modules when operated at a large concentration difference. The two units had an equal total active membrane area and stack dimensions, but different ion exchange membranes and intermembrane distances (Table 3.1). For both stacks, the open circuit voltage (OCV) improved as flow rate was increased up to a plateau at approximately 4.5 V, however this occurred at a lower flow rate of 0.5 l min^{-1} in the RED stack, compared to 1 l min^{-1} in the ED stack (Figure 3.1A). This OCV was significantly lower than the theoretically calculated OCV of 6.6 V, which is attributed to the uncontrolled migration of water and ions across the membranes [26], driven by the elevated concentration gradient. For the RED stack, current increased with flow rate up to a maximum of 9.2 A at 0.75 l min^{-1}. This can be explained by the increase in the rate of ionic transfer, facilitated by the higher flow rate which reduced concentration polarisation [27]. By contrast, current was limited to approximately 0.6 A in the ED stack and remained unchanged as flow rate was changed up to a flow rate of 2.5 l min^{-1} (Figure 3.1B). This cannot be attributed to ion exchange capacity as the FAS-50/FKS-50 membranes in the RED module and the AMH-PES/CMH-PES membranes in the ED module had a similar ion exchange capacity. However, membrane thickness varied significantly between the two modules, with those in the RED module 0.05 mm thick in comparison to 0.7 mm thick membranes in the ED module. Membrane thickness is directly correlated with resistance [12,28] and heterogeneous membranes with non-uniform charge distribution [29] such as those in the ED stack will have much higher resistance than the homogenous ones within the RED stack [11]. For seawater and river water feeds, low resistance membranes are prioritised to improve power density by RED [11,12]. However, for ED, low water permeability membranes are preferred to reduce energy requirements for desalination [5]. A maximum gross power density of 0.33 W m^{-2} was produced by the ED stack in comparison to 4.78 W m^{-2} for the RED stack (Figure 3.1C). This difference is attributed to intrinsic membrane resistance [28], however, the significant difference in intermembrane distance may also play a role.

Table 3.1. *Properties of the commercially available MemBrain and FumaTech modules.*

	MemBrain	**FumaTech**
Optimised for	Electrodialysis	Reverse Electrodialysis
Stack size	10 cm x 40 cm	10 cm x 40 cm
Cell pairs	25	25
Total Membrane Area (m^2)	2	2
Spacer Thickness (mm)	0.8	0.155
Anion Exchange Membrane	Ralex AMH-PES	Fumasep FAS-50
Cation Exchange Membrane	Ralex CMH-PES	Fumasep FKS-50
Membrane Thickness (µm)	714 - 764	45 - 55
Electrode material	Titanium MMO	Titanium MMO
Flow Direction	Co-current	Co-current

As stack dimensions and cell pair number in the two stacks were equal, the velocity at a given flow rate is determined by the intermembrane distance. The intermembrane distance of the ED stack was over four times greater than that in the RED stack, recorded as 0.8 mm and 0.15 mm respectively, and therefore residence time, τ,was similarly varied for a given flow rate($\tau = v/l$). Residence time has previously been used to estimate performance across process scales, with a deterioration in power density observed as it is increased [26]. To account for this, the performance of the two stacks was also evaluated in terms of residence time. For residence times greater than 30 s, the ED stack produced a higher OCV than the RED stack at an equivalent residence time (Figure 3.1D). This is likely to be because the increased thickness of the ED membranes mitigates exergy losses by retarding water and ionic flux. However, current was significantly lower in the ED stack (Figure 3.1E). Increased intermembrane distance is expected to increase internal ohmic resistance [10], with Długołecki et al. [11] reporting that for an intermembrane distance of > 0.6 mm, spacer resistance dominates and membrane properties have very little effect on RED performance for feeds with an equivalent concentration to seawater and river water. Therefore, in this study the increased spacer thickness which is advantageous to ED may be similarly limiting for RED with concentrated brines. Due to the reduction in current, gross power densities were significantly lower in the ED stack compared with the RED stack (Figure 3.1F). To illustrate, at a constant residence time of 20 s, a maximum current of 0.06 A was obtained compared to 7.5 A, producing gross maximum power densities of 0.33 W m^{-2} and 3.85 W m^{-2} , respectively.

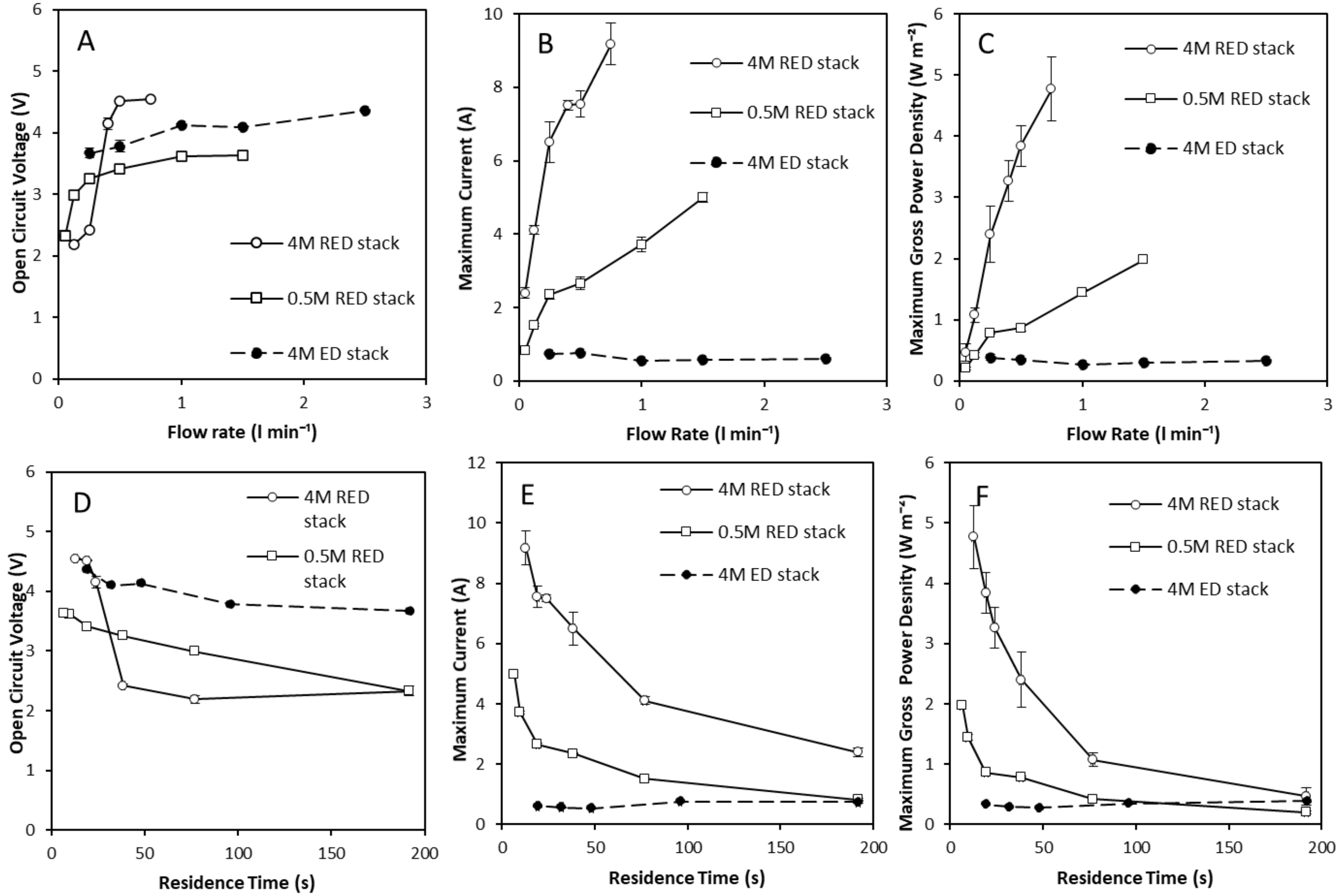

Figure 3.1. *(A) Open circuit voltage; (B) maximum current; and (C) maximum gross power density obtained by commercially available stacks optimised for RED and ED at range of flow rates; and (D) open circuit voltage; (E) maximum current; and (F) maximum power density against feed residence time. Dilute feed of 0.02M and a concentrated feed of 0.5M and 4M in single pass. Error bars represent the standard deviation of a triplicate.*

The ten-fold increase in power density using the RED stack compared to the ED stack demonstrates that this design is not suitable for delivering salinity gradient energy from concentrated brines in single pass. The distinction in ED stack design including increased intermembrane distance that promotes longer residence times, and increased membrane thickness, could however benefit total energy recovery during recycle, due to a reduction in water transport. Consequently, the two stacks were compared in recycle by fixing a high concentration gradient (4M and 0.02M feeds) at a current of 0.4 A (current density, 10 A m^{-2}), the highest current which could be sustained by the ED stack. At an equal flow rate of 0.5 l min^{-1} a maximum gross power density of 0.02 W m^{-2} was obtained in the ED stack, compared to 0.72 W m^{-2} in the RED stack (Figure 3.2A). Although maximum power densities obtained using the ED module in single pass and recycle operation are similar, maximum power output achieved by the RED module is significantly reduced. This is because the power density is limited by the reduced current utilised in recycle to enable comparison between the modules. The difference in power density obtained by the two stacks at equivalent current and flow rate can be partly explained by the difference in residence time of 96 s and 19 s, in the ED and RED stack, respectively. A total energy efficiency of 9.7 %, equivalent to 0.63 kJ kg^{-1} was achieved using the ED stack at these conditions (Figure 3.2B). However, half the energy efficiency, 4.6 %, was obtained using the RED stack. This difference is attributed to the increased water flux in the RED stack (Figure 3.2C) [15]. This introduced a sharp decline in the concentration gradient and hence electrochemical potential, as illustrated by the increased saline concentration of the dilute feed over a shorter time interval (Figure 3.2D). Significant decreases in energy efficiency due to water transport have been previously reported when using large concentration gradients [18,23]. Membranes with low water permeability are favoured for ED as they decrease exergy loss due to water transport [5], and this demonstrates that membranes with low water permeability could also improve efficiency in RED using concentrated brines and in recycle applications.

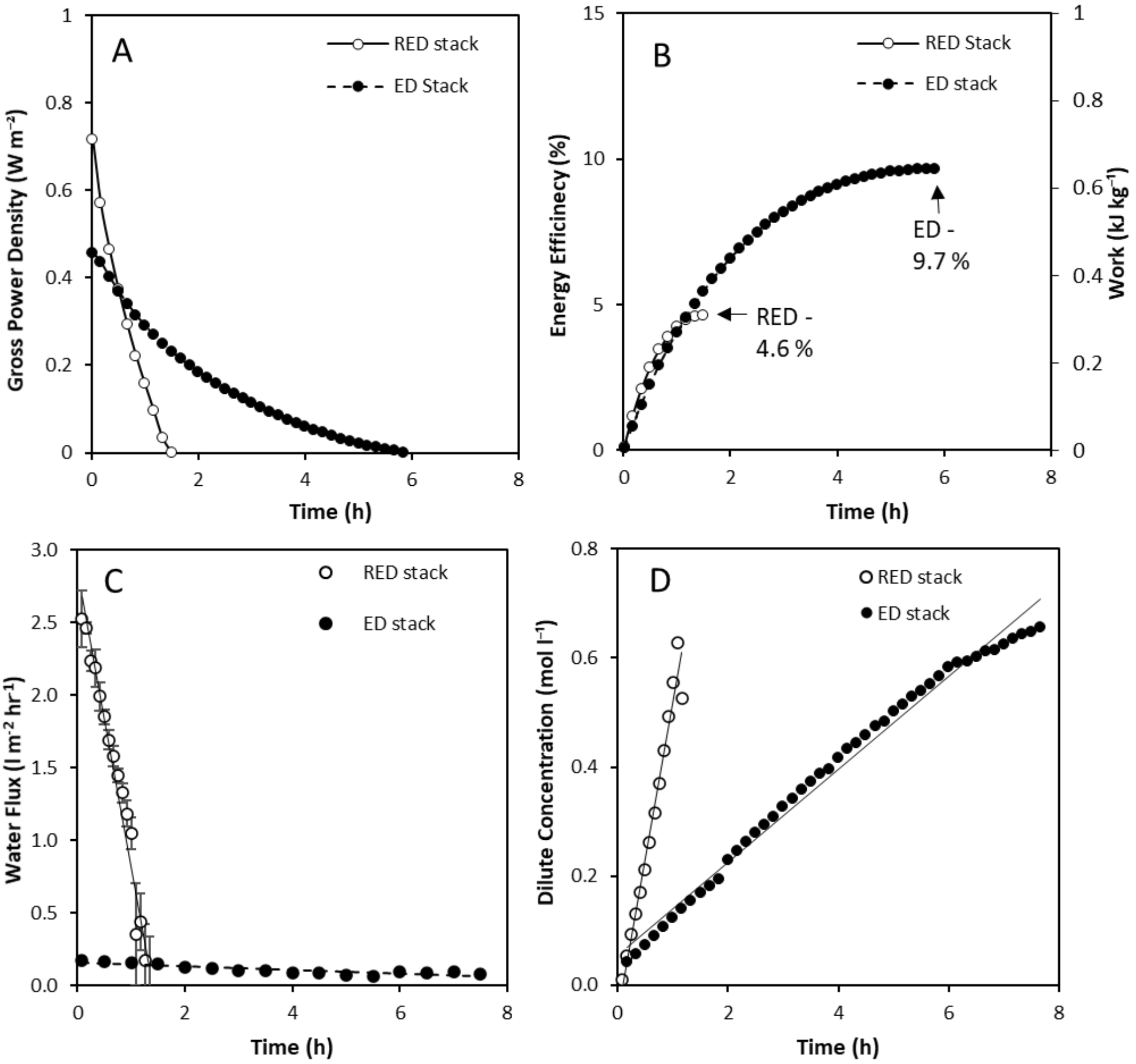

Figure 3.2. *(A) Power density; (B) energy efficiency and work produced per kg; (C) water flux; and (D) dilute concentration over time obtained using commercially available stacks optimized for RED and ED in recycle. Dilute feed, 5 kg 0.02M NaCl; concentrated feed 5 kg 4M NaCl. Flow rate, 0.5 l min^{-1}; current, 400 mA. Error bars represent the standard deviation of a triplicate.*

3.3.2 Low water permeability of membranes critical for high energy efficiency using concentrated brines

The effect of membrane properties on power density and energy efficiency using concentrated brines in recycle were discretely investigated, using five pairs of commercially available IEMs (Table 3.2), which included those used in the commercially available RED and ED stacks (Fumasep FAS-50/FKS-50 and Ralex AMH-PES/CMH-PES respectively). Current density was varied to identify an optimum energy efficiency for each IEM cell pair (Figure 3.3A). The increase in energy efficiency with current density is expected in RED, as in contrast to ED, water transport is reduced as the corresponding increase in electro-osmosis counteracts the disadvantage of osmotic flux [6,14]. However, above an optimal current density, high internal resistances inhibit performance [14]. A peak in energy efficiency was observed at 10 A m^{-2} for the Selemion ASA/CSO, Neosepta AMX/CMX, Neosepta ACS/CMS and Ralex AMH-PES/CMH-PES membranes, whereas a peak occurred at a higher current density of 20 A m^{-2} for the Fumasep FAS-50/FKS-50 membranes. This implies that higher power densities can be promoted through the Fumasep FAS-50/FKS-50 IEMs, which may explain their frequent selection for seawater/river water applications. For closed-loop RED, the energy efficiency (specifically, the work produced per kg of feed) (Figure 3.3B) is a critical determining factor in overall system efficiency [20]. Despite the increased current, the energy efficiency obtained using the Fumasep membranes was significantly lower than all other membranes pairs, at 8.5 % (Figure 3.3A). The Ralex AMH-PES/CMH-PES membranes from the ED stack obtained an improved efficiency of 14.2 %, illustrating that they can benefit the performance of RED using concentrated brines. Although both examples were exposed to the same salinity gradient that induces osmotic water transport, the improvement can be attributed to a reduction in water permeance due to an increased membrane thickness of the Ralex membranes [29].

Table 3.2. *Membrane properties from the literature on ion exchange membranes used for RED in recycle using a 4M concentrated feed and 0.02M dilute feed.*

Ion Exchange Membrane		IEC (mequiv./g dry)	Permselectivity (%)	Resistance (Ω cm^2)	Thickness (μm)	
Neosepta	AMX	1.25	90.7	2.35	134	[1]
	CMX	1.62	99	2.91	164	[1]
Neosepta	ACS	1.97 ± 0.01	100 (measured for pair) [2]	3.8 (data sheet)	117 ± 3	[3]
	CMS	2.28 ± 0.05	Monoselective for NaCl	1.8 (data sheet)	136 ± 3	[3]
Ralex	AMH-PES	1.97	89.3	7.66	714	[1]
	CMH-PES	2.34	99	11.33	764	[1]
Fumasep	FAS-50	1.6-2.0	92-96	0.6-1.5	45-55	data sheet
	FKS-50	1.2-1.4	97-99	1.8-2.5	45-55	data sheet
Selemion	ASA	2.13 ± 0.04			96 ± 3	[3]
	CSO	2.2 ± 0.02	95	1.91	97 ± 2	[3]

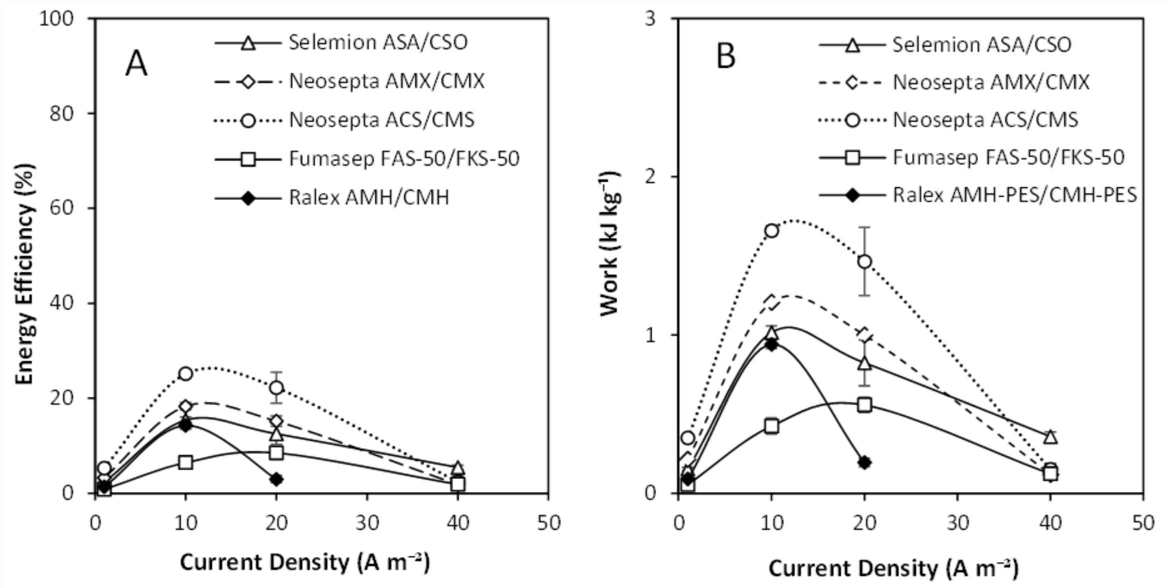

Figure 3.3. *(A) Energy efficiency obtained and (B) work produced using commercially available membranes in recycle at a range of current densities using a 10 cm x 10 cm 5-cell pair RED stack and an intermembrane distance of 0.3 mm. Dilute feed, 0.25 kg 0.02M; concentrated feed, 0.25 kg 4M; flow rate, 0.2 l min^{-1}. Error bars represent the standard deviation of a triplicate.*

For each IEM cell pair, water flux was observed to decrease over time as the concentration gradient and hence the driving force for water transport decreased (Figure 3.4A). A water flux of 1.82 l m^{-2} hr^{-1} was recorded across the Fumasep FAS-50 membranes which was the highest across the 5 IEM cell pairs tested, and was an order of magnitude greater than that of the Ralex (AMH/CMH) and Neosepta (AMX/CMX) membranes, which exhibited the lowest water flux. For this set of conditions, the maximum gross power density recorded from the Fumasep FAS-50/FKS-50 IEMs at a current density of 10 A m^{-2} was 0.7 W m^{-2}. This was comparable to both Neosepta IEMs that were characterised by comparable ohmic resistances (Table 3.2),and was quite similar to maximum power densities obtained from the Ralex AMH-PES/CMH-PES membranes used within the commercial ED stack, which confer considerably higher membrane resistances between 7.6 Ω cm^{-2} and 11.3 Ω cm^{-2} (Table 3.2). The relative insensitivity of power density to membrane resistance can be attributed to the OCV that can be sustained for Ralex IEMs, which enables comparatively higher local concentration gradients for a longer period in comparison to the thinner membranes. The increased rate of water transfer is detrimental to energy recovery, due to the faster deterioration in salinity gradient, which reduces temporal power production as the electrochemical potential tends toward 0 V (Figure 3.4B). Membranes comprising lower water permeability can reduce such exergy losses and improve energy efficiency, as theoretically demonstrated by Giacalone et al. [23]. Water permeability can be controlled through modification of membrane microstructure, or water permeance reduced by increasing the membrane thickness [22]. In this study, increasing membrane thickness is demonstrated to improve energy efficiency for RED in recycle, however, the corresponding increase in resistance reduces obtainable power densities [29] leading to a critical trade-off. In river water/sea water applications, membrane resistance has therefore been perceived as the primary membrane property governing power density [29]. Whilst results from this study broadly agree with this assertion in single pass, the highest power density and energy efficiency in recycle was obtained using the Neosepta ACS/CMS membranes, which comprise of an intermediate thickness and similar or greater resistance than competing IEMs. The apparent improvements in power density and energy efficiency can be attributed to the reduction in water transport, emphasising that a more holistic approach is required to membrane selection when subjected to high concentration gradients in recycle.

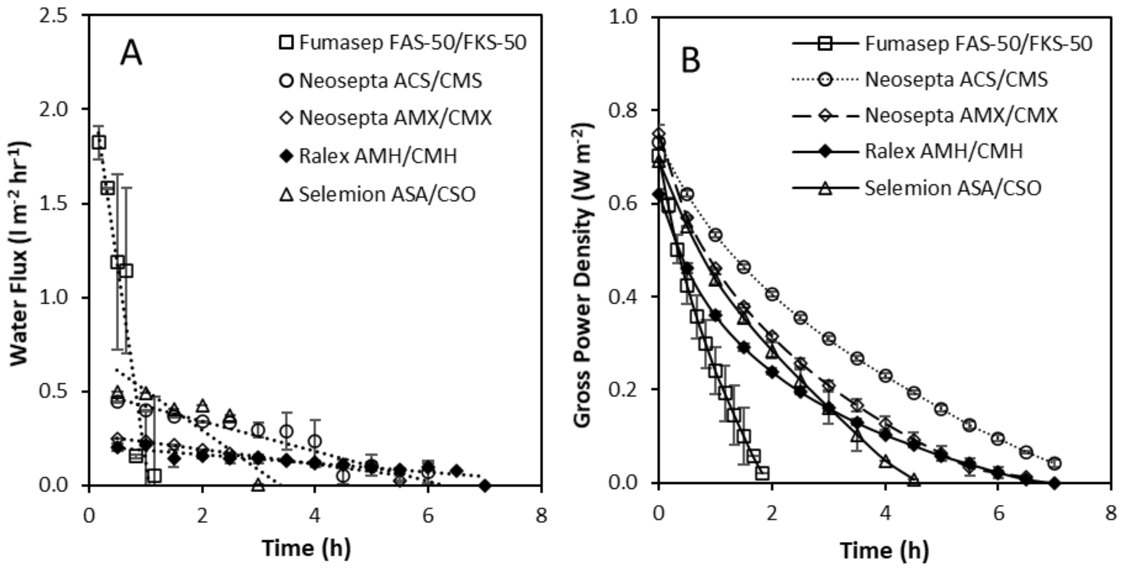

Figure 3.4. *(A) Water flux and (B) gross power density over time using commercially available membranes in recycle in a 10 cm x 10 cm 5-cell pair RED stack with an intermembrane distance of 0.3 mm. Dilute feed, 0.25 kg 0.02M; concentrated feed, 0.25 kg 4M; flow rate, 0.2 l min^{-1}, current density 10 A m^{-2}. Error bars represent the standard deviation of a triplicate.*

3.3.3 Highest energy efficiency achieved at an intermembrane distance of 0.2 mm using concentrated brine

The intermembrane distance was initially varied in single pass, to determine whether reduced intermembrane distances improve the gross and net power density obtained by RED using a large concentration gradient. At a constant flow rate of 0.2 $l\ min^{-1}$, current increased to an optimum of 68 $A\ m^{-2}$ as intermembrane distance was increased to 0.2 mm, before rapidly decreasing as intermembrane distance was increased further (Figure 3.5A). The peak current recorded at 0.2 mm was coincident with a maximum gross power density of 1.72 $W\ m^{-2}$ (Figure 3.5B). The reduction in power density above this intermembrane distance can be ascribed to ohmic and boundary layer resistances which are thought to increase as intermembrane distance increases, subsequently reducing current [10]. Net power density accounts for the hydraulic pumping losses. For small intermembrane distances of 0.1 mm, net power was negative, indicating that more pumping power was required than was produced by RED. Net power increased up to 0.2 mm due to the increased gross power density. Vermaas et al. [10] reported decreased net power below an optimal intermembrane distance of 0.1 mm using artificial seawater/river water. A thinner intermembrane distance is required for lower concentration gradients (sea/river) feeds due to the reduced gross power densities obtained, compared to the utilisation of higher concentration gradients in this study which vastly improved gross power density, enabling use of increased intermembrane distances.

The transition in intermembrane distance at a fixed flow rate results in different velocities and residence times. Consequently, experiments were undertaken at a constant velocity of 0.22 $cm\ s^{-1}$, equating to a residence time of 4.5 s for each intermembrane distance studied (Figure 3.5C). Current decreased approximately linearly as the intermembrane distance was increased (Figure 3.5C) due to ohmic and boundary layer resistance [10]. Below 0.3 mm, gross power densities are lower compared with the values obtained at 0.2 $l\ min^{-1}$. Whilst this is an artefact of the lower flow rate required to obtain a comparable velocity, RED will be scaled up based on velocity and residence time to ensure performance is consistent between process scales to account for concentration polarisation and spacer shadow effects [30]; consequently the intermembrane distance that provides the highest net power density at comparable velocity can be assumed to represent the most favourable condition. Therefore, despite identifying the highest gross power density at an intermembrane distance of 0.1 mm, the maximum net power density was recorded with a 0.3 mm intermembrane distance, which is at the upper limit of those ordinarily rationalised for seawater/river water RED. This confirms the assertion that slightly wider intermembrane distances may be appropriate for power production from high concentration brines.

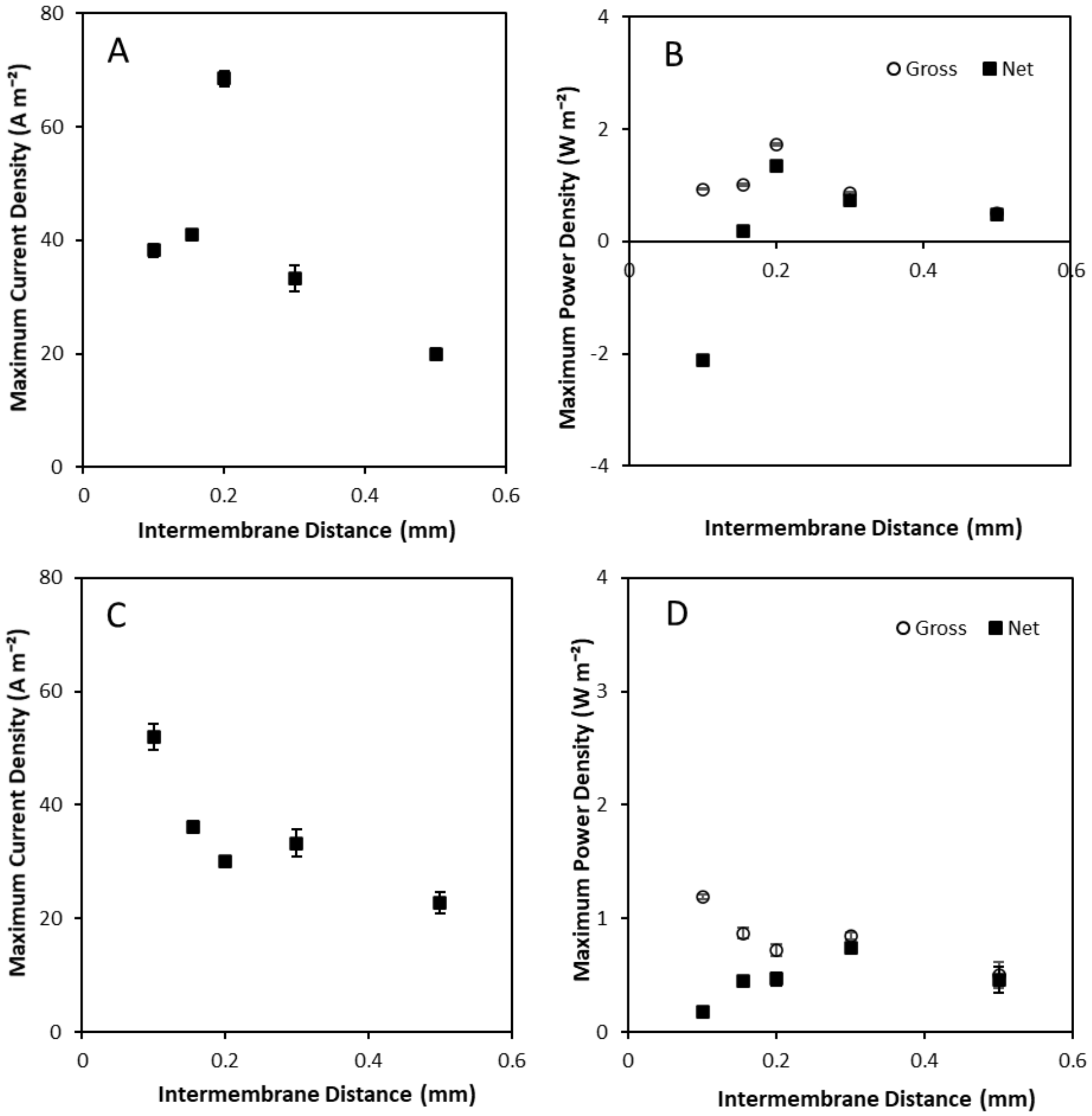

Figure 3.5. *Spacer thickness in single pass on (A) maximum current density; and (B) maximum power density at a constant flow rate of 0.2 l min^{-1}, and (C) maximum current; and (D) maximum power density at constant velocity of 0.22 cm s^{-1}, using a 10 cm x 10 cm RED stack containing 5 pairs Neosepta AMX/CMX membranes. Dilute feed, 0.25 kg 0.02M; concentrated feed, 0.25 kg 4M; current, 100 mA. Error bars represent the standard deviation of a triplicate.*

The role of intermembrane distance on energy efficiency was subsequently studied for the recycling of high concentration gradient brines. Intermembrane distances were compared at a fixed velocity of 0.22 cm s^{-1}, corresponding to a residence time of 4.5 s. An energy efficiency of just 4.5 % was obtained for an intermembrane distance of 0.1 mm (Figure 3.6A). This was attributed to the energy demanded by the higher pressure drop for very thin intermembrane distances [10]. A rapid decline in power density was also observed at 0.1 mm (Figure 3.6B) attributed to the reduced stack volume limiting power production. However, a plateau in energy efficiency of around 16 % was established for intermembrane distances exceeding 0.1 mm, coupled with comparable power densities. This indicates that, similar to ED applications, larger spacer thickness improves RED energy recovery for high concentration gradients in recycle.

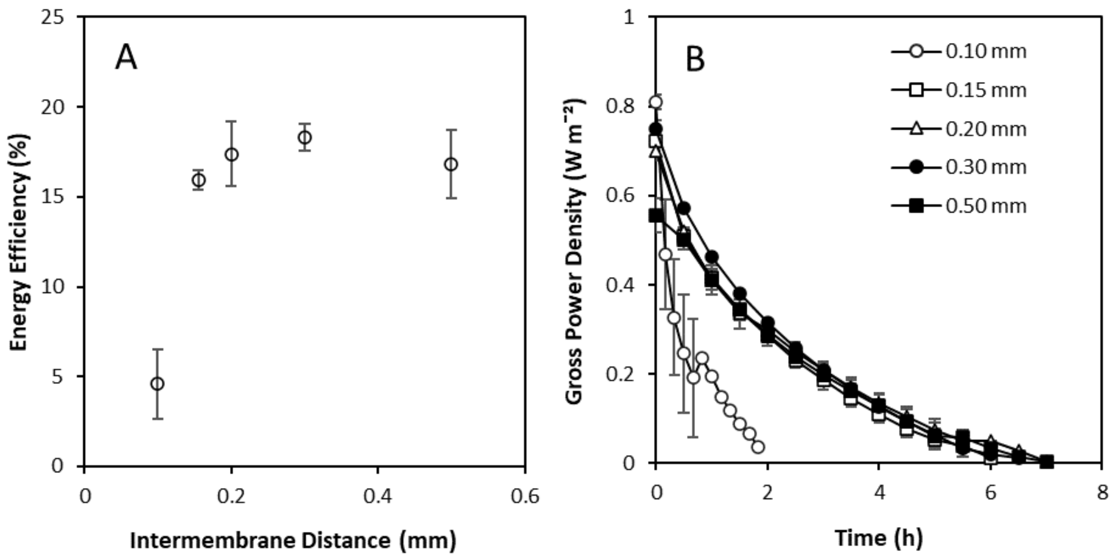

Figure 3.6. *Effect of spacer thickness on (A) energy efficiency and (B) power density over time using 4M and 0.02M feeds in recycle in a 10 cm x 10 cm RED stack containing 5 pairs Neosepta AMX/CMX membranes at a constant velocity of 0.22 cm* s^{-1}*, current 100 mA. Error bars represent the standard deviation of a triplicate.*

3.4 Conclusion

In this study, features conventionally associated with ED are demonstrated to improve energy recovery of RED utilising concentrated brines in recycle. To evidence this, commercially available ED and RED stacks were initially benchmarked in single pass. Whilst higher gross power densities were obtained in the RED module in single pass due to limited current in the ED modules, doubled energy efficiency was obtained using the ED stack when operated at low current densities in recycle. This increase in efficiency was attributed to the longer residence time at a fixed flow rate due to the larger intermembrane distance and reduced exergy losses from water transport facilitated by membrane properties. The performance of five commercially available pairs of ion exchange membranes for power production and energy recovery from a large concentration gradient was also evaluated. The highest power density and energy efficiency was obtained using Neosepta ACS/CMS membranes, attributed to the reduction in both water permeability and resistance, and an increase in membrane permselectivity. In contrast to sea/river applications where thinner intermembrane distances are typically preferred, increasing the intermembrane distance to 0.3 mm improved net power density, demonstrating that, similarly to ED, increased intermembrane distance can benefit performance when recycling concentrated brines.

Acknowledgements

This publication is based on research funded by the Bill & Melinda Gates Foundation (grant number OPP1149204). The findings and conclusions contained within are those of the authors and do not necessarily reflect positions or policies of the funders.

References

[1] A. Campione, L. Gurreri, M. Ciofalo, G. Micale, A. Tamburini, A. Cipollina, Electrodialysis for water desalination: A critical assessment of recent developments on process fundamentals, models and applications, Desalination. 434 (2018) 121–160.

[2] R.K. McGovern, S.M. Zubair, J.H. Lienhard V, The cost effectiveness of electrodialysis for diverse salinity applications, Desalination. 348 (2014) 57–65.

[3] S. Roy, S. Ragunath, Emerging membrane technologies for water and energy sustainability: Future prospects, constraints and challenges, Energies. 11 (2018) 2997.

[4] L. Liu, Q. Cheng, Mass transfer characteristic research on electrodialysis for desalination and regeneration of solution: A comprehensive review, Renew. Sustain. Energy Rev. 134 (2020) 110115.

[5] G.J. Doornbusch, M. Bel, M. Tedesco, J.W. Post, Z. Borneman, K. Nijmeijer, Effect of membrane area and membrane properties in multistage electrodialysis on seawater desalination performance, J. Memb. Sci. 611 (2020) 118303.

[6] W.J. Van Egmond, M. Saakes, S. Porada, T. Meuwissen, C.J.N. Buisman, H.V.M. Hamelers, The concentration gradient flow battery as electricity storage system: Technology potential and energy dissipation, J. Power Sources. 325 (2016) 129–139.

[7] S. Al-Amshawee, M.Y.B.M. Yunus, A.A.M. Azoddein, D.G. Hassell, I.H. Dakhil, H.A. Hasan, Electrodialysis desalination for water and wastewater: A review, Chem. Eng. J. 380 (2020) 122231.

[8] J. Veerman, D.A. Vermaas, Reverse electrodialysis: Fundamentals, in: A. Cipollina, G.M. Micale (Eds.), Sustain. Energy from Salin. Gradients, Woodhead Publishing, Cambridge, United Kingdom, 2016: pp. 77–133.

[9] M. Tedesco, H.V.M. Hamelers, P.M. Biesheuvel, Nernst-Planck transport theory for (reverse) electrodialysis: I. Effect of co-ion transport through the membranes, J. Memb. Sci. 510 (2016) 370–381.

[10] D.A. Vermaas, M. Saakes, K. Nijmeijer, Doubled power density from salinity gradients at reduced intermembrane distance, Environ. Sci. Technol. 45 (2011) 7089–7095..

[11] P. Długołecki, K. Nymeijer, S. Metz, M. Wessling, Current status of ion exchange membranes for power generation from salinity gradients, J. Memb. Sci. 319 (2008) 214–222.

[12] E. Güler, R. Elizen, D.A. Vermaas, M. Saakes, K. Nijmeijer, Performance-determining membrane properties in reverse electrodialysis, J. Memb. Sci. 446 (2013) 266–276.

[13] J. Veerman, R.M. de Jong, M. Saakes, S.J. Metz, G.J. Harmsen, Reverse electrodialysis: Comparison of six commercial membrane pairs on the thermodynamic efficiency and power density, J. Memb. Sci. 343 (2009) 7–15.

[14] W.J. van Egmond, U.K. Starke, M. Saakes, C.J.N. Buisman, H.V.M. Hamelers, Energy efficiency of a concentration gradient flow battery at elevated temperatures, J. Power Sources. 340 (2017) 71–79.

[15] R.S. Kingsbury, O. Coronell, Osmotic Ballasts Enhance Faradaic Efficiency in Closed-Loop, Membrane-Based Energy Systems, Environ. Sci. Technol. 51 (2017) 1910–1917.

[16] J. Veerman, M. Saakes, S.J. Metz, G.J. Harmsen, Reverse electrodialysis: Performance of a stack with 50 cells on the mixing of sea and river water, J. Memb. Sci. 327 (2009) 136–144.

[17] R.A. Tufa, S. Pawlowski, J. Veerman, K. Bouzek, E. Fontananova, S. Velizarov, J. Goulão, K. Nijmeijer, E. Curcio, Progress and prospects in reverse electrodialysis for salinity gradient energy conversion and storage, 225 (2018) 290–331.

[18] A. Daniilidis, D.A. Vermaas, R. Herber, K. Nijmeijer, Experimentally obtainable energy from mixing river water, seawater or brines with reverse electrodialysis, Renew. Energy. 64 (2014) 123–131.

[19] A. Tamburini, M. Tedesco, A. Cipollina, G. Micale, M. Ciofalo, M. Papapetrou, W. Van Baak, A. Piacentino, Reverse electrodialysis heat engine for sustainable power production, Appl. Energy. 206 (2017) 1334–1353.

[20] R. Long, B. Li, Z. Liu, W. Liu, Hybrid membrane distillation-reverse electrodialysis electricity generation system to harvest low-grade thermal energy, J. Memb. Sci. 525 (2017) 107–115.

[21] F. Giacalone, C. Olkis, G. Santori, A. Cipollina, S. Brandani, G. Micale, Novel solutions for closed-loop reverse electrodialysis: Thermodynamic characterization and perspective analysis, Energy. 166 (2019) 674–689.

[22] R.S. Kingsbury, S. Zhu, S. Flotron, O. Coronell, Microstructure determines water and salt permeation in commercial ion exchange membranes, ACS Appl. Mater. Interfaces. (2018) 39745–37956.

[23] F. Giacalone, P. Catrini, A. Tamburini, A. Cipollina, A. Piacentino, G. Micale, Exergy analysis of reverse electrodialysis, Energy Convers. Manag. 164 (2018) 588–602.

[24] D.A. Vermaas, J. Veerman, N.Y. Yip, M. Elimelech, M. Saakes, K. Nijmeijer, High efficiency in energy generation from salinity gradients with reverse electrodialysis, ACS Sustain. Chem. Eng. 1 (2013) 1295–1302.

[25] A.M. Hulme, C.J. Davey, A. Parker, L. Williams, S. Tyrrel, Y. Jiang, M. Pidou, E.J. McAdam, Managing power dissipation in closed-loop reverse electrodialysis to maximise energy recovery during thermal to electric conversion, Desalination. 496 (2020) 114711.

[26] J. Moreno, S. Grasman, R. Van Engelen, K. Nijmeijer, Upscaling Reverse Electrodialysis, Environ. Sci. Technol. 52 (2018) 10856–10863.

[27] P. Długołecki, P. Ogonowski, S.J. Metz, M. Saakes, K. Nijmeijer, M. Wessling, On the resistances of membrane, diffusion boundary layer and double layer in ion exchange membrane transport, J. Memb. Sci. 349 (2010) 369–379.

[28] M. Tedesco, A. Cipollina, A. Tamburini, W. van Baak, G. Micale, Modelling the Reverse ElectroDialysis process with seawater and concentrated brines, Desalin. Water Treat. 49 (2012) 404–424.

[29] J. Jang, Y. Kang, J.H. Han, K. Jang, C.M. Kim, I.S. Kim, Developments and future prospects of reverse electrodialysis for salinity gradient power generation: Influence of ion exchange membranes and electrodes, Desalination. 491 (2020) 114540.

[30] P. Długołęcki, A. Gambier, K. Nijmeijer, M. Wessling, Practical potential of reverse electrodialysis as process for sustainable energy generation, Environ. Sci. Technol. 43 (2009) 6888–6894.

4. Scale-up of reverse electrodialysis for energy generation from high concentration salinity gradients

Scale-up of reverse electrodialysis for energy generation from high concentration salinity gradients

A.M. Hulme[a], C.J. Davey[a], M. Pidou[a], E.J. McAdam[a]*

[a]Cranfield Water Science Institute, Cranfield University, Bedfordshire, MK43 0AL, UK

*Corresponding author: e.mcadam@cranfield.ac.uk

Abstract

Power production from a single reverse electrodialysis (RED) stack can be scaled-up by either increasing the size of each membrane or by increasing the number of cell pairs to increase the total membrane area, and hence power output. Whilst several studies have demonstrated the operation of large-scale RED, the effect of each scale-up strategy on performance has not been well investigated for applications utilising large concentration gradients. In this study, gross power density is demonstrated to increase as stack size and flow rate was increased for low (sea/river) concentration gradients and high concentration gradients (4M/0.02M), however, net power density was not improved due to the increased pumping power required by the larger stacks. Maximising net power density reduced total energy recovery in single pass across all stack sizes. It is therefore proposed that net power density is maximised prior to extending the path length through feed recycling, multi-stage configurations or increased cell pair number to improve both power and efficiency when scaling-up RED using concentrated brines. When a recycle configuration was adopted, the addition of cell pairs increased both power density and energy efficiency, demonstrating that this strategy should be employed to scale-up RED using high concentration gradients. An exergy analysis conducted using three stack sizes in recycle at a fixed residence time and current density determined a disproportionately large increase in exergy dissipated due to water, co-ion transport and concentration polarisation in the largest stack size. To minimise these effects, which are exacerbated by increased concentration gradients, the use of small stacks with a high cell pair number may be a preferable strategy to scale-up using these feeds.

Keywords: closed-loop; recycle; battery; thermal to electric; cell pair; membrane area

4.1 Introduction

Electricity consumption has increased to unprecedented levels due to worldwide population and economic growth [1], accelerating decarbonisation strategies to mitigate the effects of global warming [2]. This requires innovative solutions to produce ‘green’ energy in addition to technologies that can store energy from transient sources such as wind and solar to sustain the base load supply from renewables. Waste heat can be considered one relatively underexploited ‘green’ opportunity to meet electrical energy demand through thermal to electrical conversion, where around 246 PJ waste heat is available from industrial, residential and transportation sectors [3]. However, the majority of this heat energy is classified as low-grade heat (<100 ^{o}C) [3] which is not conducive to the use of organic rankine cycle [4] or thermoelectric generators [5] due to their high cost and low efficiencies. The reverse electrodialysis heat engine (RED-HE) has been theoretically demonstrated to obtain high exergy efficiency of up to 85 % using equivalent heat sources [6]. Low-grade waste heat is used in a distillation process to generate two solutions of different salinities [7,8]. The Gibbs free energy of mixing these two solutions across a reverse electrodialysis (RED) stack can then produce power by facilitating ionic transport across alternately arranged anion and cation exchange membranes, which is subsequently converted to an electrical current by a redox couple circulating across the electrode [9]. An analogous closed-loop RED configuration has been similarly demonstrated for energy storage [10], which implies that the same technology could respond to multiple demands underpinning the decarbonisation agenda.

Whilst RED has been demonstrated to produce high exergy efficiency at laboratory scale [11], successful implementation of RED technology requires that the power production estimated at laboratory scale can be realised following translation to full-scale, which includes matching the current and voltage specified. A single stack can be scaled up by increasing cell pair number [12] or increasing membrane dimensions (L x W), where both strategies increase total membrane area to deliver higher total power [9], however, the difference in outcomes yielded by these strategies have not been well investigated. Veerman et al. [13] provided the first study to demonstrate power production of RED using a larger stack of 25 cm x 75 cm, with a total membrane area of 18.75 m^2. Whilst several pilot plants have since been demonstrated on a range of feed waters and configurations (Table 4.1), there has been little research on the effect of scaling-up stack size on power and energy efficiency. Increasing cell pair number from 5 to 50 pairs in a typical laboratory stack size (10 cm x 10 cm) has been demonstrated to provide a proportionate increase in total power using artificial feeds with an equivalent concentration to sea and river water [12]. Comparable power densities have been observed for a 10 cm x 10 cm laboratory stack despite differences in cell pair number and membrane type, by fixing residence time across the different stack compositions. In a square stack, a 4Q increase is required following a doubling of length scale to match residence time, which subsequently doubles velocity. Moreno et al. [14] was similarly able to demonstrate comparable power density and energy efficiency across four stack sizes ranging from 6 cm x 6 cm to 44 cm x 44 cm by fixing residence time as a constant. At constant velocity, the authors noted that larger stack sizes led to an increase in gross energy efficiency and reduced unused exergy. In a square stack, a 2Q increase is required following a doubling of length scale to match velocity, which subsequently doubles residence time. This implies that longer residence times improve energy efficiency, due to increased utilisation of the concentration gradient.

Whilst evidence for the scalability of RED is encouraging, these studies all employed sodium chloride feeds with a fixed concentration equivalent to seawater/river water, where the electrochemical potential resulted in a maximum reported power density of 0.93 W m^{-2} [12]. Artificial saline solutions can instead be used in closed-loop applications, to increase the concentration gradient and subsequently improve power densities up to 6.7 W m^{-2} for the same salt [15]. However, the elevated concentration gradient establishes an osmotic gradient which promotes unfavourable water transport [16], which we propose can increase upon scale-up since water transport (i.e. flux) is theoretically linearly scalable. Concentration polarisation may also be exacerbated for larger membrane areas, due to the axial development of a more concentrated boundary layer induced by the high concentration gradient [17]. To illustrate, Tedesco et al. [18] obtained power densities up to 4 W m^{-2} using 5M and 0.5M sodium chloride (NaCl) feeds at 40 ^{o}C in a 10 cm x 10 cm stack. Increasing the stack size to 20 cm x 20 cm and doubling the cell pair number at constant velocity reduced power density (Table 4.1). However, energy efficiency was approximately constant at both process scales, despite an 8x increase in residence time. This contradicts behaviour reported for lower concentration salinity gradients, where significant improvement in energy efficiency has been reported as residence time was increased [14], which suggests that the approach to scale-up of RED for high concentration salinity gradients may be distinct from that studied for seawater/river water salinity gradients.

In RED, energy efficiency is defined as the percentage of available Gibbs free energy that is transformed into power production [9]. For closed-loop RED, the systems level efficiency is also determined by solution regeneration efficiency. For example, thermal utilisation efficiency [7] in the RED heat engine relates the thermal energy required for solution regeneration to the electrical energy generated by RED. This implies that energy extraction from the finite volume of regenerated working solution must be maximised to improve the thermodynamic efficiency ($\eta_{thermodynamic}$) [14]:

$$\eta_{thermodynamic} = \frac{P_{gross}}{(exergy_{in} - exergy_{out})} \quad \textbf{(4-1)}$$

This can be facilitated by increasing cell pair number [12] or introducing feed solution recycle which has been demonstrated to improve RED energy efficiency at lab-scale [11]. However, the cumulative effect of recycle may increase concentration polarisation and osmotic water transport phenomena, which must be managed to sustain power output and energy efficiency. Since these phenomena occur concomitantly, the impact is difficult to predict following scale-up. The aim of this study is therefore to investigate the scalability of RED for high concentration salinity gradients, by transitioning across three process scales: a standard 10 cm x 10 cm laboratory-scale stack, a 10 cm x 20 cm stack and a commercially available 10 x 40 cm stack. In a rectangular stack, no change in flow rate is required following a doubling of length scale to match velocity, whilst this subsequently doubles residence time. Whereas 2Q is required to sustain the same residence time, following doubling length scale of a rectangular stack, and results in doubling the crossflow velocity. The effect of scale-up is therefore comparable to Moreno et al. [13] for low concentration salinity gradients (seawater/river water). Specific objectives are to: (i) use a widely studied low concentration gradient (seawater/river water) to benchmark the high concentration salinity gradient across three stack sizes; (ii) challenge stack sizes at these concentration gradients to compare across flow rate, velocity and residence time to describe the scalability of power density at high concentration gradients; (iii) establish how energy efficiency improvements with recycle translate across stack sizes for high concentration salinity gradients; and (iv) compare the impact of increasing membrane area via stack size or cell pair number, to inform on stack design for high concentration gradients.

Table 4.1. *Summary of scaled-up RED systems in the literature using NaCl solutions or naturally-occurring sources with a salinity gradient.*

Concentrated Feed (M)	Dilute Feed (M)	Stack dimensions (cm x cm)	Cell Pairs	Total membrane area (m^2)	Spacer thickness (μm)	Feed Temp. (◦C)	Feed Velocity (cm s^{-1})	Power Density (W m^{-2})	Power (W)	Ref
0.51	0.017	25 x 74	50	18.75	200	25	0.1	0.62	-	[13]
0.51	0.017	10 x 10	10-50	0.2-1	200	25	1	≥ 0.93	0.2 - 0.93	[12]
0.48	0.003 - 0.009	-	-	-	-	-	-	-	Aim: 50 kW	[20]
5	0.5	20 x 20	100	8	270	40	1-3	3		[21]
4-5[a,b]	0.03[a,b]	44 x 44	125	48	280	17-31[a] 25-28[b]	1	0.8[a] 1.4[b]	40[a] 65[b]	[18]
4[a,b]	0.007 – 0.06[a,b]	44 x 44	1x 125 2x 500c	>400	280	17-31[a] 25[b]	0.5-0.9[a] 0.9[b]	1.7[a] 2.1[b]	330[a] 700[b]	[22]
0.5	0.01-0.06[d]	43 x 29	1000	250	100	16-22	1.5	0.38	95	[23]
0.51	0.017	6 x 6 10 x 10 22 x 22 44 x 44	50	0.36 1.00 4.84 19.36	0.155	25	0.25-2	1.4	-	[14]

–Indicates where no data is available. [a]Concentrated brine and brackish water with a conductivity equivalent to these concentrations. [b]Artificial solutions with a conductivity equivalent to these concentrations. [c]Modules operated in parallel. [d]Municipal wastewater and seawater with a conductivity equivalent to these concentrations.

4.2 Materials and Methods

4.2.1 Experimental setup for reverse electrodialysis stacks

Three reverse electrodialysis stacks with progressively increasing dimensions of 10 x 10 cm, 10 x 20 cm and 10 cm x 40 cm were used in these experiments, with fluid flowing across the longest length. The largest stack was a commercially available RED module (RED-800-2-25, FumaTech, Bietigheim-Bissingen, Germany) equipped with Titanium mixed metal oxide electrodes. The module had a total membrane area of 2 m^2, with 25 pairs of alternately stacked FAS-50 anion exchange and FKS-50 cation exchange membranes, separated by 0.155 mm integrated polyester spacers. Membranes and spacers from this stack were laser cut to size and alternately stacked between custom-made acetal endplates (Model Products LT, Bedfordshire, UK) for the two smaller stack sizes. Titanium mesh electrodes coated with a mixed metal oxide (MAGNETO special anodes, Schiedam, The Netherlands) were fixed inside the endplates.

Feed and electrode rinse solutions were pumped to the stack by peristaltic pumps (Watson Marlow, Cornwall, UK). Inline conductivity meters (2 CDH-SD1, Omega Engineering Limited, Manchester, UK and 2 Mettler Toledo Seven2Go Pro S7, Wolf Laboratories, York, UK) were fitted on the stack inlets and outlets, and the feed reservoirs were placed on balances (Kern SFB 20K2HIP, Scales and Balances, Thetford, UK). This enabled the water flux for each cell to be quantified at a range of conditions, following a simple mass balance. Stack size was initially varied at a constant cell pair number of 25 pairs, corresponding to a total membrane area of 0.5 m^2 in the smallest stack to 2 m^2 in the largest stack. To decouple the effect of stack size from total membrane area, stack size was also varied at a constant membrane area of 0.8 m^2. Cell pair number was varied from 5 to 25 cell pairs in the largest module (10 cm x 40 cm).

4.2.2 Preparation of solutions

Aqueous sodium chloride solutions were prepared using 99 % NaCl (Alfa-Aesar, Lancashire, UK) and deionised water. A 0.51M concentrated feed and 0.02M dilute feed, corresponding to standard sea/river water equivalent concentrations, were prepared, in addition to a 4M concentrated feed, previously identified as the best conditions to promote high power density. To enable comparison with the literature, experiments were initially carried out in single pass, using reservoirs with an excess of feed volume. For experiments carried out in 'recycle mode', reservoirs containing a fixed feed volume were prepared, with total feed volume normalised to membrane area. The electrode rinse solution contained 0.1M $K_3Fe(CN)_6$, 0.1M $K_4Fe(CN)_6$ (Fisher

Scientific, Leicestershire, UK) and 2M NaCl (Alfa-Aesar, Lancashire, UK). The electrode rinse volume was normalised to membrane area for all experiments.

4.2.3 Electrochemical Measurements

A potentiostat (IviumStat.h, Alvatek, UK) was used to carry out electrochemical measurements, with data logged using proprietary software (IviumSoft). Feeds were pumped through the stack until a stable open circuit voltage of <0.01 V s^{-1} was obtained before beginning experiments to ensure steady-state was achieved. All experiments were carried out in triplicate. Results are reported as mean and standard deviation. For single pass experiments, chronopotentiometry was carried out at a constant current until the voltage stabilised. The theoretical open circuit voltage was calculated using the Nernst equation [24]:

$$OCV = \frac{2nRT}{zF} \ln \frac{\gamma_c C_c}{\gamma_d C_d} \qquad \textbf{(4-2)}$$

Where n is the number of cell pairs, R is the universal gas constant (J K^{-1} mol^{-1}), T is the temperature (K), z is the valency of the ion, F is the Faraday constant (96,485 C mol^{-1}), γ is the mean activity coefficient of the counter-ion and C is the concentration of the counter-ion (mol), with the subscripts c and d referring to the concentrated and dilute feeds respectively. Maximum current was determined from the roots of the power/current curve produced. Power density, P_d (W m^{-2}), was obtained from the current and voltage produced, and was normalised to the total active membrane area in the module:

$$P_d = \frac{UI}{A} \qquad \textbf{(4-3)}$$

Where U is the voltage (V), I is the current (A), and A is the total membrane area (m^2). Net power is calculated to account for the power required for pumping [9]:

$$P_{net} = P_{RED} - P_p \qquad \textbf{(4-4)}$$

Where P_{net} is the net power (W), P_{RED} is the power produced by RED and P_p is the power required for pumping, calculated from:

$$P_p = \Delta p_C Q_C + \Delta p_D Q_D \qquad \textbf{(4-5)}$$

Where Δp is the pressure drop (Pa) and Q is the volumetric flow rate (m^3 s^{-1}). The pressure drop across the channel can be estimated from [25]:

$$\Delta p = \frac{12\mu l v}{h^2} \qquad \textbf{(4-6)}$$

Where μ is the viscosity (Pa s), l is the channel length (m), v is the fluid velocity (m s^{-1}) and h is the intermembrane thickness (m).

Experiments in which feeds were continuously recycle were carried out at a constant current until the voltage reached 0 V. Current density was normalised to the area of one electrode, with each stack tested at a range of current densities. Energy efficiency can be calculated from the work produced by RED, W_{RED}, and the total available Gibbs free energy of mixing in the system, ΔG_{mix}:

$$\eta_{RED} = \frac{W_{RED}}{\Delta G_{mix}} \times 100\% \quad \textbf{(4-7)}$$

The total work recovered can be calculated from:

$$W_{RED} = \sum_{t_o}^{t_{end}} UI \bigtriangleup t \quad \textbf{(4-8)}$$

where $\bigtriangleup t$ is the time interval (s), t_0 and t_{end} are the times at which work production by RED started and ended (when the voltage reached 0V), respectively [15]. The Gibbs equation is used to calculate the total energy available in the system:

$$\Delta G_{mix} = \Delta G_m - (\Delta G_c + \Delta G_d) \quad \textbf{(4-9)}$$

where $\bigtriangleup G$ is the energy available in each stream (J) with the subscripts m, c and d referring to the mixed outlet stream, the concentrated and the dilute feeds, respectively. For ideal solutions, and assuming total mixing of the concentrated and dilute streams, $\bigtriangleup G_{mix,}$ is calculated from

$$\Delta G_{mix} = -(N_c + N_d)T\Delta S_m - (-N_c T\Delta S_c - N_d T\Delta S_d) \quad \textbf{(4-10)}$$

where N is the number of moles (mol), T is the temperature (K) and $\bigtriangleup S$ is the molar entropy (J K^{-1} mol^{-1}). $\bigtriangleup S$ can be obtained as follows:

$$\Delta S = -R \sum_i x_i \ln x_i \quad \textbf{(4-11)}$$

where x is the mole fraction of species i.

4.3 Results and discussion

4.3.1 Highest gross power achieved using the largest stack size at the highest flow rates

The three stacks (10 cm x 10 cm, 10 cm x 20 cm and 10 cm x 40 cm) were initially compared in single pass to evidence the effect of stack size on power density. To set a benchmark, initial experiments were carried out using a concentration gradient equivalent to seawater/river water and repeated using a 4M feed to establish the effect of a higher concentration gradient. For seawater/river water, a minimum open circuit voltage (OCV; indicating electrochemical potential) was recorded at the lowest flow rate. Once flow rate was increased above 0.3 l min^{-1}, a plateau was achieved at 3.42 ± 0.09 V for all three stack sizes (Figure 4.1A), which was attributed to a reduction in concentration polarisation [26]. Notably, this plateau was reached at lower flow rates for the smaller stacks, due to the increasing boundary layer thickness which developed axially along the extended path length as stack size increased [17]. Consequently, higher flow rates are required to achieve similar voltages as stack size is increased. To illustrate, an OCV of 3.2 V was obtained using the smallest stack at a flow rate of 0.06 l min^{-1}, in comparison to 2.9 and 2.3 V by the 10 cm x 20 cm and 10 cm x 40 cm stacks, respectively, at an equal flow rate. For the 4M concentrated feed, a similar trend was observed with each of the stacks producing an OCV of around 4.73 V (Figure 4.1D). Estimation of the maximum theoretical OCV based on the Nernst Potential (Equation 4-2) indicated that whilst the OCV obtained using the 0.5M concentrated feed was close to the theoretical maximum of 3.84 V, the maximum obtained using the 4M concentrated feed was significantly lower than the theoretical OCV of 6.66 V. This is likely due to the uncontrolled movement of ions [14] occurring because of the increased driving force provided by the larger concentration gradient; an effect exacerbated by the increased membrane area in the larger stacks.

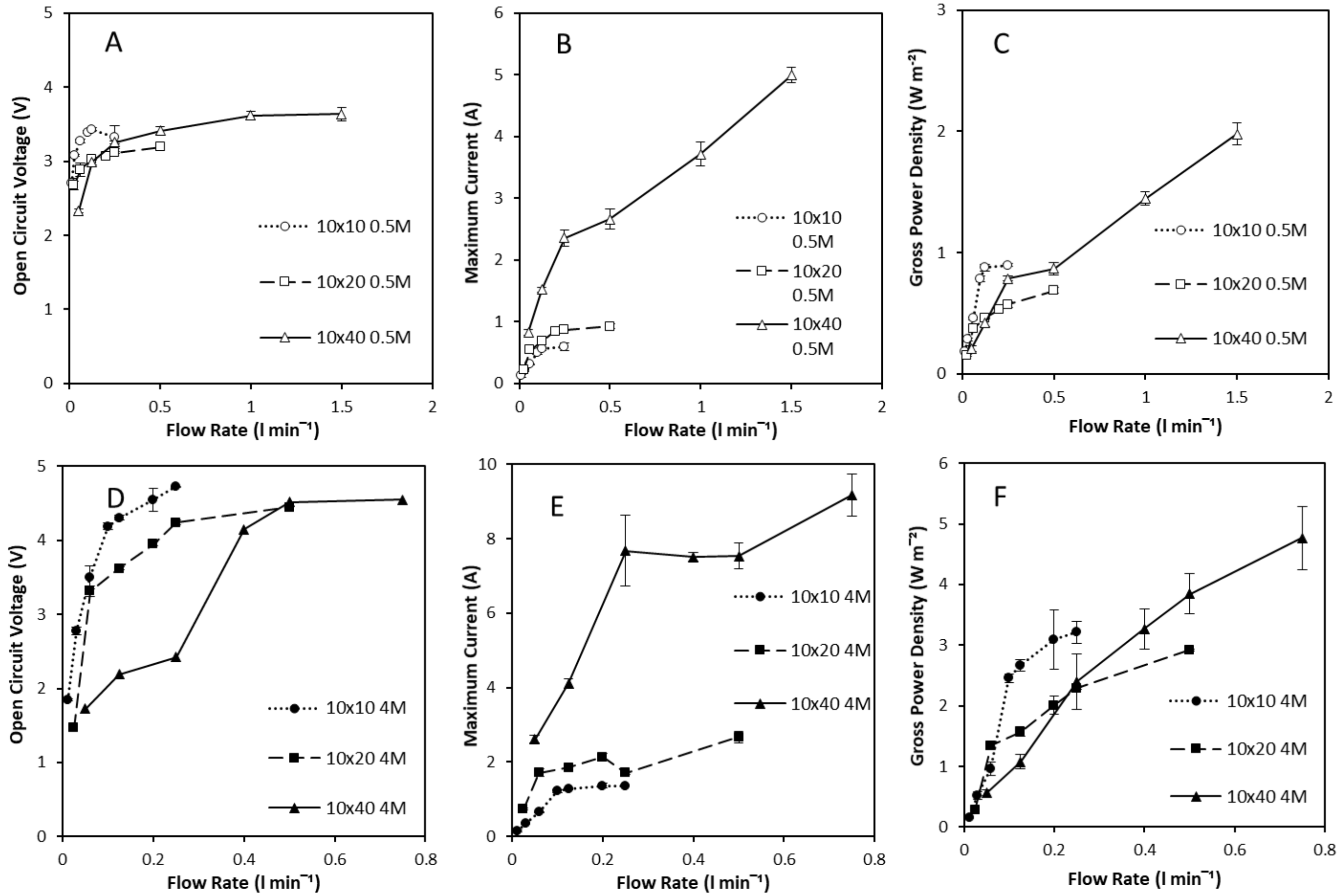

Figure 4.1. *Effect of stack size and flow rate at constant cell pair number on (A) power density; (B) open circuit voltage; and (C) maximum current using 0.51M and 0.02M feeds in single pass, and (D) maximum power density (E) open circuit voltage and (F) maximum current using 4M and 0.02M feeds in single pass. Cell pair number was fixed at 25 pairs; feed temperature, 25 °C. Error bars represent the standard deviation of a triplicate.*

For both concentrations gradients, the current recorded at a fixed flow rate increased with stack size. Maximum current was achieved through increasing flow rate for both the 0.5M and 4M feeds (Figure 4.1B, E). This is because the increased membrane surface area facilitates greater total ionic transfer; the ionic flux further benefitting from reducing concentration gradient at the membrane-fluid boundary with higher flow rates [26]. This accords with the gross power density (Pd) in which the highest Pd of 1.98 W m^{-2} and 4.77 W m^{-2} was recorded for the largest stack at the highest flow rate using a 0.5M and 4M concentrated feed, respectively. As power output is the product of current and voltage, it can be inferred that this is mainly due to the contribution of the significantly increased current, as voltage remains approximately constant across all stack sizes. However, at a constant flow rate, the highest power density is obtained in the smallest stack (Figure 4.1C). For example, for the 4M concentrated feed at a flow rate of 0.25 L min^{-1}, power densities of 3.2 W m^{-2}, 2.4 W m^{-2} and 2.3 W m^{-2} are obtained with the 10 cm x 10 cm, 10 cm x 20 cm and 10 cm x 40 cm stacks respectively (Figure 4.1F). This discontinuity can be explained by the cumulative effect of the increase in current coupled with the development of a more concentrated boundary layer. Since the length scale increases in only one dimension for rectangular stacks, a fixed flow rate for each stack size is equivalent to fixing velocity. When the path length is short, high power densities are obtained despite the lower current, as concentration polarisation is negligible which increases the voltage. Conversely, once the path length is extended at an equivalent velocity, the current increases due to the increase in membrane surface area and feed side residence time. This drives the development of a more concentrated boundary layer when complemented by the extension in path length, subsequently diminishing the potential such that lower gross power densities are achieved for these conditions at larger stack sizes; an effect exacerbated for high concentration gradients.

To compensate for the extended path length, Moreno et al. [14], proposed that residence time could be used to achieve comparable performance between square RED stacks of increasing size when applied to seawater/river water concentration gradients:

$$\tau = \frac{l}{v} \tag{4-12}$$

where τ is residence time (s), v is velocity (m s^{-1}), and L is path length (m). When doubling the length of the rectangular stack from 10 cm x 10 cm to 10 cm x 20 cm, flow rate must be increased 2Q to fix an equivalent residence time, which consequently doubles feed velocity. The implication is that at an equivalent residence time, ionic flux becomes comparable across stack sizes [14], whilst a secondary implication is that the increased polarisation phenomenon observed for larger stack sizes may be compensated for by the higher feed side velocity imposed.

For the low concentration gradient, similar OCVs were obtained for each stack size at a constant residence time when a 0.5M concentrated feed was used (Figure 4.2A). For residence times in the range 30 to 190s, the maximum current increased approximately in proportion to the stack membrane area (Figure 4.2B). Consequently, power densities recorded for the low concentration gradient within this range of residence times were comparable for each stack size (Figure 4.2C)., which accords with experience in scaling-up RED for seawater/river water [14]. For residence times below 30s, divergence of the power density data was evident, due to the disproportionate increase in current created by the largest stack size. This can be accounted for by the significantly higher feed velocity applied at comparable residence times, which reduced concentration polarisation to improve ionic transport. For the high concentration salinity gradient, OCV was approximately constant across stack sizes for residence times <20 s (Figure **4.2**D). However, for longer residence times, a considerably lower OCV was recorded for the large stack. Whilst current was higher for the 4M feed, the trend was comparable to the low concentration gradient where an approximately proportionate relationship between membrane area and current was identified between residence times of 80 s and 190 s. However, power densities were not comparable between stack sizes, indicating that the higher ionic transport, and subsequent complex polarisation phenomena made it difficult to predict scale-up for high concentration gradients (Figure 4.2F); an effect that could be made more complex at longer residence times due to the enhanced water transport observed for high concentration gradients [19].

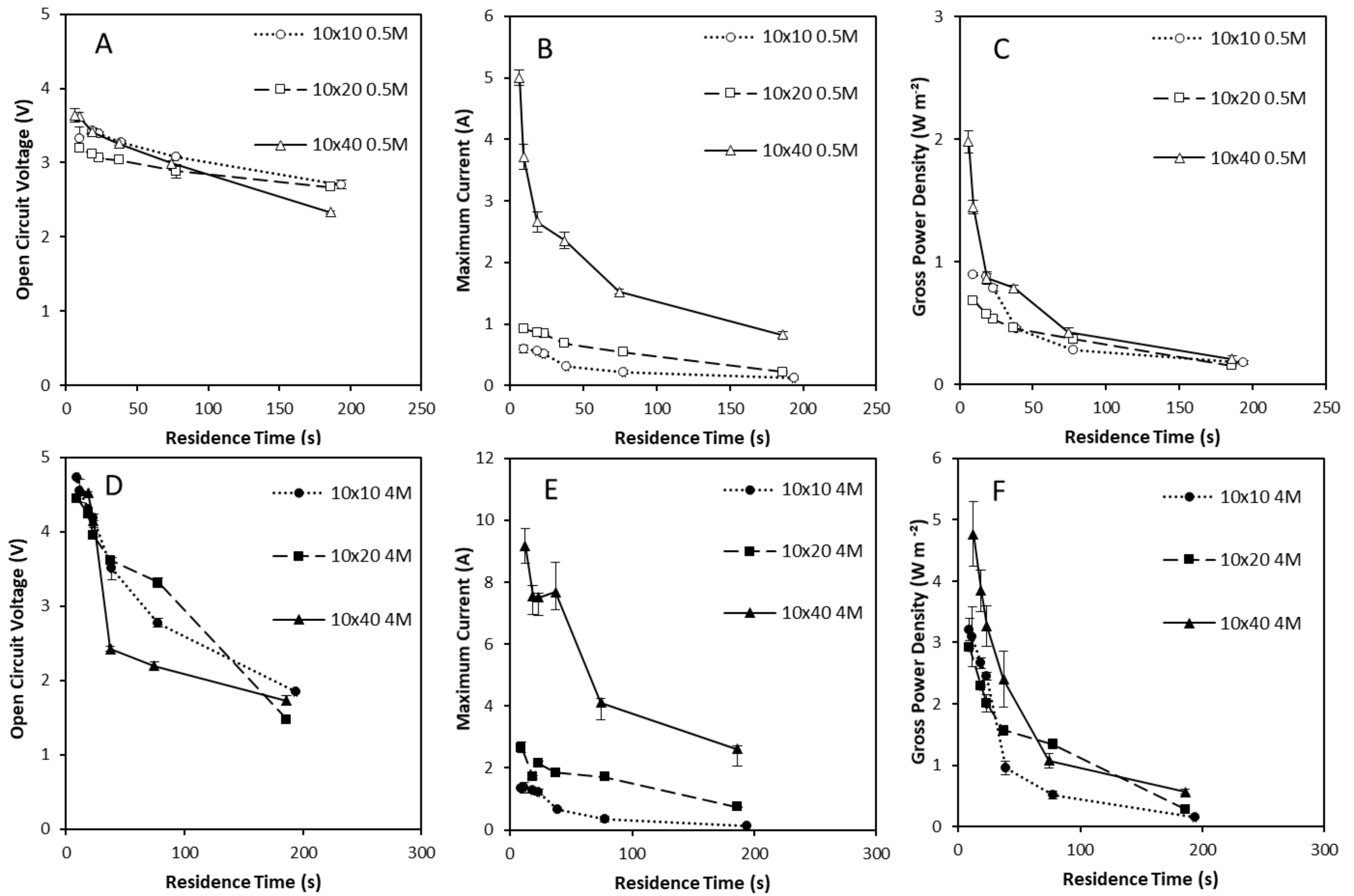

Figure 4.2. *Effect of stack size and residence time at constant cell pair number on (A) power density; (B) open circuit voltage; and (C) maximum current using 0.51M and 0.02M feeds in single pass, and (D) maximum power density: (E) open circuit voltage; and (F) maximum current using 4M and 0.02M feeds in single pass. Cell pair number was fixed at 25 pairs; feed temperature, 25 °C. Error bars represent the standard deviation of a triplicate.*

4.3.2 Net power density and energy efficiency trade-off when scaling-up in single pass

The highest gross power density was recorded at the shortest residence time for the 10 cm x 40 cm stack (Figure 4.2C). However, due to the increased pressure drop imposed by higher flow rates (4Q versus the 10 cm x 10 cm) and longer channel length within the larger stack, a negative net power density was recorded with the lower concentration gradient for residence times <20 s, making it impractical for implementation (Figure 4.3A). In contrast, at the higher concentration gradient, net power density was consistently positive, with the highest net power densities recorded at the shortest residence times (Figure 4.3B). This can be ascribed to the concentration gradient promoting high electrochemical potential coupled with the relative increase in fluid velocity that corresponds to a decrease in residence time, which reduces boundary layer thickness, subsequently improving ionic transport [15,27].

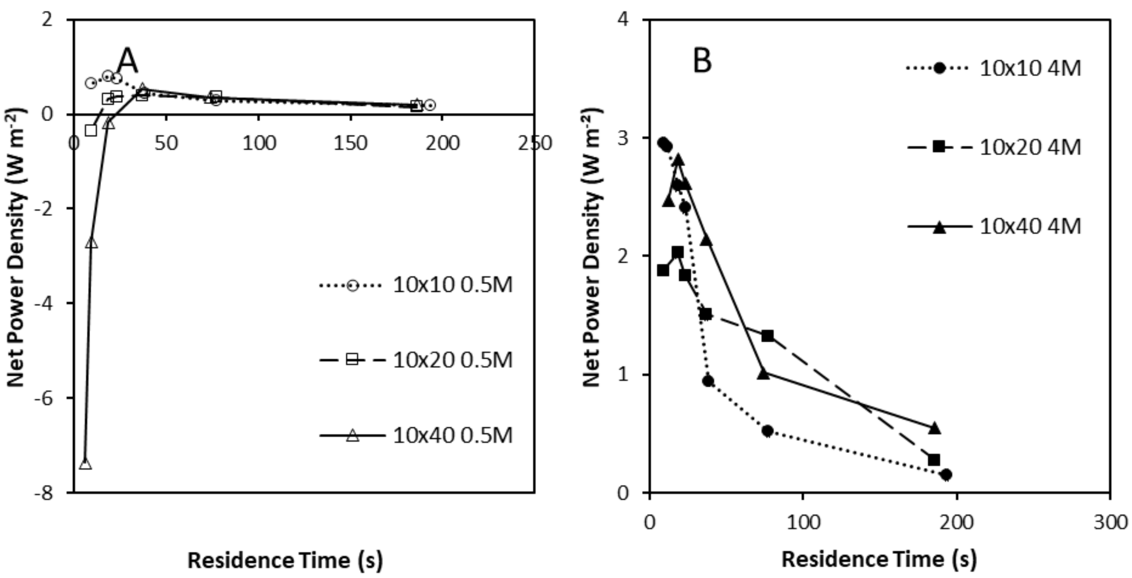

Figure 4.3. *Effect of stack size and flow rate on net power density for (A) 0.5M concentrated feed and (B) 4M concentrated feed in single pass. Cell pair number was fixed at 25 pairs; feed temperature, 25 °C.*

Whilst gross power density was considerably higher for the largest stack with the 4M feed, comparison between the 10 cm x 10 cm and 10 cm x 40cm stack demonstrates comparable net power densities owing to the increased pressure drop of the larger stack compensating for the gain in net power density [15,27]. Consequently, the comparative unitary membrane cost (€ kWh^{-1}) between the small and large stacks can be considered comparable; selection is therefore likely to be based on a systems engineering approach between the relative capital cost of the increased pump duty for the larger stack versus the reduced current provided by the small stack. This is illustrated by comparing the net energy generated per unit of feed (Wh m^{-3}) versus the net power density created at each residence time studied (Figure 4.4). Maximum power density is realised at the shortest residence time that corresponds to the lowest volumetric energy recovery, and conversely the minimum power density is recorded for the residence time which provides the highest volumetric energy recovery. For closed-loop applications, this implies a trade-off between system efficiency and the capital cost required for power generation, to minimise exergy destruction and improve efficiency of the combined system (RED with regenerative step). An alternative perspective is to approach stack design for closed loop application as a classical mass transfer problem [28]:

$$\frac{C}{C_0} = e^{-\frac{kal}{v}} \tag{4-13}$$

which identifies that in order to maximise utilisation of the feedside concentration (C/C_0), the mass transfer coefficient (k, m s^{-1}) is first optimised through limiting the boundary layer thickness, by increasing fluid velocity (short residence time), followed by extending path length in order to extend residence time (l/v, s). The proposed approach is therefore to maximise net power density from the stack, and extend path length, by increasing the number of RED stacks in series, or recycling the feed to reduce unused exergy leaving the stack [15,29]. A similar design approach was proposed by Weiner et al [30] for RED systems using sea and river water feeds following pre-treatment. This work indicates that such a strategy is also applicable to concentrated brines for closed-loop applications where pre-treatment is not required.

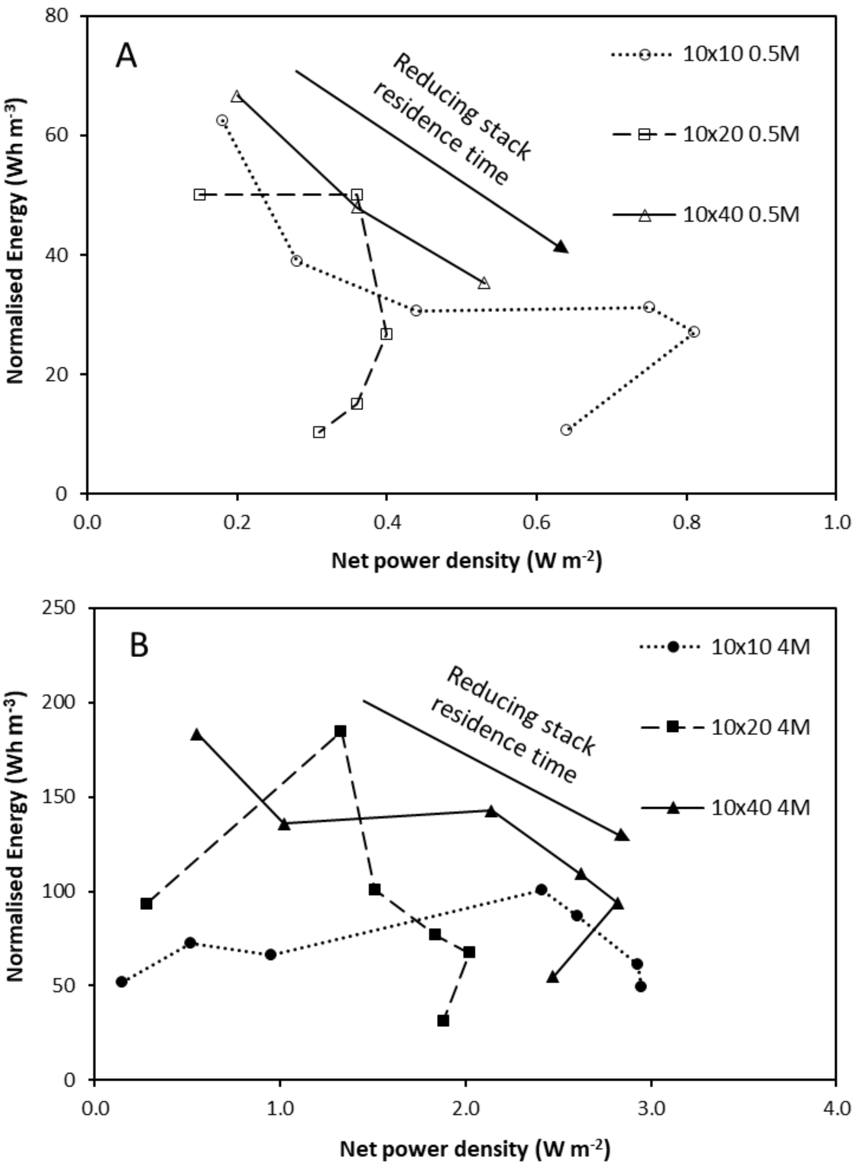

Figure 4.4. *Normalised energy and net power density for (A) 0.5M concentrated feed and (B) 4M concentrated feed in single pass at varying residence times. Cell pair number was fixed at 25 pairs; feed temperature, 25 °C.*

4.3.3 Gross energy efficiency increases as cell pair number is increased for concentrated brines in recycle

Cell pair number was varied in the largest stack (5 to 25 cell pairs) to establish the impact on power density and energy generation from a high concentration gradient. In single pass, power density and current density increased with cell pair number (Figure 4.5A). Open circuit voltage increased linearly with an increase in cell pair number, in accordance with the Nernst Equation (Figure 4.5B). Consequently, net power density increased with an increase in cell pair number and is comparable in effect to operating RED stacks in parallel (Figure 4.5C). However, current density (normalised to the area of one electrode) also increased with cell pair number (Figure 4.5D), which can be ascribed to the increased ionic transport imparted by the higher flow rate required to sustain a comparable residence time with increasing cell pair number. This contrasts with Veerman et al. [12] who observed a constant current density as cell pair number increased when using seawater and river water. We propose that the distinction arises from the concentration gradient employed, where ionic transport is comparatively less effected by concentration polarisation at lower concentration gradients and is comparable to previous work [31].

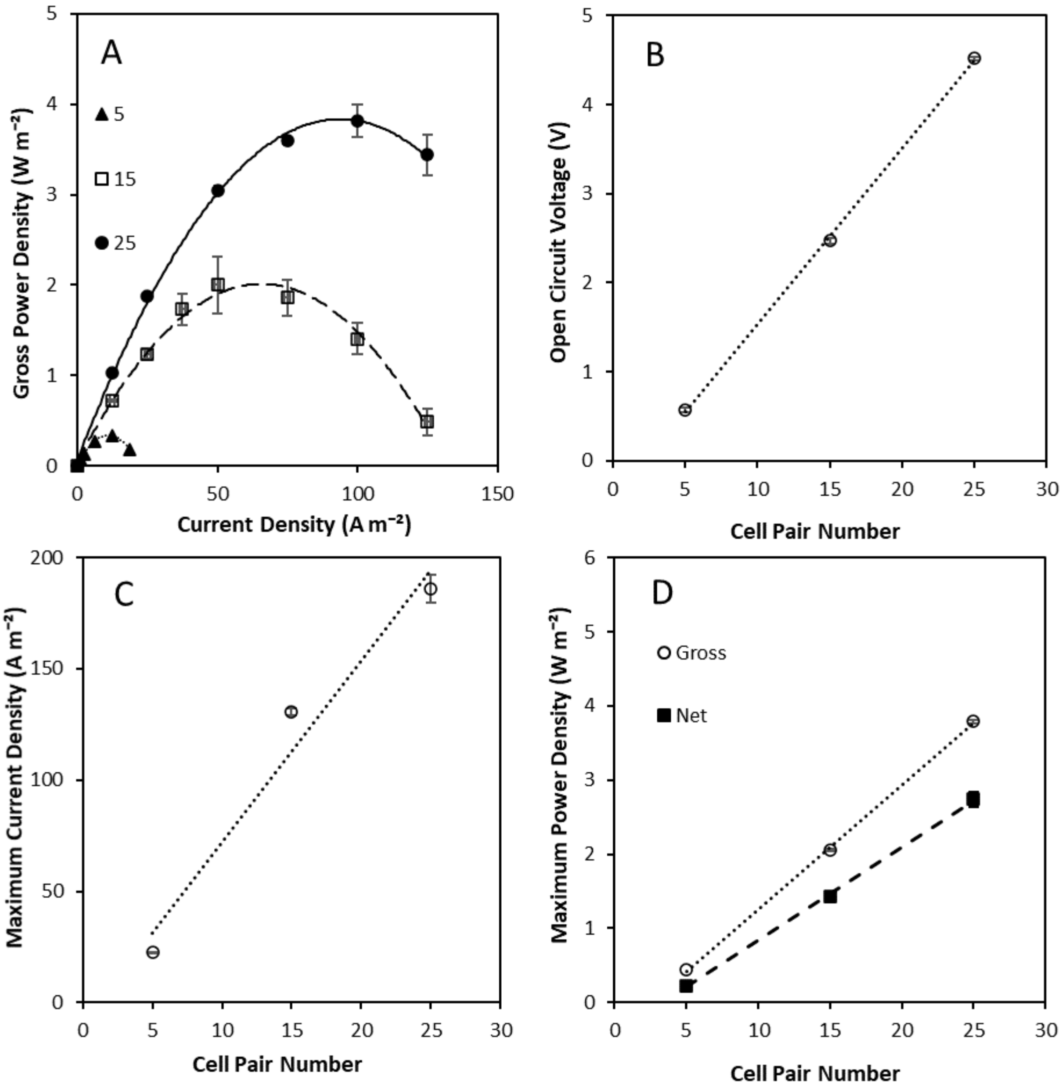

Figure 4.5. *Effect of varying cell pair number on (A) power density and current density; (B) open circuit voltage; and (C) maximum current density and (D) maximum gross and net power density obtained using 4M and 0.02M feeds in single pass in a 10 cm x 40 cm RED stack. Residence time fixed at 20 s; and feed temperature, 25 °C. Error bars represent the standard deviation of a triplicate.*

The effect of increasing cell pair number when utilising a large concentration gradient in recycle was also established. An increase in energy efficiency was observed when cell pair number was increased in recycle at a constant current density (Figure 4.6A)**.** This is likely to be because of the increased ionic transport facilitated by the increased membrane area, enabling greater power production. Water flux was approximately constant across all cell pair numbers (Figure 4.6B). The improvement in power density and energy efficiency indicates that increasing the cell pair number is an effective strategy to improve performance and scale-up RED for concentrated brine applications.

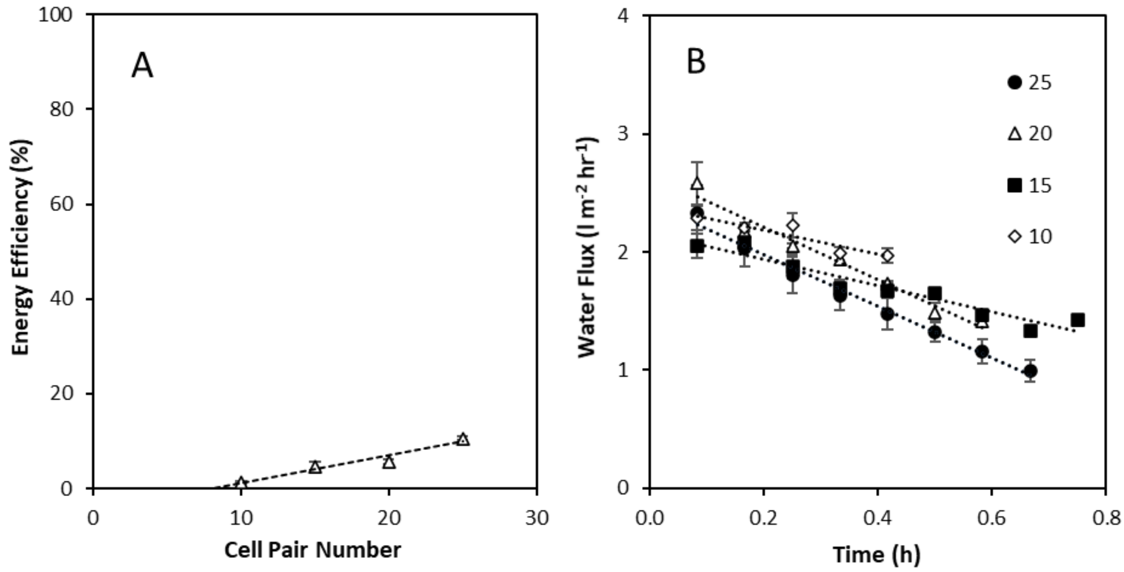

Figure 4.6. *Effect of cell pair number on (A) energy efficiency and (B) water flux. 4M and 0.02M feeds in recycle using a 10 cm x 40 cm RED stack. Feed volume was normalised to membrane area and residence time fixed at 20 s; feed temperature, 25 °C; current density, 60 A m^{-2}. Error bars represent the standard deviation of a triplicate.*

4.3.4 Increased exergy dissipation at large stack sizes reduces efficiency

A high concentration gradient (4M and 0.02M) was established across the three stacks, and the solutions operated in recycle. The electrochemical potential declined as feeds were recirculated (Figure 4.7A), comparable to the discharge of a battery [29]. Energy efficiency subsequently improved during discharge, which reflected the increased utilisation of the concentration gradient (Figure 4.7B). The discharge curve was characterised by two phases, an initial linear decline in energy generation, followed by a non-linear phase, which terminated in a plateau (Figure 4.7B). At a fixed current density (40 A m^{-2}) and residence time (20 s), the smallest stack achieved the highest energy efficiency. The higher exergy losses for larger stack sizes was due to the increased water transport, induced by the increase in membrane surface area (Figure 4.7C,D). For both stacks, power production is observed to terminate whilst a residual concentration difference remains. This is attributed to the effect of concentration polarisation on the dilute feed, due to osmosis from the dilute to the concentrated feed, prohibiting the movement of ions and hence power production.

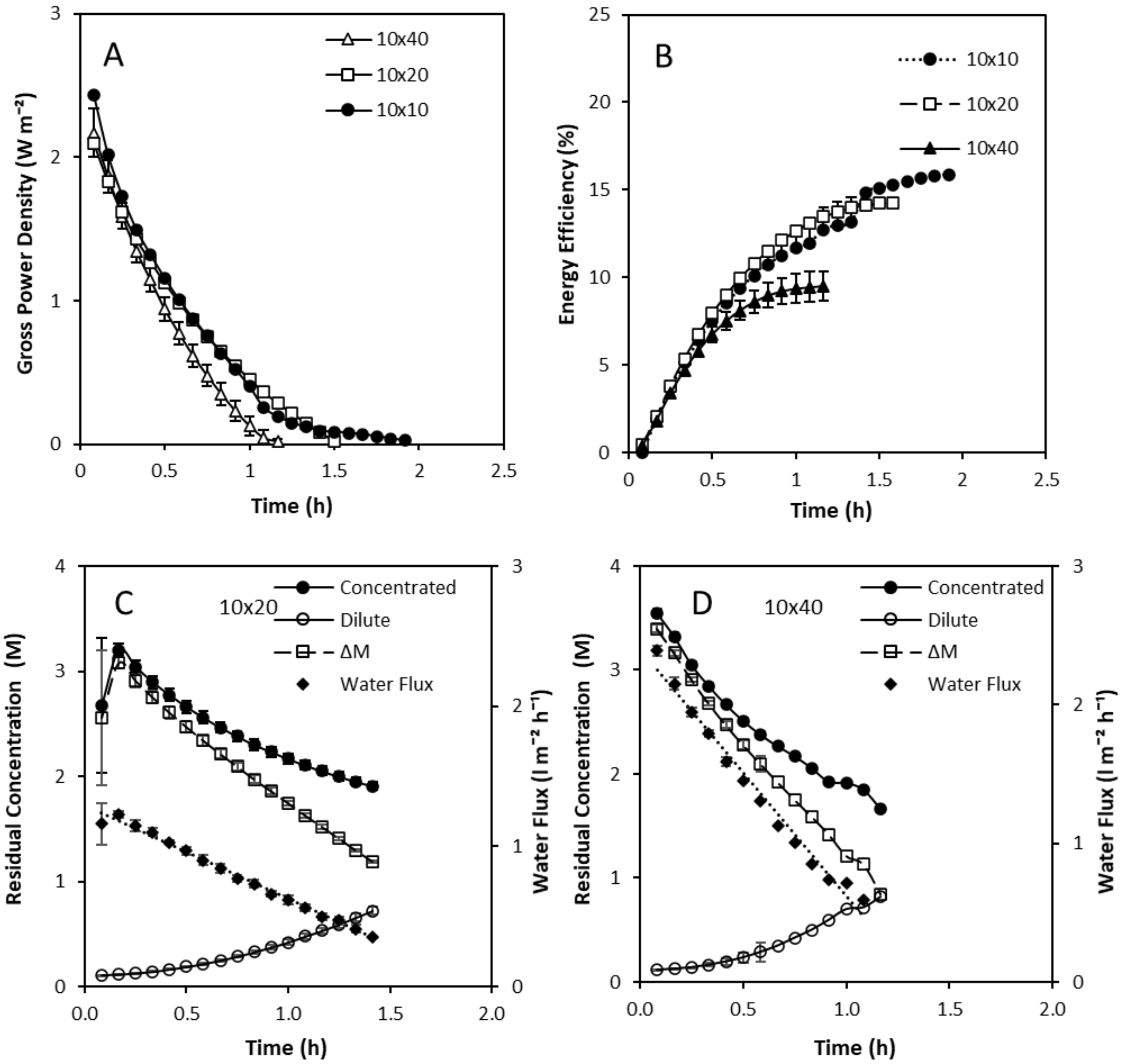

Figure 4.7. *Effect of stack size on (A) Gross power density over time and (B) energy efficiency over time from 4M and 0.02M feeds in recycle. Feed volume was normalised to membrane area; residence time fixed at 20 s; current density, 40 A m⁻²; feed temperature, 25 °C. Concentration profile and water flux at stack size of: (C) 10 cm x 20 cm; and (D) 10 cm x 40 cm.*

An exergy analysis of the three stacks demonstrates that recycling feeds minimises the unused exergy in the effluent, however, the majority of exergy provided to each stack was dissipated and not used for power production (Figure 4.6F). These exergy losses were greatest for the largest stack at 89 %, resulting in just 10 % of the available energy being utilised for power production, compared to 13 % and 14 % in the 10x10 and 10x20 stacks, respectively (Figure 4.8A). Moreno et al. [14] similarly determined an increase in exergy loss due to water flux and co-ion transport as stack size increased for sea and river water feeds in single pass at an equal velocity, with 55 % of exergy dissipated in the 44 cm x 44 cm stack compared to 15 % in a 6 cm x 6 cm stack. Increased exergy losses are expected as the concentration gradient is increased due to greater water and co-ion transport [16,29]. However, in this study, the increase in water flux (normalised for membrane surface area) was not proportional to membrane surface area, and instead increased for larger stack sizes. This can be explained by the higher velocity required for the largest stack size, to sustain a comparable residence time, which was four times greater for the 10 cm x 40 cm compared to the 10 cm x 10 cm stack. Water transport from the low concentration compartment, dilutes the salinity concentration within the high concentration boundary layer, which is compensated for by surface renewal at higher velocities. This re-establishes the concentration gradient within the high concentration boundary layer, which serves to enhance osmotic transport at the higher velocities imposed in the 10 cm x 40 cm stack; an effect exacerbated by the higher ionic transport imposed with the larger surface area, resulting in the increased exergy dissipated observed (Figure 4.8B). Whilst an increase in gross efficiency was observed by Moreno et al. [14] as stack size was increased, this was not observed in this study due to the non-linearity of exergy losses resulting in the highest energy efficiency being achieved by the intermediate stack (Figure 4.8B). As recycling the feeds minimised the unused exergy leaving the stack, thermodynamic efficiency (Equation 4-1) was similar to the gross energy efficiency (Equation 4-7) in this study. The improved efficiency achieved by the intermediate stack despite recording the lowest gross power density in single pass (Figure 4.1), demonstrates the trade-off which must be made between power density and efficiency [32] when scaling systems using a large concentration gradient in recycle.

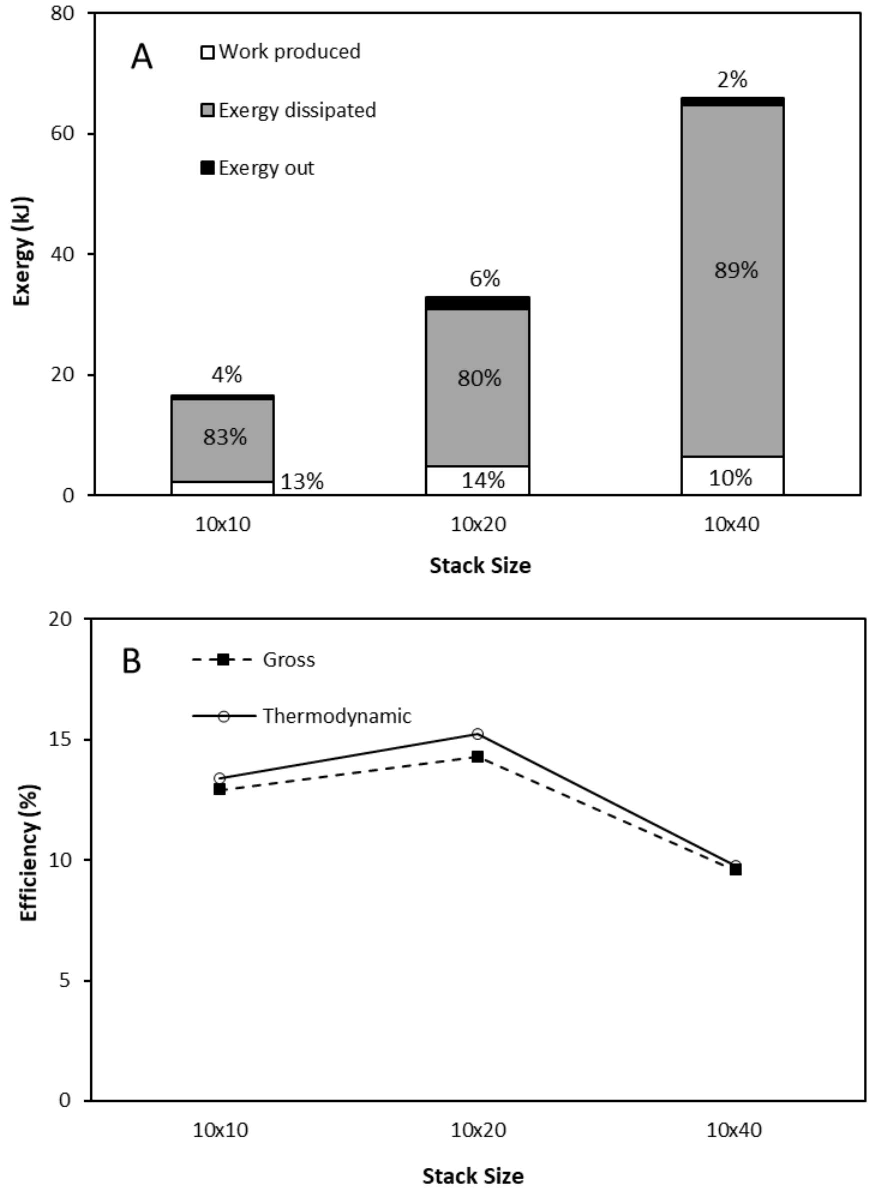

Figure 4.8. *(A) Exergy analysis and (B) gross and thermodynamic efficiency obtained by the three stack sizes from 4M and 0.02M feeds in recycle. Feed volume was normalised to membrane area; residence time fixed at 20 s; current density, 40 A m^{-2}; and feed temperature, 25 °C. Error bars represent the standard deviation of a triplicate.*

Increasing current density decreased water flux for all stack sizes (Figure 4.9), suggesting that an increase in electro-osmosis counteracts water transport [29]. The optimum current, for which maximum energy efficiency was recorded, increased with stack size (Figure 4.10), which is likely due to the higher flow rate required for an equivalent residence time facilitating greater ionic transport [14] and indicates that improved performance could be obtained by larger stacks by operating at an increased current density.

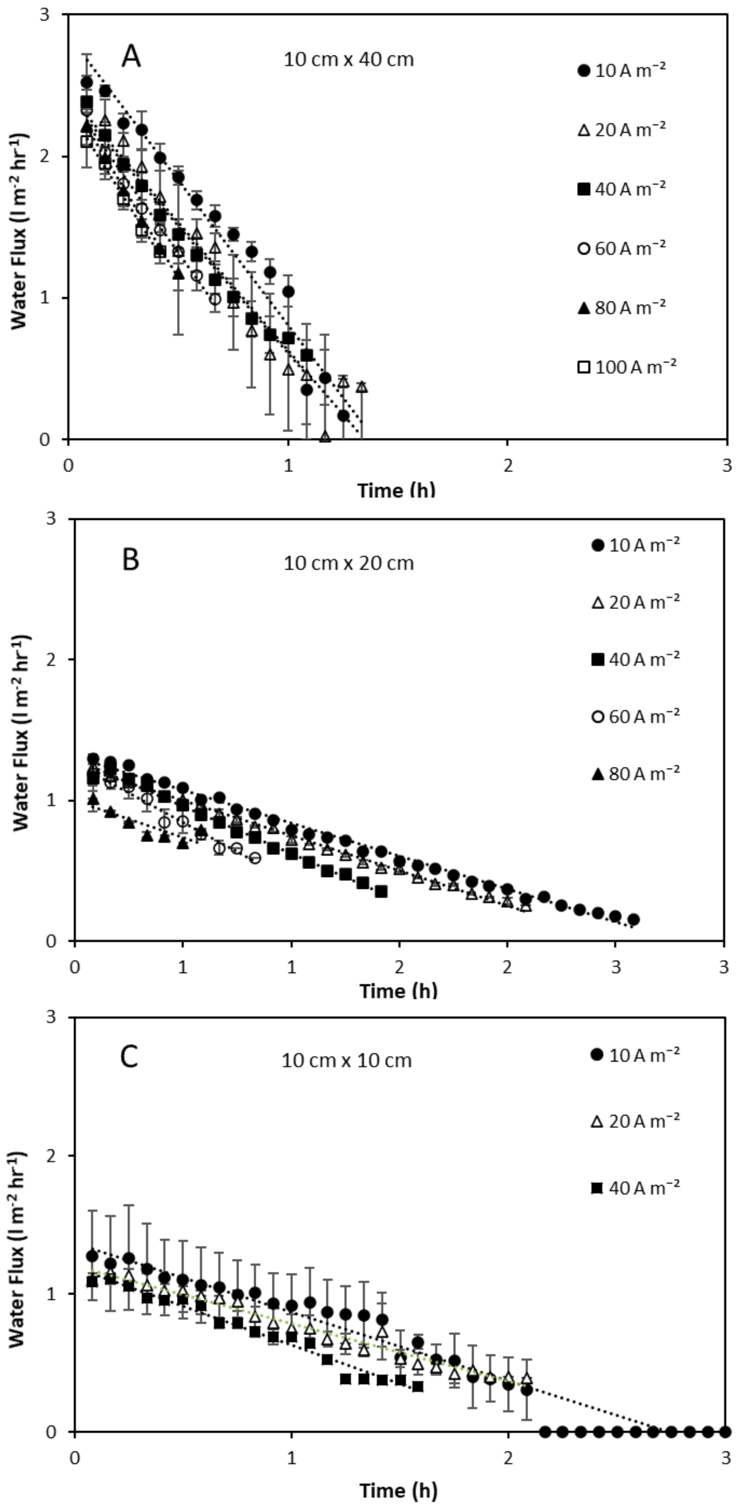

Figure 4.9. *Effect of current density on water flux over time for (A) 10 cm x 40 cm (B) 10 cm x 20 cm and (C) 10 cm x 10 cm at fixed cell pair number. Feed volume was normalised to membrane area and residence time fixed at 20 s. Cell pair number was fixed at 25 pairs; feed temperature, 25 °C. Error bars represent the standard deviation of a triplicate.*

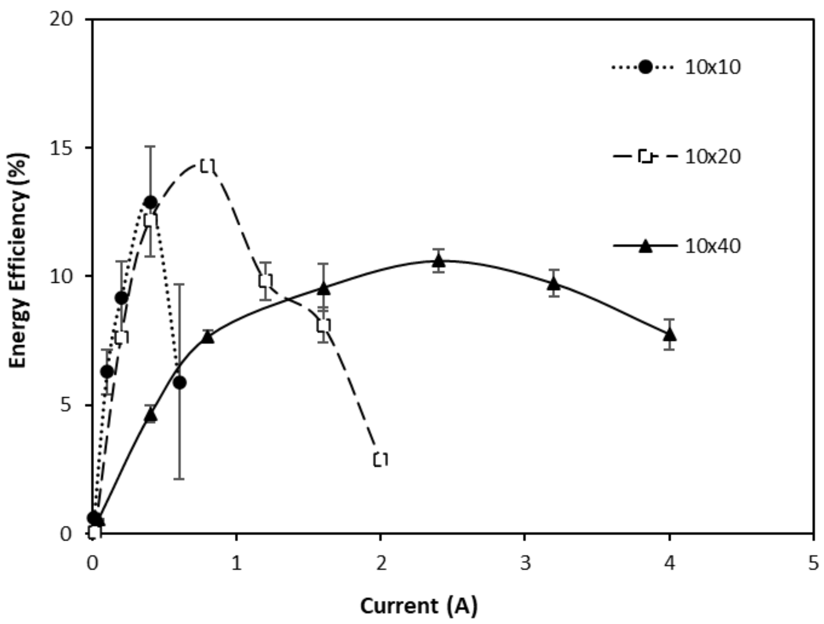

Figure 4.10. *Effect of stack size and current on energy efficiency from 4M and 0.02M feeds in recycle. Feed volume was normalised to membrane area and residence time fixed at 20 s. Cell pair number was fixed at 25 pairs; feed temperature, 25 °C; current density, 40 A m^{-2}. Error bars represent the standard deviation of a triplicate.*

Cell pair number was varied to decouple stack size from membrane area, by fixing stack membrane area at 0.8 m^2. For a fixed current density (60 A m^{-2}) and residence time (20 s), an initial power density of 3.0, 2.6 and 1.1 W m^{-2} was produced by the smallest, intermediate and largest stack size respectively (Figure 4.11A). Voltage decreased as stack size was increased (Figure 4.11B) which can be explained by the decreased cell pair number required to maintain an equivalent membrane area. Energy efficiencies of 1.3 % and 10.9 % were identified in the largest and smallest stack respectively (Figure 4.11C), where the lower efficiency can be explained by concentration polarisation developing axially along the extended channel [17] subsequently decreasing concentration gradient [14]. As the current density was normalised to electrode area, the absolute current increased as stack size increased which could have inhibited voltage, as voltage decreases as current is increased [33]. Consequently, membrane area must be considered when selecting an optimal current for operation in recycle. To minimise concentration polarisation and maximise the use of a fixed membrane area, a small stack size with a large number of cell pairs offers improved energy efficiency and power, and is preferable to large stacks which promote water transport leading to greater exergy loss.

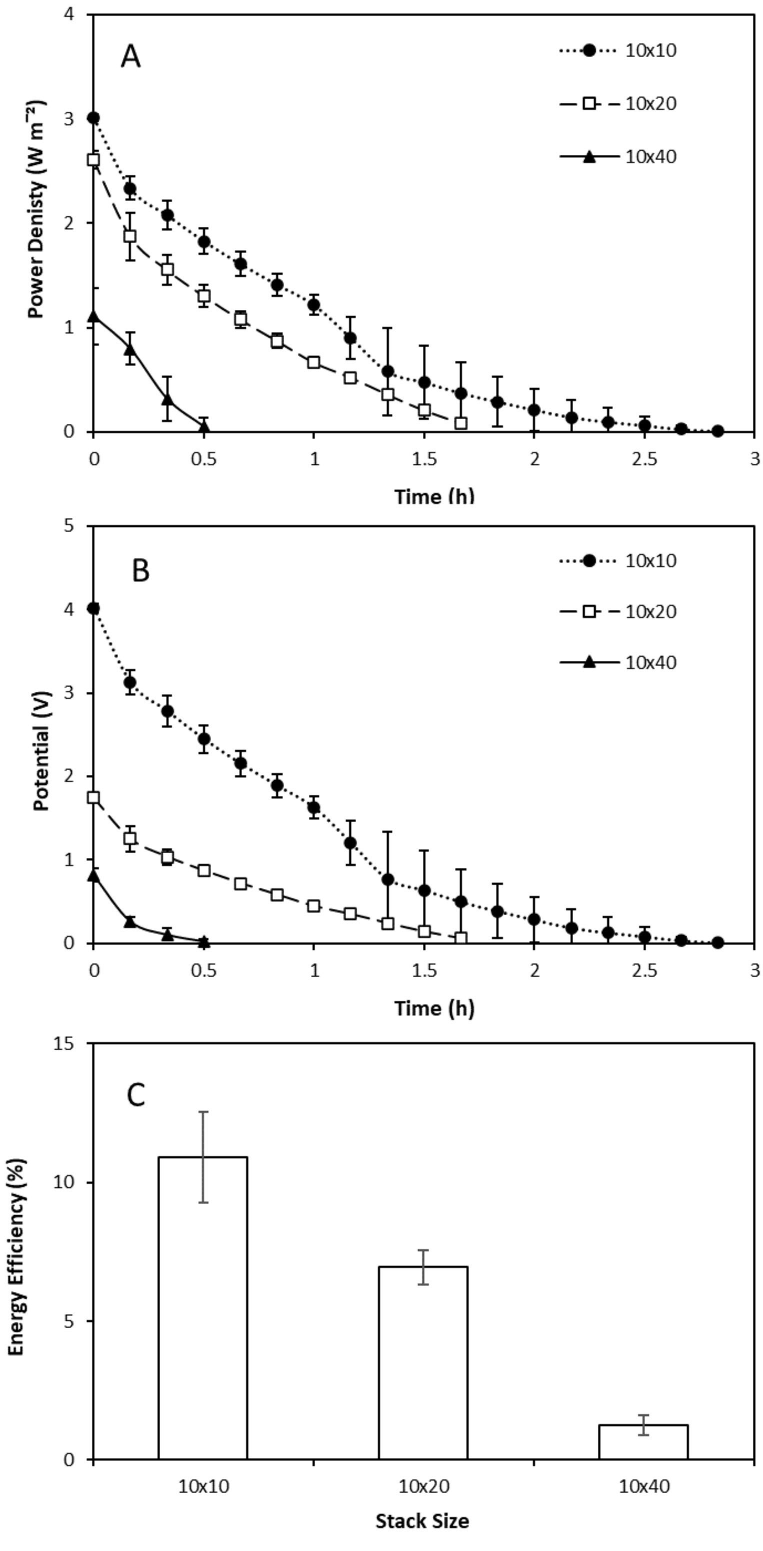

Figure 4.11. *Effect of stack size at a constant membrane area of 0.8 m^2 on (A) power density over time (B) voltage over time and (C) energy efficiency using 4M and 0.02M feeds in recycle. Residence time fixed at 20 s; feed temperature, 25 °C; current density, 60 A m^{-2}. Error bars represent the standard deviation of a triplicate.*

4.4 Conclusions

In this study, small stack sizes have been demonstrated to produce equivalent or even improved performance in comparison to larger stacks when using concentrated brines. Gross power density was determined to increase as stack size and flow rate was increased for both a typical sea/river matrix and a larger concentration gradient using a 4M NaCl feed. However, the additional pumping power required for these conditions counteracted the improvements in gross power density, resulting in reduced net power. Whilst negative net power densities were obtained using the 0.5M concentrated feed at flow rates greater than 0.5 L min^{-1}, the increased chemical potential of larger concentration gradients produced positive power densities at all conditions examined, demonstrating the improved potential of these feeds for large-scale applications. The maximum net power densities obtained by all stack sizes were comparable, however, stack design and operation must manage a trade-off between net power density and normalised energy. This can be done by maximising net power density in single pass before subsequently increasing the path length to improve energy recovery. Increasing cell pair number up to 25 pairs was observed to improve both power density and energy efficiency obtained from a fixed volume, indicating that the addition of cell pairs to increase total membrane area provides a suitable strategy for scaling up RED in recycle. An exergy analysis conducted across the three stack sizes at an equivalent residence time demonstrated that increasing stack size resulted in increased exergy dissipated due to water transport, co-ion transport and concentration polarisation. The superior performance of small stack sizes in recycle when total membrane area is equal indicates that future efforts to scale-up RED for thermal to electric conversion should centre on multi-stage RED using small stacks with a high cell pair number.

Acknowledgements

This publication is based on research funded by the Bill & Melinda Gates Foundation (grant number OPP1149204). The findings and conclusions contained within are those of the authors and do not necessarily reflect positions or policies of the funders.

References

[1] EnerData, Global Energy Statistical Yearbook 2020, (2020). https://yearbook.enerdata.net/electricity/electricity-domestic-consumption-data.html (accessed August 17, 2020).

[2] J. Rogelj, D. Shindell, K. Jiang, S. Fifita, Mitigation Pathways Compatible with 1.5°C in the Context of Sustainable Development, in: Glob. Warm. 1.5°C. An IPCC Spec. Rep. Impacts Glob. Warm. 1.5°C above Pre-Industrial Levels Relat. Glob. Greenh. Gas Emiss. Pathways, Context Strength. Glob. Response to Threat Clim. Chang., IPCC, 2018: pp. 93–174.

[3] C. Forman, I.K. Muritala, R. Pardemann, B. Meyer, Estimating the global waste heat potential, Renew. Sustain. Energy Rev. 57 (2016) 1568–1579.

[4] S. Iglesias Garcia, R. Ferreiro Garcia, J. Carbia Carril, D. Iglesias Garcia, A review of thermodynamic cycles used in low temperature recovery systems over the last two years, Renew. Sustain. Energy Rev. 81 (2018) 760–767.

[5] D. Champier, Thermoelectric generators: A review of applications, Energy Convers. Manag. 140 (2017) 167–181.

[6] A. Tamburini, M. Tedesco, A. Cipollina, G. Micale, M. Ciofalo, M. Papapetrou, W. Van Baak, A. Piacentino, Reverse electrodialysis heat engine for sustainable power production, Appl. Energy. 206 (2017) 1334–1353.

[7] R. Long, B. Li, Z. Liu, W. Liu, Hybrid membrane distillation-reverse electrodialysis electricity generation system to harvest low-grade thermal energy, J. Memb. Sci. 525 (2017) 107–115.

[8] M. Micari, A. Cipollina, F. Giacalone, G. Kosmadakis, M. Papapetrou, G. Zaragoza, G. Micale, A. Tamburini, Towards the first proof of the concept of a Reverse ElectroDialysis - Membrane Distillation Heat Engine, Desalination. 453 (2019) 77–88.

[9] J. Veerman, D.A. Vermaas, Reverse electrodialysis: Fundamentals, in: A. Cipollina, G.M. Micale (Eds.), Sustain. Energy from Salin. Gradients, Woodhead Publishing, Cambridge, United Kingdom, 2016: pp. 77–133.

[10] W.J. Van Egmond, M. Saakes, S. Porada, T. Meuwissen, C.J.N. Buisman, H.V.M. Hamelers, The concentration gradient flow battery as electricity storage system: Technology potential and energy dissipation, J. Power Sources. 325 (2016) 129–139.

[11] D.A. Vermaas, J. Veerman, N.Y. Yip, M. Elimelech, M. Saakes, K. Nijmeijer, High efficiency in energy generation from salinity gradients with reverse electrodialysis, ACS Sustain. Chem. Eng. 1 (2013) 1295–1302.

[12] J. Veerman, M. Saakes, S.J. Metz, G.J. Harmsen, Reverse electrodialysis: Performance of a stack with 50 cells on the mixing of sea and river water, J. Memb. Sci. 327 (2009) 136–144.

[13] J. Veerman, M. Saakes, S.J. Metz, G.J. Harmsen, Electrical power from sea and river water by reverse electrodialysis: A first step from the laboratory to a real power plant, Environ. Sci. Technol. 44 (2010) 9207–9212.

[14] J. Moreno, S. Grasman, R. Van Engelen, K. Nijmeijer, Upscaling Reverse Electrodialysis, Environ. Sci. Technol. 52 (2018) 10856–10863.

[15] A. Daniilidis, D.A. Vermaas, R. Herber, K. Nijmeijer, Experimentally obtainable energy from mixing river water, seawater or brines with reverse electrodialysis, Renew. Energy. 64 (2014) 123–131.

[16] F. Giacalone, P. Catrini, A. Tamburini, A. Cipollina, A. Piacentino, G. Micale, Exergy analysis of reverse electrodialysis, Energy Convers. Manag. 164 (2018) 588–602.

[17] S. Pawlowski, P. Sistat, J.G. Crespo, S. Velizarov, Mass transfer in reverse electrodialysis: Flow entrance effects and diffusion boundary layer thickness, J. Memb. Sci. 471 (2014) 72–83.

[18] M. Tedesco, C. Scalici, D. Vaccari, A. Cipollina, A. Tamburini, G. Micale, Performance of the first reverse electrodialysis pilot plant for power production from saline waters and concentrated brines, J. Memb. Sci. 500 (2016) 33–45.

[19] A.M. Hulme, C.J. Davey, A. Parker, L. Williams, S. Tyrrel, Y. Jiang, M. Pidou, C. Water, B. Mk, Managing power dissipation in closed-loop reverse electrodialysis to maximise energy recovery during thermal to electric conversion, Desalination. 496 (2020) 114711.

[20] A. Cipollina, G. Micale, A. Tamburini, M. Tedesco, L. Gurreri, J. Veerman, S. Grasman, Reverse electrodialysis: Applications, in: A. Cipollina, G.M. Micale (Eds.), Sustain. Energy from Salin. Gradients, Woodhead Publishing, Cambridge, United Kingdom, 2016: pp. 135–180.

[21] M. Tedesco, E. Brauns, A. Cipollina, G. Micale, P. Modica, G. Russo, J. Helsen, Reverse electrodialysis with saline waters and concentrated brines: A laboratory investigation towards technology scale-up, J. Memb. Sci. 492 (2015) 9–20.

[22] M. Tedesco, A. Cipollina, A. Tamburini, G. Micale, Towards 1 kW power production in a reverse electrodialysis pilot plant with saline waters and concentrated brines, J. Memb. Sci. 522 (2017) 226–236.

[23] J.-Y. Nam, K.-S. Hwang, H.-C. Kim, H. Jeong, H. Kim, E. Jwa, S. Yang, J. Choi, C.-S. Kim, J.-H. Han, N. Jeong, Assessing the behavior of the feed-water constituents of a pilot-scale 1000-cell-pair reverse electrodialysis with seawater and municipal wastewater effluent, Water Res. 148 (2019) 261–271.

[24] E. Mercer, C.J. Davey, D. Azzini, A.L. Eusebi, R. Tierney, W. Leon, Y. Jiang, P. Alison, K. Athanasios J., T. Sean, C. Elise, P. M., E. McAdam, Hybrid membrane distillaion reverse electrodialysis configuration for water and energy recovery from human urine: An opportunity for off-gride decentralised sanitation, J. Memb. Sci. 584 (2019) 343–352.

[25] D.A. Vermaas, E. Guler, M. Saakes, K. Nijmeijer, Theoretical power density from salinity gradients using reverse electrodialysis, Energy Procedia. 20 (2012) 170–184.

[26] P. Długołecki, P. Ogonowski, S.J. Metz, M. Saakes, K. Nijmeijer, M. Wessling, On the resistances of membrane, diffusion boundary layer and double layer in ion exchange membrane transport, J. Memb. Sci. 349 (2010) 369–379.

[27] X. Zhu, W. He, B.E. Logan, Influence of solution concentration and salt types on the performance of reverse electrodialysis cells, J. Memb. Sci. 494 (2015) 154–160.

[28] J. Cookney, A. Mcleod, V. Mathioudakis, P. Ncube, A. Soares, B. Jefferson, E.J. McAdam, Dissolved methane recovery from anaerobic effluents using hollow fibre membrane contactors, J. Memb. Sci. 502 (2016) 141–150.

[29] W.J. van Egmond, U.K. Starke, M. Saakes, C.J.N. Buisman, H.V.M. Hamelers, Energy efficiency of a concentration gradient flow battery at elevated temperatures, J. Power Sources. 340 (2017) 71–79.

[30] A.M. Weiner, R.K. McGovern, J.H. Lienhard V, A new reverse electrodialysis design strategy which significantly reduces the levelized cost of electricity, J. Memb. Sci. 493 (2015) 605–614.

[31] O. Scialdone, A. Albanese, A. D'Angelo, A. Galia, C. Guarisco, Investigation of electrode material - Redox couple systems for reverse electrodialysis processes. Part II: Experiments in a stack with 10-50 cell pairs, J. Electroanal. Chem. 704 (2013) 1–9.

[32] N.Y. Yip, D.A. Vermaas, K. Nijmeijer, M. Elimelech, Thermodynamic, energy efficiency, and power density analysis of reverse electrodialysis power generation with natural salinity gradients, Environ. Sci. Technol. 48 (2014) 4925–4936.

[33] M. Turek, B. Bandura, Renewable energy by reverse electrodialysis, Desalination. 205 (2007) 67–74.

5. Discussion

5.1 How can RED systems be configured and operated?

5.1.1 Configuration and operation of a single stack

RED systems should be configured and operated according to the source of the salinity gradient (Figure 5.1). Where sources with a high concentration difference are not limited (for example concentrated brines), stack designs that promote short residence times may be preferred to maximise power density (Chapter 2). However, the availability of freshwater or low salinity sources which can be utilised for the dilute feed often limits power production by RED [1]. In these cases, sources of salinity with a low concentration may not be viable due to the low work (Chapter 2) and net power densities which can be produced using these feeds (Chapter 3 & 4). For source waters with a large concentration gradient which are limited in quantity, recirculating feeds can maximise both the work produced, and energy efficiency achieved by the finite source of salinity gradient available for power production (Chapter2. Increased exergy conversion can also be facilitated by extended residence times, but at the cost of reduced power density (Chapter 3). An increase in cell pair number could compensate for this as the increased total membrane area enables increased power output despite the reduction of power density (Chapter 3).

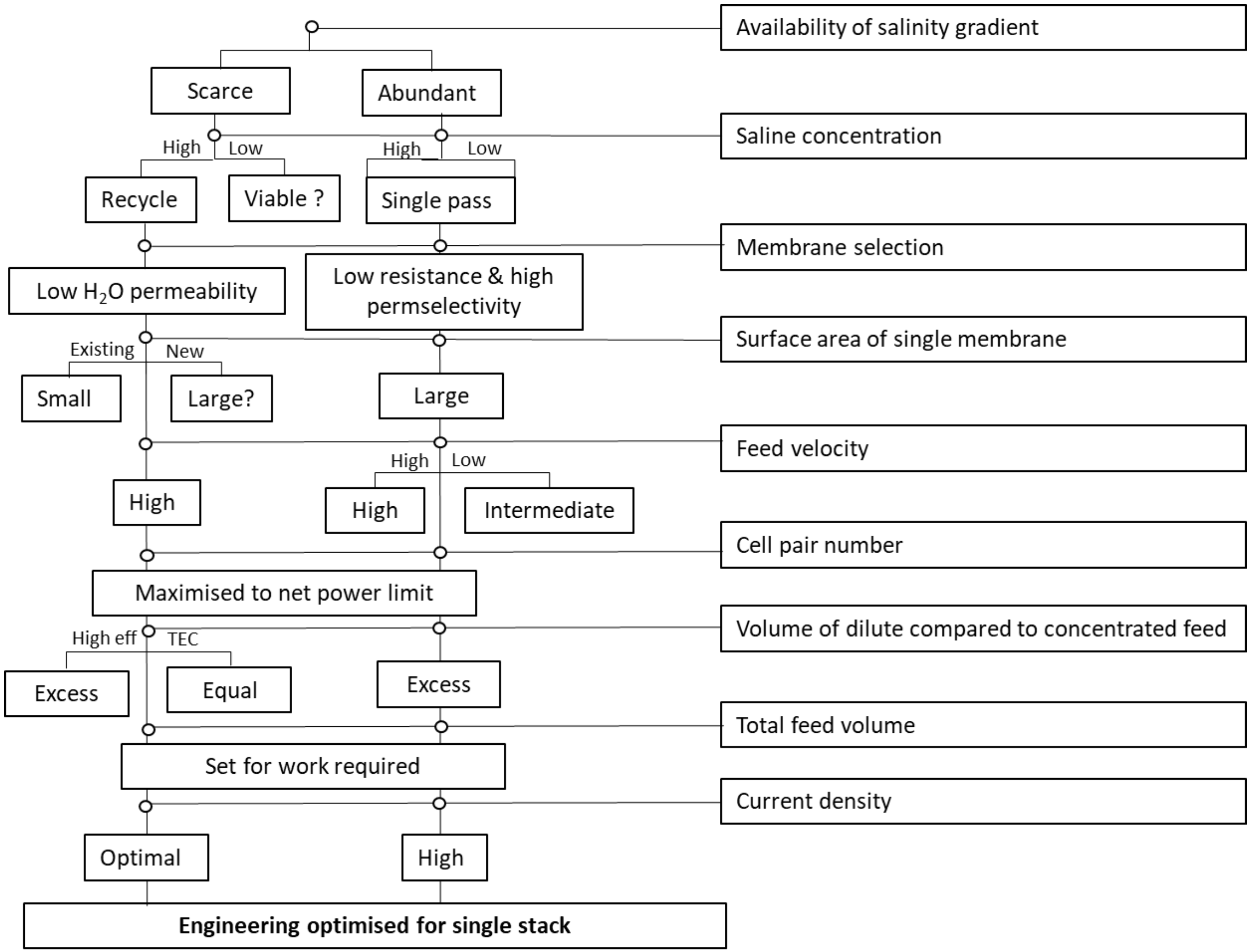

Figure 5.1. *Flow chart for the configuration and operation of a single RED stack.*

Membranes for RED applications are required to have low membrane resistance and high permselectivity for both low concentration (sea/river) applications [2] and increased concentrations (Chapter 3), however, for larger concentration gradients in recycle, consideration of water permeability is also critical (Chapter 3). Large membranes are preferable to improve power output when low salinity gradients are utilised. However, where the osmotic gradient across the membrane is significant, as in the case of large concentration gradients, the surface area of a single membrane should be reduced to minimise water transport (Chapter 4). In the future, the development of improved membranes with low resistance and low water permeability could reduce water transport and enable the use of larger membranes for these applications (Chapter 3). The minimisation of concentration polarisation through selection of velocity is critical [3] particularly when using large concentration gradients (Chapter 2). The selective movement of anions and cations across the ion exchange membranes from low concentration to high concentration compartments leads to concentration polarisation developing on the dilute feed (Figure 5.2). This phenomenon is exacerbated by osmosis, which is particularly significant when large concentration gradients are utilised (Chapter 2). Although osmosis is somewhat counteracted by electro-osmosis at increased currents, water flux from the dilute to concentrated feed remains a significant source of exergy destruction when large concentration gradients are utilised (Chapter 2). Gross power density improved as feed velocity was increased using these feeds, however a plateau was observed at a velocity of 0.55 cm s^{1} indicating that concentration polarisation was minimised (Chapter 2). When using low concentration gradients care must be taken to ensure high feed velocity does not lead to negative net power, however, this problem was not observed using larger concentration gradients (Chapter 4).

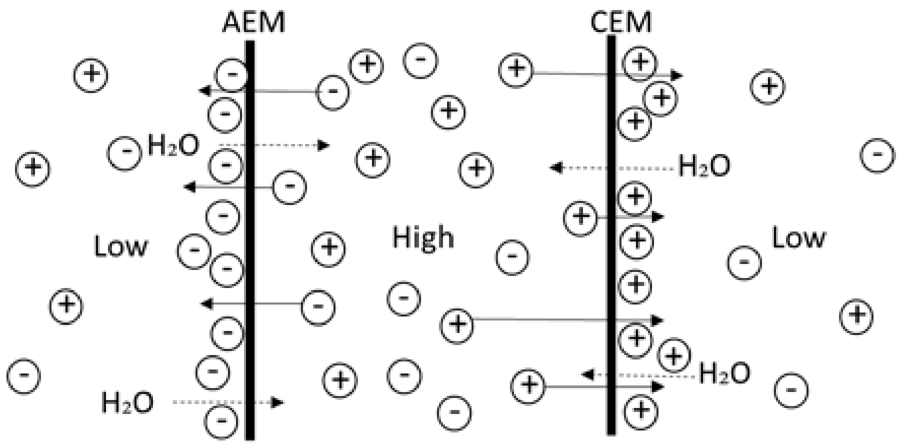

Figure 5.2. *Schematic of concentration polarisation in a reverse electrodialysis cell.*

Increasing cell pair number has been demonstrated to improve both power density and energy efficiency from a fixed volume in recycle (Chapter 4). However, Pawlowski et al. [4], demonstrated that net power reduces above a critical cell pair number due to the increased pumping requirements. Therefore, cell pair number should be fixed to maximise net power density, which will vary according to the velocity, intermembrane distance and feed properties. For RED applications where high energy efficiency is required, for example when the source of salinity is scarce, using an excess of dilute feed has been demonstrated to increase the Gibbs free energy which is recovered for sea/river feeds [5]. By contrast, for thermal to electric applications in which RED is integrated with a distillation stage to regenerate the concentration gradient, the increased volume of dilute feed to be evaporated necessitates an increase in heat energy and is therefore unlikely to be favourable. The total mass or volume of feed which is recirculated can be selected to achieve a desired output. To illustrate, the total mass of feeds recirculated through a 10 cm x 40 cm stack was varied from 2.5 to 10 kg. An initial power density of approximately 3 W m^{-2} was obtained regardless of the total mass of feeds, however, an increased mass enabled high power production to be maintained for an extended duration (Figure 5.3A). The total work extracted from the system also increased as the mass of feeds recirculated was increased as is expected due to the increased Gibbs free energy provided to the system. After fully depleting the concentration gradient for maximal extraction of work, an energy efficiency of 10.5 % was achieved using 10 kg of feeds compared, to 10.8 % and 12.3 % for 5 kg and 2.5 kg, respectively (Figure 5.3B). This indicates that total work produced scales approximately linearly when an equal mass of concentrated and dilute feeds is utilised. For recycle applications, an optimal current, which depends on the concentration gradient (Chapter 2) and appropriate membrane selection (Chapter 3), enable improved energy efficiency to be obtained at equivalent power densities. For high power applications where the source of salinity is abundant and energy efficiency is a secondary consideration, increased current maximises power densities.

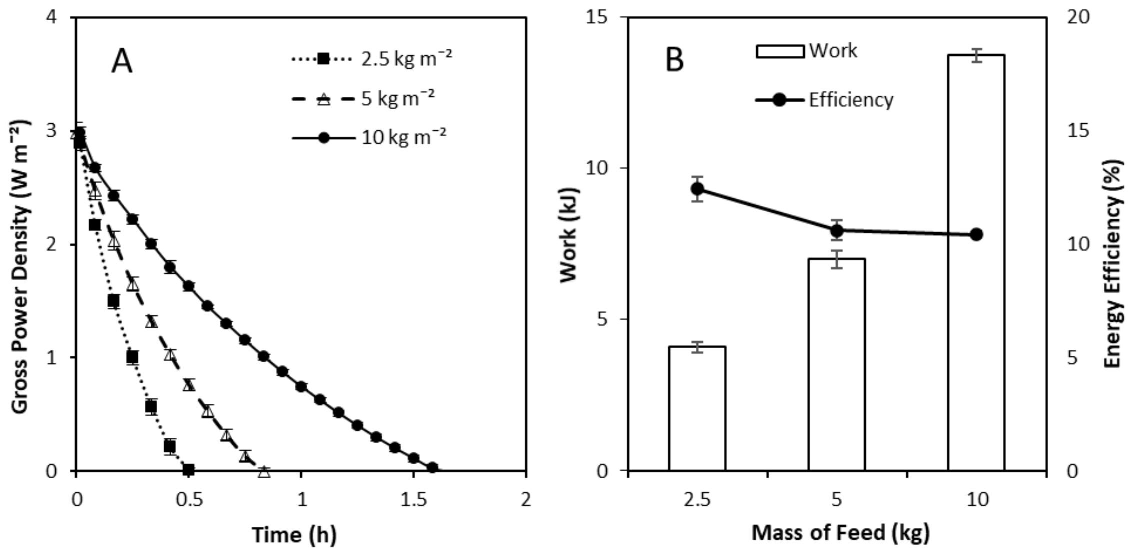

Figure 5.3. *(A) Gross power density over time and (B) total work and energy efficiency obtained by recirculating 2.5 kg, 5 kg and 10 kg of 4M concentrated feed and 0.02 M dilute feed. Stack size, 10 cm x 40 cm; 25 cell pairs; flow rate, 200 ml min^{-1}; current, 0.4 A. Error bars represent standard deviation of triplicate.*

5.1.2 Configuration and operation of multi-stage RED

To meet specified power output for large-scale applications, the operation of multiple stacks in series is likely to be required [6]. Multi-stage RED (MSRED) has been demonstrated to increase energy recovery and improve total power output [7,8] and can be operated in series or parallel configurations. When feeds are abundant and a constant, high power output is required, multiple stacks should be operated in parallel, to enable the highest power output to be produced. A disadvantage of this configuration is that limited feed volumes will be quickly exhausted quickly, with low energy recovery. By contrast, when feeds are scarce, and maximising energy efficiency is the criticality, operating MSRED in series can extend the duration of power production and improve work produced per kg of feeds. To benchmark the performance of MSRED using a large concentration gradient, four stages were carried out experimentally utilising a large concentration gradient in single pass at a uniform current. A gross power density of 1.9 W m^{-2} was obtained in the initial stage with power density decreasing in each subsequent stage, to 1.3 W m^{-2} in the 4th and final stage, attributed to the reduction in in the residual concentrated feed concentration from 4M to 3.6M over the four stages (Figure 5.4A). Despite the reduction in power density over the stages, total power output is significantly improved by the addition of stages with up to 2.6 W achieved by operating the four stages simultaneously, compared to a maximum of 0.90 W for a single stage (Figure 5.4B). Hu et al. [8], also observed increased net power output as the stage number was increased, up to a maximum of 1.42 W obtained at ten stages using similar feed concentrations. The difference in total power output can be attributed to the increased total membrane area in each stage used in this study (Total membrane area, A = 0.5 m^2), compared to Hu et al. [8] (A = 0.1 m^2) and differences in stack properties and hydrodynamics. Energy recovery also benefits from an increase in stage number, with the cumulative energy efficiency observed to increase approximately linearly from 1.4 % to 4.6 % as stage number increased from 1 to 4 (Figure 5.4B). Similarly, Veerman et al reported that increasing the number of stages improved energy efficiency up to 18 % at three stages, using artificial sea water and river water feeds in a 50 cell-pair stack [6]. The difference in energy efficiency obtained between these studies can be partly attributed to the doubled cell pair number, with increased cell pair number expected to improve energy efficiency. Additionally, lower energy efficiency is expected when utilising concentrated brine feeds, as a result of the increased exergy losses due to water and salt transport promoted by the increased driving force for diffusion [9]. Modelling by Hu et al. [7] demonstrated that energy efficiency could be expected to increase as stage number increased and this was experimentally verified in a subsequent study [8]. In this work, a residual concentration of 3.6M remained in the concentrated feed (Figure 5.4A), after 4 stages representing a significant amount of unused energy. Whilst energy efficiency could be improved further by the addition of further stages, this would incur additional capital costs and a more cost-efficient alternative would be to continuously recirculate the feeds to maximise energy recovery.

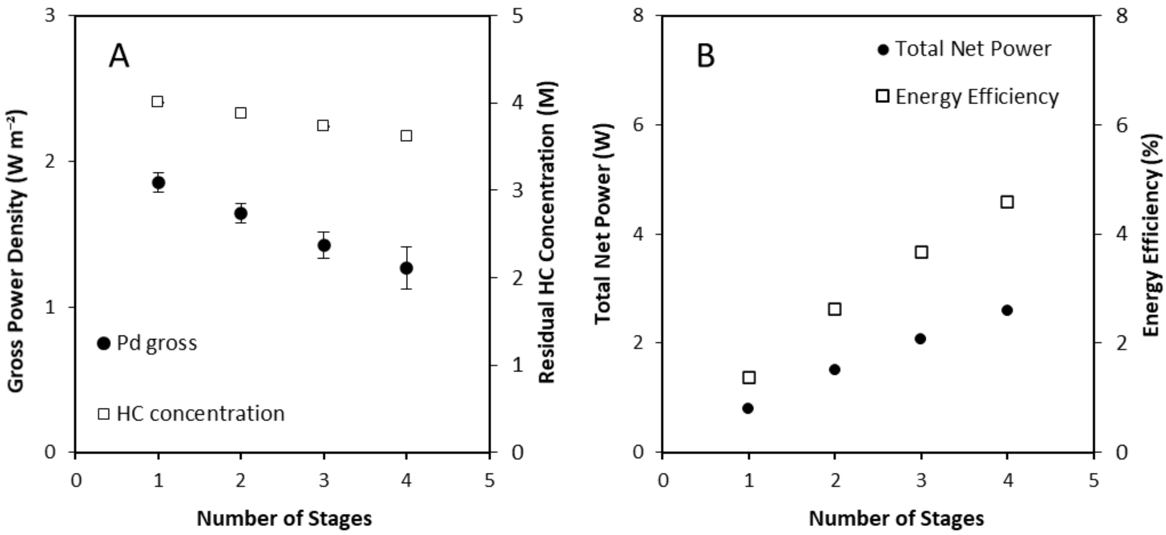

Figure 5.4. *(A) Gross power density and residual concentrated feed concentration and (B) total net power and cumulative energy efficiency obtained from 4 stages of MSRED in series operating in single pass. Stack size, 10 cm x 10 cm; 25 cell pairs; flow rate 200 ml min^{-1}, 1 kg 4M concentrated feed, 1kg 0.02M concentrated feed; current, 0.4A. Error bars represent standard deviation of triplicate.*

To evidence the maximum power output, energy efficiency and solution unit work potential achievable using one stack, feeds were continuously recirculated throughout the stack until the voltage reached 0 V. Power output using one stack in recycle reached a maximum of 0.87 W (Figure 5.5A) compared to 2.6 W achieved by 4 stages of MSRED operated in series (Figure 5.4B). However, doubled energy efficiency of 12 % was obtained in a single stack in recycle (Figure 5.5A), indicating the benefits of this configuration compared to MSRED. A hybrid configuration consisting of MSRED with feed recirculation may be preferable to enable improved power and energy efficiency to be achieved simultaneously.

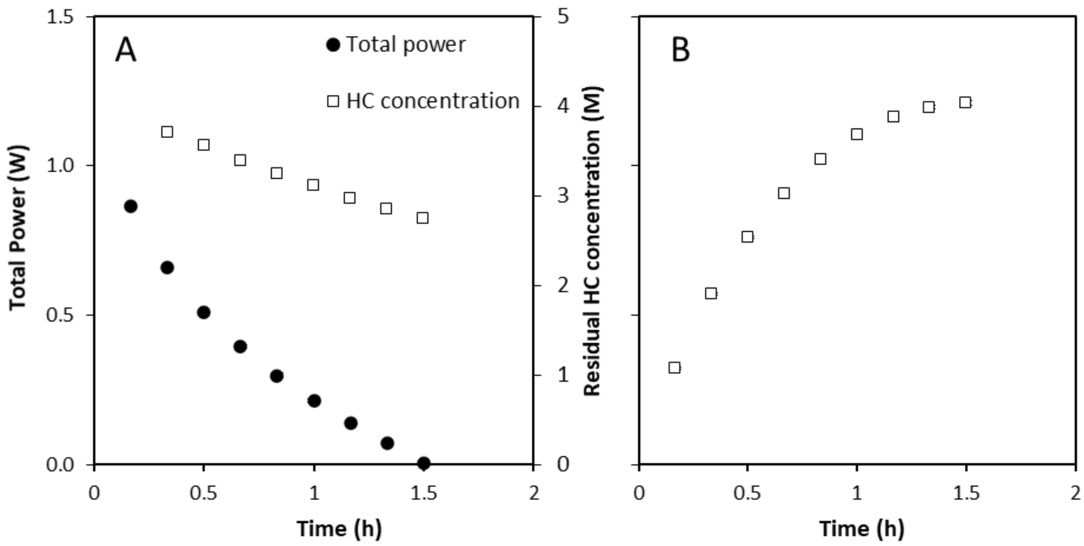

Figure 5.5. *(A) Total power output and (B) energy efficiency obtained by 1 reverse electrodialysis stack operating in recycle. Stack size, 10 cm x 10 cm; 25 cell pairs; 1 kg 4M concentrated feed; 1 kg 0.02M dilute feed; flow rate 200 ml min^{-1}, current 0.4 A. Error bars represent standard deviation of triplicate.*

Despite the improved utilisation of the available salinity gradient in recycle compared to single pass, a residual concentration of 2.75M (Figure 5.5B) remained in the concentrated feed effluent even after the voltage had decreased to 0V when operating in recycle. This indicates that the dilute feed prohibited further power production, thus limiting the energy efficiency which could be achieved. An excess of dilute feed could overcome this limitation. Vermaas et al. [5] demonstrated that energy efficiency up to 95 % could theoretically be obtained by an RED stack with multiple electrodes fed with sea and river water by utilising an excess of river water. Whilst this is not generally practical in conventional RED applications due to the lack of availability of fresh water [10], this limitation can be avoided in RED for thermal to electric applications where a limited feed volume is reused following thermal regeneration. To experimentally determine the effect of an excess of dilute feed using a larger concentration gradient for MSRED applications, 9 stages of MSRED in recycle were carried out using 1 kg of concentrated feed, with an additional 1 kg of 0.02M dilute feed added at each stage. The use of an excess of dilute feed enabled more of the salinity source to be utilised for power production, with the residual concentration of the concentrated feed reduced to 0.4M after nine stages (Figure 5.6A). This resulted in improved energy efficiency of 18 % (Figure 5.6B), demonstrating that this can benefit the performance of RED for high efficiency applications where the availability of dilute feed is not limited.

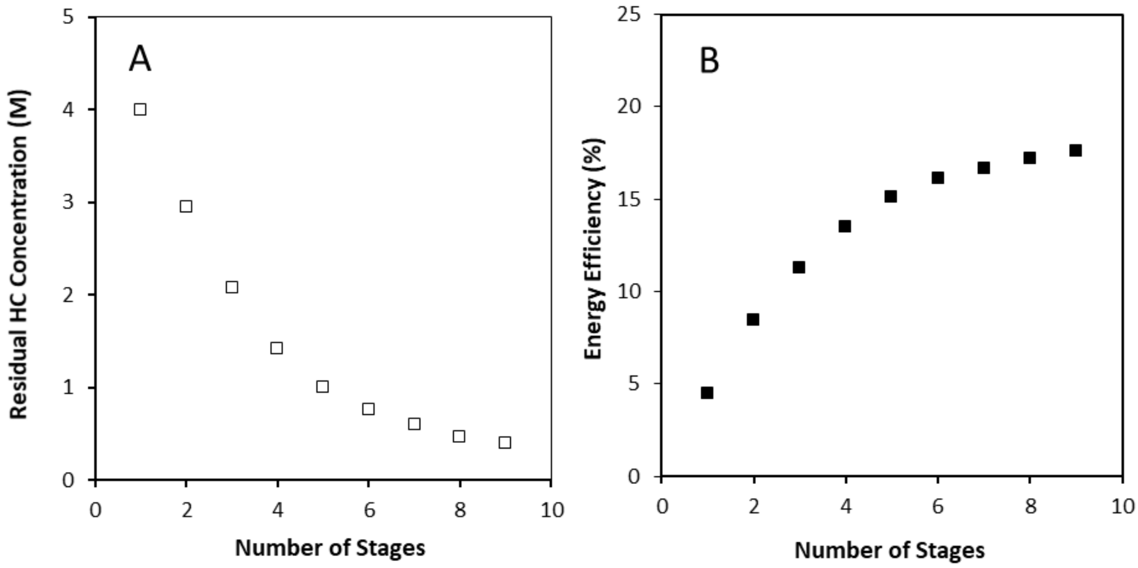

Figure 5.6. *(A) Residual concentration of the concentrated feed following10 stages with a new volume of dilute added each stage and (B) Cumulative energy efficiency as number of stages increased 9 stacks in series, 25 cell pairs. 1 kg 4M concentrated feed; 1 kg 0.02M added every stage; flow rate 200 ml min^{-1}; current 0.4 A. New stage started when conductivity of the dilute reached 50 mS cm^{-1} or 0 V produced by the system.*

The use of MSRED or recycle configurations introduces a dynamic concentration gradient which decreases over time as mixing occurs, causing a temporal shift in solution and stack resistances [11]. This gives rise to a variation in optimal current density, as the external resistance should equal the internal resistance to maximise power output [12]. Electrode segmentation, in which the electrode is split up into several sections to enable the external load to be matched to varying resistance throughout a single RED stack, has been proposed to overcome this [13]. In MSRED, an analogous strategy is to individually alter current for each stage [7,14]. Veerman et al. [15], first reported that electrode segmentation improved power density up to 15 % in a 25 cm x 75 cm RED stack using artificial sea/river water feeds at low flow rates [12]. A subsequent study by Simões et al. [13], demonstrated that electrode segmentation improved gross power density and energy efficiency, and could reduce capital and operating costs in a cross-flow stack. The use of feeds with an increased salinity difference to conventionally used sea/river feeds can be expected to cause a greater disparity in optimal current throughout the stages in MSRED and therefore it is hypothesised that current control will be even more significant utilising these salinities. Whilst Hu et al. [7], modelled MSRED with individual current control using a 4M concentrated feed and 0.05M dilute feed, and experimentally investigated the effect of process conditions in a subsequent study [8], the effect of non-uniform current with an excess of dilute feed has not previously been considered for concentrated brine applications.

In this work, non-uniform current was applied using MSRED in recycle using an excess of dilute feed for the first time. A small improvement in the energy which was recovered by each stage was observed (Figure 5.7A). This led to an improvement in total work which was produced by the 4 stages from 4.6 kJ when current is uniform compared to 6.1 kJ with non-uniform current (Figure 5.7B). Similarly, Hu et al. [7] theoretically demonstrated an increase in total work produced by individual control of current using an equivalent concentration gradient but equal volumes of dilute and concentrated feed. Total energy efficiency was also observed to improve across the four stages to a maximum of 18 % (Figure 5.7C). The increased energy recovery facilitated by the current control strategy improves the solution unit work potential compared to when current is uniform across all stages. However, for integration of RED with a thermal separation stage, the effect of an excess of dilute feed on the solution unit work potential must also be determined, to ensure that hypothesised improvements in power are sufficient to offset any increase in thermal consumption necessitated by increased latent heat which will be required to distil the increased volume of water. The solution unit work potential decreased every stage due to the excess of dilute feed (Figure 5.7D), indicating that this is not a favourable configuration for an RED heat engine. The use of MSRED in recycle offers flexibility of operation and increased power output, with individual current control improving performance. However, a disadvantage of serial and recycle operation is that power output decreases over time (Chapter 2). This can be managed through using power produced by RED to charge a battery for energy storage applications. Alternatively, discharge from multiple stages could be off-set to provide a steady power output.

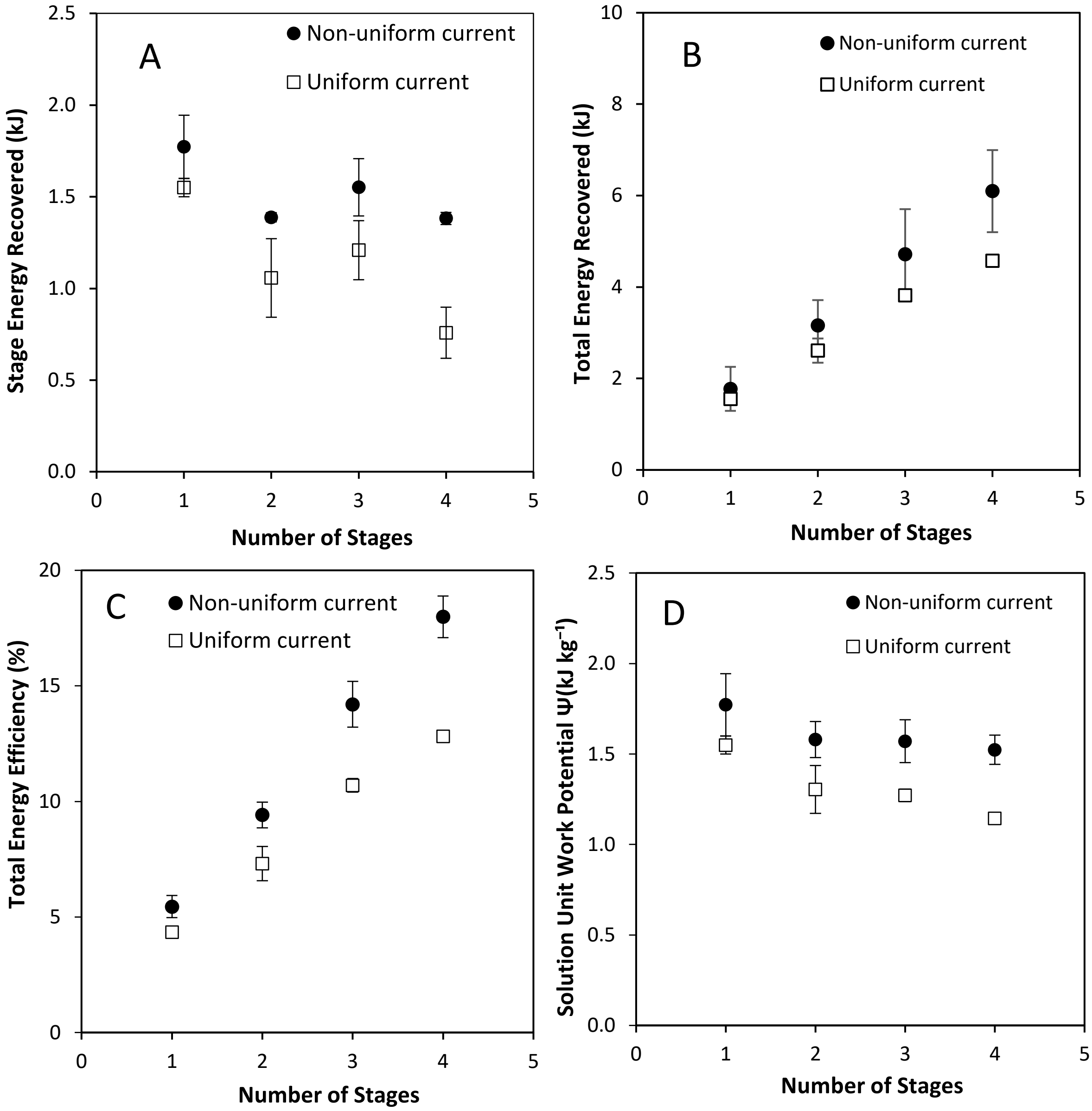

Figure 5.7. *(A) Energy recovered and (B) Energy efficiency of each stage with constant current and optimised current in recycle. 4 stacks in series, 25 cell pairs. 1 kg 0.02M added every stage; flow rate 200 ml min^{-1}; current 0.4 A. Error bars represent standard deviation of triplicate.*

5.2 How can the levelised cost of electricity of RED be reduced?

The levelised cost of electricity (LCOE) is defined as the cost per unit of electricity, and accounts for total costs incurred and total power produced by a system over its lifetime [16]. The LCOE for an RED system can be calculated from:

$$LCOE = \frac{NPV}{(P_{d,net}wl)CAF} \qquad \textbf{(5-1)}$$

where NPV is the net present value ($), $P_{d,net}$ is the net power density, w is the channel width (m), l is the stack length (m) and CAF is the capital amortization factor [3]. The NPV can be determined from:

$$NPV = K_{mem}wl + 2K_{PT}vhw \quad \textbf{(5-2)}$$

Where K_{mem} is membrane cost ($ m^{-2}) and K_{PT} is the cost of pre-treatment ($ m^{-3} day^{-1}), v is the feed velocity (m s^{-1}), and h is the channel height (m). The CAF is calculated from:

$$CAF = \frac{1}{r}\left[1 - (\frac{1}{1+r})^{\Gamma}\right] \quad \textbf{(5-3)}$$

Where r is an annualised cost of capital (6 %). and Γ is the plant life (years). Net power density accounts for the pumping required for pumping and pre-treatment:

$$P_{d,net} = P_{d,gross} - P_{d,PT} - P_{d,pump} \quad \textbf{(5-4)}$$

Where $P_{d,\,gross}$ is the gross power density, $P_{d,PT}$ is the power density required for pre-treatment and $P_{d,pump}$ is the power density required to pump solutions through the stack, all in W m^{-2}. For RED applications utilising synthetic saline solutions, the cost of pre-treatment can be assumed to be negligible, and the LCOE is therefore simplified to:

$$LCOE = \frac{1}{P_{D,net}}(\frac{K_{mem}}{CAF}) \quad \textbf{(5-5)}$$

For systems using artificial solutions, the process scale will be limited by feed availability and for closed-loop systems, the inclusion of a stage such to regenerate the concentration gradient such as thermal separation or electrodialysis can be expected to incur additional costs.

An LCOE in the range of $0.01 kWh^{-1} to $0.14 kWh^{-1} (80 to 120 € MWh^{-1}) is required for RED to be a competitive technology [16]. The LCOE of RED has previously been evaluated across a range of scales and scenarios (Table 5.1). Turek et al. [17], first estimated an LCOE of $6.79 kWh^{-1} for an industrial RED module fed with synthetic sea and river water feeds, assuming capital costs of $100 m^{-2} of membrane. In 2010, Post et al. [18] demonstrated that an LCOE of $0.01 kWh^{-1} (0.08€ kWh^{-1}) could theoretically be achieved by a 200 kW module producing a power density of 2 W m^{-2}, following a reduction in ion exchange membrane costs to 2 € m^{-2}. However, despite the availability of heterogeneous membranes <$5 m^{-2}, the cost of low resistance ion exchange membranes suitable for RED applications remains prohibitively high (>$100m^{-2}) [18–20] with membranes < $5 m^{-2} required for cost-effective RED [19]. Utilising relatively low salinity gradients such as sea and river water limits the achievable net power density and total power output per m^3 of feed, due to the availability of Gibbs free energy [21], and therefore lower LCOEs can be expected from the use of increased salinity gradients. To illustrate, the highest net power density achieved using artificial saline solutions with an equivalent concentration to sea and river water in this work was 0.81 W m^{-2} producing an LCOE of \$0.50 kWh^{-1}, assuming a constant power output for 20 years (160,000h) and negligible pre-treatment requirements. By contrast, a net power density of up to 2.95 W m^{-2} was achieved by the same stack using an increased concentration gradient of 4M and 0.02M, reducing the LCOE to \$0.14 kWh^{-1}. Whilst this demonstrates that increased concentration gradients can improve the unitary cost of electricity produced by RED, this does not account for the cost of thermal regeneration of the salinity gradients which would increase the LCOE, with thermal separation stages such as multi-effect distillation or membrane distillation expected to cost between \$0.50 m^{-3} and \$11 m^{-3} (0.38 € m^{-3} to 9.60 € m^{-3}) [22].

Table 5.1. *Levelised cost of electricity from the literature and calculated in this work.*

Feeds	Power density (W m^{-2})	Membrane cost (\$ m^{-2})	Lifetime (years)	Scale	LCOE (\$ kWh^{-1})	Refs
Sea/river (artificial)	0.46	Total installed cost, \$100 m^{-2}	10 (80,000 h)	Industrial	6.79	[17]
Sea/river	2	Membrane cost, 2 € m^{-2}	7	200 kW module	0.1 (0.08 € kWh^{-1})	[18]
Sea/river	1.65	Total installed cost, \$750 m^{-2}	20	200 kW module	6.33 - 30	[3]
Sea/river		Membrane cost, \$10 m^{-2}– \$70 m^{-2}	20	10,000 m^3 day^{-1}	0.02 - 0.06	[23]
Sea/river	0.81	Total installed cost, \$750 m^{-2}		10 cm x 10 cm lab-scale module	0.50	This work
Synthetic brines	2.95	Total installed cost, \$750 m^{-2}	20	10 cm x 10 cm lab-scale module	0.14	This work

The LCOE can be reduced by increasing power production or by decreasing the capital costs or operating costs of an RED system [20] (Equation 5-1). In addition to increasing the salinity gradient (Chapter 2), power production can be improved through selection of operating conditions (Chapter 2), configurations (Chapter 2 and 4), and stack design (Chapter 3 and 4). Consequently, a range of design strategies to minimise the LCOE have been developed. Modelling by Weiner et al. [3], demonstrated that the LCOE could be minimised through selection of resistance which maximised gross power density, prior to fixing residence time and optimising velocity by varying stack length. An LCOE of \$6.33 kWh^{-1} was achieved using this strategy. Conversely, Kim et al. [23] demonstrated that the LCOE could be improved by increasing the cell pairs in a single RED stack to maximise power production from a fixed volume. In this work, feed recirculation was demonstrated to increase work produced per kg of feed, whilst minimising the total membrane area required (Chapter 2). By operating RED to produce peak power output and subsequently recycling the feeds to improve efficiency, a reduction in the LCOE can be expected. However, a disadvantage of this configuration is decreasing power output over time. To circumvent this, an RED stack could instead be designed to maximise energy efficiency in single pass. However, as maximised energy efficiency occurs when net power density is minimised (Chapter 4), reduced power output is expected from this configuration. Increasing the cell pair number can counteract this (Chapter 4) but the increase in membrane area necessitates additional capital investment. Adding a recycle to a stack with a high cell pair number designed for high energy efficiency can further maximise the energy recovery from the feeds.

For multi-stage RED (MSRED) applications, increased total capital investment is expected to be offset by increased power production for parallel configurations where power production can be expected to scale to the number of stacks, assuming a constant stack size is utilised. However, when operating MSRED in series, power density will decrease in each successive stack, and it must therefore be ensured that additional stacks increase power production sufficiently to offset increased costs. An excess of dilute feed can improve energy efficiency in MSRED by enabling improved power output to be produced for an extended duration and therefore could reduce the LCOE of RED for closed-loop applications, where pre-treatment costs are negligible.

Selection of stack components such as membranes, electrodes and spacer and gasket thicknesses play a role in power output and efficiency which can be obtained from a single RED stack (Chapter 3). Whilst increased power densities can be obtained at no extra capital cost by reducing spacer and gasket thickness for a smaller intermembrane distance (Chapter 3), a trade-off in cost and power density is likely to be required to further reduce the unitary cost of electricity through selection of membranes and electrodes. Installed costs per membrane area are estimated to be as high as \$750 m^{-2} [3]. Whilst this includes all equipment required for power production by RED [3], membrane cost is acknowledged to be a barrier to the implementation of RED [18–20]. Despite the existence of cheap homogeneous membranes (>\$5 m^{-2}), these are unfeasible due to the low power output they can achieve due to high internal resistance [18]. It is expected that the cost of low resistance ion exchange membranes suitable for RED applications will decrease significantly with time as technologies for the large-scale manufacturing of these materials improves [3,9].

The titanium electrodes with a Ir/Ru mixed metal oxide coating conventionally used in RED applications also increase the capital costs of an RED stack as electrode cost scales to stack size. Veerman et al. [25], evaluated a range of electrode systems in terms of health and safety, environmental impact, cost, and technical feasibility, identifying graphite electrodes as a potential cheap alternative. In a study to establish the performance of graphite electrodes for RED, Lee et al. [26], reported similar performance to titanium electrodes using a typical seawater/river water matrix. Conversely, Scialdone et al. [27], noted signs of micro-erosion of the graphite electrode, reporting that the anode collapsed at low concentrations of redox couple (0.1 mol dm^{-3}). However, these studies were limited to relatively low salinity gradients. In this thesis, 4M and 0.02M feeds were used to create a high concentration gradient. A gross power density of 0.04 W m^{-2} was produced using graphite electrodes however, a gross power density 55 times higher, of 2.2 W m^{-2} was obtained using conventional titanium electrodes with a mixed metal oxide coating (Figure 5.8). This is likely due to the increased resistance of this material [26]. Accounting for pumping power, net power density is negative, highlighting that despite the reduced capital costs, graphite electrodes are not feasible for RED using concentrated brines. Despite this, the use of cheaper materials which limit power density but at reduced capital investment can play a role to in improving the unitary cost of electricity of RED where reductions in power density are counteracted by significantly reduced capital investment.

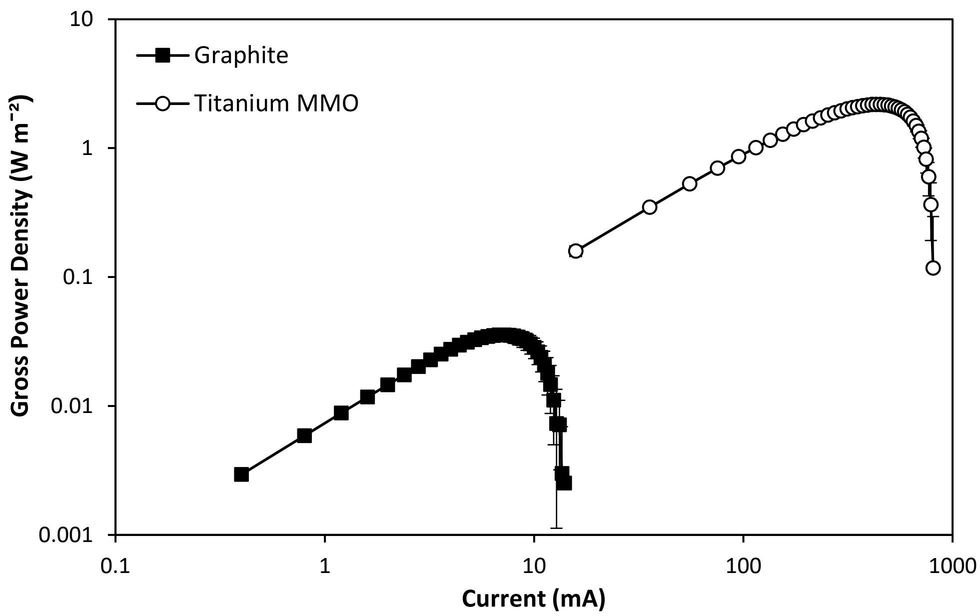

Figure 5.8. *Gross power density obtained by reverse electrodialysis with graphite electrodes and titanium electrodes with a Ir/Ru mixed metal oxides coating. 4M concentrated feed and 0.02M dilute feed in single pass, flow rate 200 ml min^{-1}.*

5.3 Where can closed-loop RED offer most value?

Whilst conventional RED has focussed on power production from sea and river water, closed-loop RED provides further opportunities to produce sustainable electricity through the thermal to electric conversion of widely-available waste and sustainable heat sources (Table 5.2). Operating in a closed-loop removes the limitation on feed availability and enables a wide range of solutions to be utilised for power production, including the use of alternative salts to NaCl, such as lithium bromide (LiBr) [28,29] and binary mixtures of salts [30] which have been demonstrated to improve power density. The highest experimentally power density recorded using NaCl is 6.7 W m^{-2}, achieved by maximising both the concentration gradient and feed temperature (60 °C) [21]. Power densities up to 8 W m^{-2} have been experimentally obtained using a binary mixture of ammonium chloride and lithium chloride in a conventional RED stack, with power densities up to 18 W m^{-2} theoretically achievable using LiBr [28]. This is because the increased solubility of these salts enables higher concentration gradients to be exploited for power productions, whilst the increased conductivity reduces solutions resistance and large activity coefficients facilitate an increased potential according to the Nernst Equation. The challenges pertaining to power production from NaCl feeds with a large concentration gradient, such as water transport and concentration polarisation, are expected to be similarly limiting when utilising these alternative saline solutions, due to the increased solubility, facilitating even greater osmotic gradients. The strategies developed in this thesis for the selection of operating conditions and configurations to mitigate exergy losses and maximise power production will also be applicable to these alternative feeds.

The availability of waste or sustainable heat energy enables higher feed temperatures to be utilised for RED. Daniilidis et al. [21], previously demonstrated that increased temperatures can produce higher power densities, however this has the adverse effect of increasing exergy loss and reducing energy efficiency (Chapter 2). Therefore, feeds should only be heated in applications where power density is prioritised over energy efficiency. Concentrated brines produced by processes such as desalination also provide an opportunity for power production, reducing electricity consumption from fossil fuels [31]. The combination of RED with a regeneration stage such as electrodialysis be used for energy storage applications such as the concentration gradient flow battery [32,33]. Closed-loop RED could also be used to provide decentralised power in low-income settings where heat energy is readily available from biomass boilers, biogas, or propane, for example, but networked electricity is unavailable. Whilst these are not green energy sources, thermal to electric conversion could provide an opportunity for reliable decentralised power in this case. Micari et al. [24], determined an LCOE for an RED-MD heat engine [24] which is competitive with photovoltaics, where the LCOE is in the region of \$0.1 kWh^{-1} to \$0.8 kWh^{-1} [34]. In contrast to photovoltaics, membrane modules can be stacked resulting in land requirements of 0.1 m^2 kW^{-1} to 2 m^2 kW^{-1} [16], compared to between 5 m^2 kW^{-1} and 25 m^2 kW^{-1} for photovoltaics [35]. RED-HE provides reliable power production and is not subject to temporal variations in power production due to seasonal effects, clouds and shadows, obstacles, with dirt and dust necessitating regular cleaning to maximise power output in photovoltaics [11,12].

Table 5.2. *Classifications and sources of energy for RED applications*

Category	Source
Waste heat	Industry, power generation, transportation, buildings
Sustainable heat	Solar, Geothermal
Energy storage	Synthetic brine
Energy recovery from waste	Concentrated brines from desalination, salt works, wastewater
Off-grid power	Heat generated from biomass, biogas, or propane

References

[1] B.E. Logan, M. Elimelech, Membrane-based processes for sustainable power generation using water, Nature. 488 (2012) 313–319.

[2] J. Veerman, R.M. de Jong, M. Saakes, S.J. Metz, G.J. Harmsen, Reverse electrodialysis: Comparison of six commercial membrane pairs on the thermodynamic efficiency and power density, J. Memb. Sci. 343 (2009) 7–15.

[3] A.M. Weiner, R.K. McGovern, J.H. Lienhard V, A new reverse electrodialysis design strategy which significantly reduces the levelized cost of electricity, J. Memb. Sci. 493 (2015) 605–614.

[4] S. Pawlowski, J.G. Crespo, S. Velizarov, Pressure drop in reverse electrodialysis: Experimental and modeling studies for stacks with variable number of cell pairs, J. Memb. Sci. 462 (2014) 96–111.

[5] D.A. Vermaas, J. Veerman, N.Y. Yip, M. Elimelech, M. Saakes, K. Nijmeijer, High efficiency in energy generation from salinity gradients with reverse electrodialysis, ACS Sustain. Chem. Eng. 1 (2013) 1295–1302.

[6] J. Veerman, M. Saakes, S.J. Metz, G.J. Harmsen, Reverse electrodialysis: Performance of a stack with 50 cells on the mixing of sea and river water, J. Memb. Sci. 327 (2009) 136–144.

[7] J. Hu, X. Wu, Q. Leng, D. Jin, P. Wang, S. Xu, D. Wu, Multi-stage reverse electrodialysis: Strategies to harvest salinity gradient energy, Energy Convers. Manag. 183 (2019) 803–815.

[8] J. Hu, S. Xu, X. Wu, S. Wang, X. Zhang, S. Yang, R. Xi, D. Wu, L. Xu, Experimental

investigation on the performance of series control multi-stage reverse electrodialysis, Energy Convers. Manag. 204 (2020) 112284.

[9] F. Giacalone, P. Catrini, A. Tamburini, A. Cipollina, A. Piacentino, G. Micale, Exergy analysis of reverse electrodialysis, Energy Convers. Manag. 164 (2018) 588–602.

[10] B.E. Logan, M. Elimelech, Membrane-based processes for sustainable power generation using water, Nature. 488 (2012) 313–319.

[11] W.J. van Egmond, U.K. Starke, M. Saakes, C.J.N. Buisman, H.V.M. Hamelers, Energy efficiency of a concentration gradient flow battery at elevated temperatures, J. Power Sources. 340 (2017) 71–79.

[12] J. Veerman, M. Saakes, S.J. Metz, G.J. Harmsen, Reverse electrodialysis: A validated process model for design and optimization, Chem. Eng. J. 166 (2011) 256–268.

[13] C. Simões, D. Pintossi, M. Saakes, Z. Borneman, W. Brilman, K. Nijmeijer, Electrode segmentation in reverse electrodialysis: Improved power and energy efficiency, Desalination. 492 (2020) 114604.

[14] G. Doornbusch, H. Swart, M. Tedesco, J. Post, Z. Borneman, K. Nijmeijer, Current utilization in electrodialysis: Electrode segmentation as alternative for multistaging, Desalination. 480 (2020) 114243.

[15] J. Veerman, M. Saakes, S.J. Metz, G.J. Harmsen, Electrical power from sea and river water by reverse electrodialysis: A first step from the laboratory to a real power plant, Environ. Sci. Technol. 44 (2010) 9207–9212.

[16] M. Papapetrou, K. Kumpavat, Environmental aspects and economics of salinity gradient power (SGP) processes, in: A. Cipollina, G.M. Micale (Eds.), Sustain. Energy from Salin. Gradients, Woodhead Publishing, Cambridge, United Kingdom, 2016: pp. 315–335.

[17] M. Turek, B. Bandura, Renewable energy by reverse electrodialysis, Desalination. 205 (2007) 67–74.

[18] J.W. Post, C.H. Goeting, J. Valk, S. Goinga, J. Veerman, H.V.M. Hamelers, P.J.F.M. Hack, Towards implementation of reverse electrodialysis for power generation from salinity gradients, Desalin. Water Treat. 16 (2010) 182–193.

[19] A. Daniilidis, R. Herber, D.A. Vermaas, Upscale potential and financial feasibility of a reverse electrodialysis power plant, Appl. Energy. 119 (2014) 257–265.

[20] M. Papapetrou, G. Kosmadakis, F. Giacalone, B. Ortega-Delgado, A. Cipollina, A. Tamburini, G. Micale, Evaluation of the Economic and Environmental Performance of Low-Temperature Heat to Power Conversion using a Reverse Electrodialysis – Multi-

Effect Distillation System, Energies. 12 (2019) 3206.

[21] A. Daniilidis, D.A. Vermaas, R. Herber, K. Nijmeijer, Experimentally obtainable energy from mixing river water, seawater or brines with reverse electrodialysis, Renew. Energy. 64 (2014) 123–131.

[22] D. Amaya-Vías, J.A. López-Ramírez, Techno-economic assessment of air and water gap membrane distillation for seawater desalination under different heat source scenarios, Water. 11 (2019). 2117.

[23] H. Kim, S. Yang, J. Choi, J. Kim, N. Jeong, Optimization of the number of cell pairs to design efficient reverse electrodialysis stack, Desalination. (2020) 114676.

[24] M. Micari, A. Cipollina, F. Giacalone, G. Kosmadakis, M. Papapetrou, G. Zaragoza, G. Micale, A. Tamburini, Towards the first proof of the concept of a Reverse ElectroDialysis - Membrane Distillation Heat Engine, Desalination. 453 (2019) 77–88.

[25] J. Veerman, M. Saakes, S.J. Metz, G.J. Harmsen, Reverse electrodialysis: Evaluation of suitable electrode systems, J. Appl. Electrochem. 40 (2010) 1461–1474.

[26] S.Y. Lee, Y.J. Jeong, S.R. Chae, K.H. Yeon, Y. Lee, C.S. Kim, N.J. Jeong, J.S. Park, Porous carbon-coated graphite electrodes for energy production from salinity gradient using reverse electrodialysis, J. Phys. Chem. Solids. 91 (2016) 34–40.

[27] O. Scialdone, A. Albanese, A. D'Angelo, A. Galia, C. Guarisco, Investigation of electrode material - Redox couple systems for reverse electrodialysis processes. Part II: Experiments in a stack with 10-50 cell pairs, J. Electroanal. Chem. 704 (2013) 1–9.

[28] A. Tamburini, M. Tedesco, A. Cipollina, G. Micale, M. Ciofalo, M. Papapetrou, W. Van Baak, A. Piacentino, Reverse electrodialysis heat engine for sustainable power production, Appl. Energy. 206 (2017) 1334–1353.

[29] F. Giacalone, C. Olkis, G. Santori, A. Cipollina, S. Brandani, G. Micale, Novel solutions for closed-loop reverse electrodialysis: Thermodynamic characterization and perspective analysis, Energy. 166 (2019) 674–689.

[30] M. Micari, M. Bevacqua, A. Cipollina, A. Tamburini, W. Van Baak, T. Putts, G. Micale, Effect of different aqueous solutions of pure salts and salt mixtures in reverse electrodialysis systems for closed-loop applications, J. Memb. Sci. 551 (2018) 315–325.

[31] R.A. Tufa, E. Curcio, E. Brauns, W. van Baak, E. Fontananova, G. Di Profio, Membrane Distillation and Reverse Electrodialysis for Near-Zero Liquid Discharge and low energy seawater desalination, J. Memb. Sci. 496 (2015) 325–333.

[32] W.J. Van Egmond, M. Saakes, S. Porada, T. Meuwissen, C.J.N. Buisman, H.V.M. Hamelers,

The concentration gradient flow battery as electricity storage system: Technology potential and energy dissipation, J. Power Sources. 325 (2016) 129–139.
[33] R.S. Kingsbury, K. Chu, O. Coronell, Energy storage by reversible electrodialysis: The concentration battery, J. Memb. Sci. 495 (2015) 502–516.
[34] K. Branker, M.J.M. Pathak, J.M. Pearce, A review of solar photovoltaic levelized cost of electricity, Renew. Sustain. Energy Rev. 15 (2011) 4470–4482.
[35] A.A.A. Al-khazzar, The Required Land Area for Installing a Photovoltaic Power Plant, Iran. J. Energy Environ. (2017) 11–18.

6. Conclusions and Further Work

6.1 Conclusions

This thesis has demonstrated how RED can be configured and operated for thermal to electric conversion applications.

1. At an optimised current density, higher salinity gradients maximise the work which can be produced from a fixed volume despite complex temporal effects due to ionic transport, water flux and concentration polarisation, and are therefore likely to be favourable for integration with a thermal separation stage (Objective 1).
2. Recycling feeds improves the energy efficiency and cost effectiveness of power production by enabling an improved power density from a fixed volume to be sustained for an extended duration compared with conventional single pass operation, thereby minimising the total membrane area required and hence the unitary cost of electricity (Objective 1).
3. Whilst increasing feed temperatures from room temperature to 40 °C doubled power density, increased exergy losses due to water transport reduced the total work produced from a fixed feed volume in recycle and an increased feed temperature is therefore not recommended for closed-loop applications where high efficiency from a small feed volume is required (Objective 1).
4. For RED applications utilising large concentrations in recycle, the increased residence time facilitated by an increased intermembrane distance up to 0.3 mm was demonstrated to improve net power density and is favoured for high power applications (Objective 2). Membranes with low water permeability enabled improved energy efficiency from RED using feeds with a large concentration, as exergy losses due to water transport were minimised, however, low membrane resistance is also required to improve power output from these feeds (Objective 2).
5. Positive net power densities were achieved using a large concentration gradient (4M/0.02M) at all operating conditions and stack sizes investigated in this study, demonstrating the suitability of these feeds for use at increased process scale (Objective 3).
6. Despite an improvement in gross power density as stack size was increased in single pass, maximum net power density, accounting for pumping power, was comparable across all stack sizes due to the increased pressure drop as the path length was extended, demonstrating that power production does not scale linearly with process scale (Objective 3).

7. A trade-off between power density and energy recovery must be managed when scaling-up RED, and the recommended design strategy is to maximise net power density through selection of appropriate velocity or residence time, prior to extending the path length to improve energy recovery (Objective 3).
8. An exergy analysis showed that exergy dissipation from feeds with a large concentration gradient increased as RED stack size was increased, indicating that smaller stacks may be preferable for applications where sources of salinity difference are scarce and high energy efficiency is required (Objective 3). Increasing the cell pair number within a single stack was demonstrated to improve both power density and energy efficiency for a large concentration gradient in recycle, and is therefore a suitable strategy for scaling-up RED using large concentration gradients (Objective 3).

6.2 Further Work

Further research is recommended in the following areas.

1. In this work, operating conditions for RED using sodium chloride solutions in recycle have been identified for thermal to electric applications. Whilst improved power density has been theoretically [1] and experimentally [2] demonstrated using alternative saline solutions with a high solubility due to the increased availability of Gibbs free energy provided, further research is required to determine the maximum power densities which can be experimentally obtained by RED using these feeds and existing ion exchange membranes.
2. Whilst this work is limited to sodium chloride solutions, the same challenges due to water flux, ionic transport and concentration polarisation are anticipated when utilising alternative saline solutions with a large concentration gradient and operating conditions such as current density, flow rate and temperature which minimise these phenomena must be determined.
3. Water transport has been identified as a barrier to high energy efficiency in RED when using concentrated brines in recycle. For improved power density and energy efficiency when using feeds with a large concentration gradient, membranes with low water permeability to limit exergy dissipation due to water transport and low membrane resistance to improve power output must be developed.
4. Electrode segmentation has previously been demonstrated to improve the power density and energy efficiency achieved by RED using NaCl feeds with concentrations equivalent to sea water and river water [3]. Whilst it can be expected that the

performance of RED with large concentration gradients and alternative saline solutions will be similarly improved, it must be determined whether electrode segmentation can counteract the effect of exacerbated exergy dissipation when using these feeds, and reduce the levelised cost of electricity.

5. The effect of RED effluent concentration, temperature, and flow rate on the performance of a thermal separation stage must be investigated, to determine the overall efficiency which could be achieved an integrated RED heat engine.

References

[1] A. Tamburini, M. Tedesco, A. Cipollina, G. Micale, M. Ciofalo, M. Papapetrou, W. Van Baak, A. Piacentino, Reverse electrodialysis heat engine for sustainable power production, Appl. Energy. 206 (2017) 1334–1353.

[2] M. Micari, M. Bevacqua, A. Cipollina, A. Tamburini, W. Van Baak, T. Putts, G. Micale, Effect of different aqueous solutions of pure salts and salt mixtures in reverse electrodialysis systems for closed-loop applications, J. Memb. Sci. 551 (2018) 315–325.

[3] C. Simões, D. Pintossi, M. Saakes, Z. Borneman, W. Brilman, K. Nijmeijer, Electrode segmentation in reverse electrodialysis: Improved power and energy efficiency, Desalination. 492 (2020) 114604.